eTransportation 1 (2019) 100011

Contents lists available at ScienceDirect

eTransportation

journal homepage: www.journals.elsevier.com/etransportation

Lithium-ion battery fast charging: A review

Anna Tomaszewska [a, *], Zhengyu Chu [b], Xuning Feng [b, **], Simon O'Kane [c, d], Xinhua Liu [a], Jingyi Chen [a], Chenzhen Ji [a], Elizabeth Endler [e], Ruihe Li [b], Lishuo Liu [b], Yalun Li [b], Siqi Zheng [b], Sebastian Vetterlein [f], Ming Gao [g], Jiuyu Du [b], Michael Parkes [f], Minggao Ouyang [b], Monica Marinescu [c, d], Gregory Offer [c, d], Billy Wu [a, d, ***]

[a] Dyson School of Design Engineering, Imperial College London, Exhibition Road, London, SW7 2AZ, UK
[b] State Key Laboratory of Automotive Safety and Energy, Tsinghua University, Beijing, 100084, PR China
[c] Department of Mechanical Engineering, Imperial College London, Exhibition Road, London, SW7 2AZ, UK
[d] The Faraday Institution, Quad One, Harwell Science and Innovation Campus, Didcot, OX11 0RA, UK
[e] Shell International Exploration & Production Inc., 3333 Hwy 6 South, Houston, TX, 77082, USA
[f] Shell Global Solutions UK, 40 Bank Street, Canary Wharf, London, E14 5NR, UK
[g] Shell (Shanghai) Technology Limited, Building 4, 4560 Jinke Road, Pudong District, Shanghai, 201210, PR China

ARTICLE INFO

Article history:
Received 26 June 2019
Received in revised form
9 August 2019
Accepted 10 August 2019
Available online 16 August 2019

Keywords:
Lithium-ion battery
Fast charging
Lithium plating
Charging protocols
Electric vehicles

ABSTRACT

In the recent years, lithium-ion batteries have become the battery technology of choice for portable devices, electric vehicles and grid storage. While increasing numbers of car manufacturers are introducing electrified models into their offering, range anxiety and the length of time required to recharge the batteries are still a common concern. The high currents needed to accelerate the charging process have been known to reduce energy efficiency and cause accelerated capacity and power fade. Fast charging is a multiscale problem, therefore insights from atomic to system level are required to understand and improve fast charging performance. The present paper reviews the literature on the physical phenomena that limit battery charging speeds, the degradation mechanisms that commonly result from charging at high currents, and the approaches that have been proposed to address these issues. Special attention is paid to low temperature charging. Alternative fast charging protocols are presented and critically assessed. Safety implications are explored, including the potential influence of fast charging on thermal runaway characteristics. Finally, knowledge gaps are identified and recommendations are made for the direction of future research. The need to develop reliable onboard methods to detect lithium plating and mechanical degradation is highlighted. Robust model-based charging optimisation strategies are identified as key to enabling fast charging in all conditions. Thermal management strategies to both cool batteries during charging and preheat them in cold weather are acknowledged as critical, with a particular focus on techniques capable of achieving high speeds and good temperature homogeneities.

1. Introduction

In recent years, efforts to limit the effects of climate change and local air pollution have driven rapid progress in the development of lithium-ion (Li-ion) battery powered electric vehicles (EVs). While manufacturers race to introduce electrified options in their ranges, customer acceptance of EVs, and particularly battery electric vehicles (BEVs) that are not hybridised with internal combusion engines (ICEs), is still limited. Range anxiety and long charging times compared to the refuelling of petrol vehicles are often quoted among the main issues hindering wider adoption of EVs [1]. Fast charging capability has therefore become one of the key features targeted by battery and EV industries. However, charging at high rates has been shown to accelerate degradation, causing both the capacity and power capability of batteries to deteriorate. Low ambient temperatures, prevalent in many key EV markets,

* Corresponding author.
** Corresponding author.
*** Corresponding author. Dyson School of Design Engineering, Imperial College London, Exhibition Road, London, SW7 2AZ, UK.
E-mail addresses: a.tomaszewska18@imperial.ac.uk (A. Tomaszewska), fxn17@tsinghua.edu.cn (X. Feng), billy.wu@imperial.ac.uk (B. Wu).

https://doi.org/10.1016/j.etran.2019.100011

Abbreviations

AC	Alternating current
BMS	Battery Management System
CC-CV	Constant current - constant voltage
CCS	Combined Charging System
CEI	Cathode electrolyte interphase
CP-CV	Constant power - constant voltage
DC	Direct current
DCFC	DC fast charging
DEC	Diethyl carbonate
DMC	Dimethyl carbonate
DVA	Differential voltage analysis
EC	Ethylene carbonate
ECM	Equivalent circuit model
EIS	Electrochemical impedance spectroscopy
EV	Electric vehicle
FOM	Full order model
ICA	Incremental capacity analysis
LAM	Loss of active material
LCO	Lithium cobalt oxide
LFP	Lithium iron phosphate
LLI	Loss of lithium inventory
LMO	Lithium manganese oxide
LTO	Lithium titanium oxide
MCC	Multistage constant current
N/P	Negative-to-positive electrode
NCA	Lithium nickel cobalt aluminium oxide
NFRA	Nonlinear frequency response analysis
NMC	Lithium nickel manganese cobalt oxide
NMR	Nuclear magnetic resonance
P2D	Pseudo-two-dimensional
PCM	Phase change material
PDE	Partial differential equation
ROM	Reduced order model
SEI	Solid electrolyte interphase
SEM	Scanning electron microscopy
SOC	State-of-Charge
SP	Single particle
UVP	Universal Voltage Protocol

exacerbate the problem even further due to the slower diffusion of Li^+ ions in the electrodes and the electrolyte and the sluggish kinetics of intercalation. On the other hand, the heat generated during fast charging due to resistive heating is often difficult to remove in a uniform and efficient manner, leading to accelerated degradation and safety concerns. The behaviour of cells and packs subjected to fast charging depends on a multitude of factors spanning multiple scales from atomic to system level, as illustrated in Fig. 1. This paper looks to review the existing literature and identify some of the key knowledge gaps at each of these length scales.

EVs can be charged using either alternating current (AC) or direct current (DC) infrastructure. Out of these, DC offers significantly higher charging speeds. The most common DC fast charging (DCFC) posts can charge at a power of 50 kW using CHArge de MOve (CHAdeMO), Combined Charging System (CCS) or GB/T standard connectors. Tesla were the first to introduce 120 kW charging posts (Tesla Superchargers) equipped with custom connectors. CCS has since followed suit, developing 150 kW chargers. In 2017, Porsche pioneered 350 kW charging by unveiling two CCS charging posts rated to this power at the company's office in Berlin [2,3]; however, the first light duty EV capable of accepting the full 350 kW is only scheduled to become available in 2019, when Porsche's debut electric model, the Taycan, is released. This is because today's EV battery packs are normally rated at 400 V. 350 kW and higher power charging necessitates higher voltage packs to avoid extremely high charging currents and to limit resistive heat generation. The Porsche Taycan as well as the recently unveiled Audi e-tron GT concept (also expected to charge at up to 350 kW) will both be equipped with 800 V Li-ion battery packs [4,5]. In December 2018, a prototype 450 kW CCS charger was tested on two research vehicles in Bavaria, Germany [6]. Both the charger and the vehicles were developed as a result of the 'Fast-Charge' research project, conducted by a consortium led by the

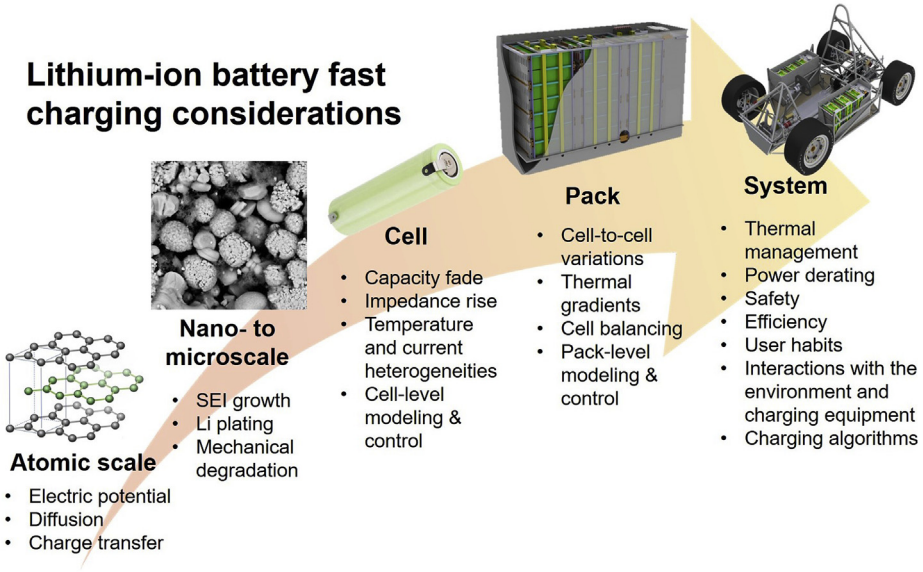

Fig. 1. Key factors affecting Li-ion battery fast charging at different length scales.

BMW Group and involving Porsche and Siemens.

While impressive progress has been made in increasing the power capability of EV chargers, these improvements do not always translate directly into fast charging in all circumstances. Continuous charging power is normally derated compared to the power rating of the charger and depends on the specifications of the EV as well as the environmental conditions. In particular, charging speeds are significantly decreased at low ambient temperatures: according to the Nissan LEAF Owner's Manual [7], charging up to 80% State-of-Charge (SOC) with a 50 kW charger can take from 30 min to over 90 min depending on the temperature. Furthermore, fast charging rates are typically only achievable up to about 80% SOC level [8,9] due to safety limitations. At high SOCs, the current needs to be gradually decreased to avoid exceeding the maximum cell voltage limits, resulting in much longer times required to charge to full capacity. The maximum charging power is limited not only by the charger but also by the Battery Management System (BMS) on the vehicle. Typically, EVs with smaller battery packs such as the Nissan LEAF (40–62 kWh) or BMW i3 (22–42 kWh) can only charge at a maximum power of 50 kW [7,10], whereas vehicles equipped with larger packs accept higher power levels. This is due to the fact that the charging C-rate that can be safely accepted by the batteries used in EVs is still limited to about 1–1.5C in most cases. However, according to the current specifications, the aforementioned Porsche Taycan is expected to defy this trend with a maximum charging rate of around 3C. Given the increasing industrial interest in battery fast-charging, there is a need to understand rate limiting processes and lifetime implications of different charging approaches.

The progress in understanding various aspects of fast charging has recently been analysed and reviewed in a number of publications, with notable works highlighted here. Zhu et al. [11] discussed some of the key strategies to improve electrode rate capabilities and electrolyte conductivities in both traditional Li-ion and solid state systems, with a thorough consideration of the issues related to solid electrolyte/electrode interfaces. Liu et al. [12] reviewed the recent developments in battery materials to tackle challenges with the mass transport in electrolytes and charge transfer in electrodes, while also describing useful characterisation techniques for material research. Some of the common charging algorithms were discussed from a control and implementation perspective by Shen et al. [13], but with little consideration of the implications on cycle life. Gao et al. [14] recently published a review of charging algorithms with a focus on model-based optimisation. Chen et al. [15] published a technological review on EV fast charging, discussing the thermal management issues and charger design. The authors also listed some of the available charging algorithms, however little critical commentary was provided and no links were made to the electrochemical aspects of battery charging. This work aims to highlight the multiscale and multidisciplinary nature of fast charging, establishing the links between microscale processes, material characteristics, cell and pack design, and charging strategy optimisation. Recent progress in each of these aspects is analysed in a critical way to identify the key questions that remain unanswered, to understand the limitations of the current technologies, and to highlight possible directions for future research.

The discussion of key aspects of Li-ion battery fast charging is arranged according to scale, starting from atomic to pack and system level. Section 2 describes the rate limiting processes that restrict fast charging capability in Li-ion batteries. Degradation phenomena that result from these processes, and which are exacerbated by fast charging, are discussed along with detection and mitigation methods in Section 3. Approaches to material, cell and pack design to reduce degradation are discussed in Section 4. Section 5 evaluates the existing charging protocol optimisation strategies, while the implications of fast charging capability on battery thermal management are outlined in Section 6. Particular attention is paid to the effects of extreme temperatures on fast charging performance. Section 7 deals with the safety implications of fast charging, including the effect on thermal runaway characteristics. Finally, recommendations are made on the existing knowledge gaps and directions for future research in Section 8.

2. Principles of battery fast charging

An ideal battery would exhibit a long lifetime along with high energy and power densities, enabling both long range travel on a single charge and quick recharge anywhere in any weather. Such characteristics would support broad deployment of EVs for a variety of applications. Unfortunately, the physics of each of these requirements results in tradeoffs [16]; for example, thicker electrodes needed for high energy density suffer more acutely from the concentration and potential gradients resulting from fast charging [17,18]. The combination of physical properties of materials and devices with temperature dependent behaviour defines the operating envelope for batteries. As ambient temperatures decrease, charge rates and recommended maximum voltages are typically kept low to improve safety and performance, making operating temperature a key barrier to fast charging [16]. The risk of lithium plating during charging significantly increases with decreasing temperatures, impacting capacity retention. The temperature threshold below which lithium plating becomes likely depends on many factors, including the cell parameters, age and C-rate. Although many authors have reported lithium plating at temperatures below 25°C [19–21], it can also occur at higher temperatures, particularly when high C-rates or high energy density cells are used [22,23]. Additionally, the efficiency of fast charging equipment is often strongly dependent on temperature, with power conversion efficiencies of 50 kW chargers reported at up to 93% and as low as 39% for operation at 25°C and -25°C, respectively, primarily due to the derating of power levels requested by BMSs at lower temperatures [24]. Efficiency in this case is defined as the ratio between the instantaneous DC power delivered by the charger to the vehicle and the instantaneous AC power supplied to the charger by the grid. The level of this temperature-dependency varies between charger models, with some still able to maintain about 70% efficiencies at -25°C and others failing to function at all [24]. This section looks to provide insights into the fundamental phenomena involved in fast charging and their resulting impacts.

2.1. Rate-limiting processes

A Li-ion battery typically includes a graphite anode, a lithium metal oxide cathode with a layered, spinel, or olivine structure, a liquid electrolyte containing a mixture of organic carbonates, salts, and additives, as well as copper/aluminium current collectors and a porous polymer separator. Processes that take place within the battery, whether within electrodes or at key interfaces, are central to enabling reliable operation and fast charging [16] and are dependent on factors such as ion transport and temperature. As shown in Fig. 2, when a Li-ion battery is charged, ions move from the cathode, through the electrolyte, to the anode. Key mechanisms that influence this journey are ion transport 1) through the solid electrodes, 2) across the electrode/electrolyte interface for both anode and cathode, and 3) through the electrolyte, including Li^+ solvation and desolvation [25]. In an ideal situation, these primary phenomena involved in battery charging would be favoured. However, battery operating conditions can lead to a range of side reactions that compromise performance and lifetime. In addition, the thermal behaviour of the battery is strongly dependent on the conditions: factors such as high charging/discharging currents,

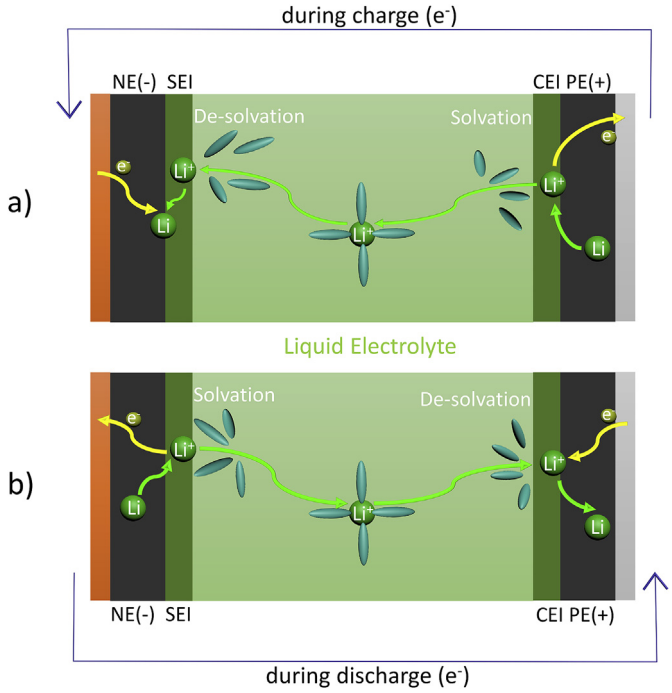

Fig. 2. A schematic view of Li^+ ion transfer during a) charge, b) discharge.

high cell resistance or high concentration polarisation increase the heat generation rates, affecting the efficiency and safety of the process.

The anode receives a lot of the attention during the charging process, since multiple studies have explored the role of cathode degradation and cathode electrolyte interphase (CEI) layer growth and concluded that these processes, while important, are generally not rate-limiting for traditional Li-ion systems [22,25,26]. At the anode, lithium metal can begin to deposit on the surface of the graphite under certain conditions during charging. This can result from a lack of accessible intercalation sites within the electrode if lithium reaches the surface when the surface concentration is already high. Understanding the site accesibility is a complex process, with studies showing that lithium diffusion into the electrode along the edge plane of graphite is significantly more likely compared to the basal plane of graphite [27,28]. Under certain circumstances, the lithium may continue to deposit preferentially where deposits already exist, forming needle-like structures known as dendrites which pose a risk of piercing the separator and causing a short circuit. As the cell is repeatedly cycled, the dendrites may also break and become electrically disconnected from the anode, reducing the amount of cyclable lithium. However, even relatively uniform lithium plating removes significantly more lithium from active availability than typical solid electrolyte interphase (SEI) layer formation on graphite, leading to dramatic capacity losses. The reactivity of lithium metal and the chemical instability of electrolyte components near the Li/Li^+ potential result in the formation of gas by-products and new SEI material, removing active materials from the system [28].

Factors that influence lithium deposition and resulting structures include lithium diffusion rates within the anode [18], limited ion transport in the electrolyte leading to concentration gradients across the anode and salt depletion at the current collector [29], and reactions at electrode/electrolyte interfaces [30]. Both materials and cell designs have been studied in detail to manage the impacts of fast charging on these phenomena [23]. Managing internal resistances, including those associated with the transport through the electrolyte and electrodes as well as charge transfer at interfaces, is important to good charging characteristics, performance, and lifetime [31], with low temperatures increasing these transport resistances and requiring more sophisticated control strategies [24]. In studies of electrolyte additives to mitigate lithium plating under fast charging conditions, Liu et al. [32] found significant differences in cell capacity losses between C/2 and 1C charging rates at 20°C which were attributed to lithium plating. They concluded that many of the phenomena occurring at the anode could be combined into a single guideline relating the area specific resistance for the anode to the onset current of lithium plating for the conditions tested. Additionally, work on charge transfer by Jow et al. demonstrated that reducing the anode resistance, which dominates overall cell resistance, is important for improving fast charging performance [25].

Regarding temperature, work by Waldmann et al. [33] explored the main aging mechanisms at both low (0°C) and high temperatures (45°C) at 0.5C in lithium nickel cobalt aluminium oxide (NCA)/graphite systems to better understand implications related to different aging mechanisms. Cells that experienced aging at higher temperatures by consumption of active materials through SEI growth show higher temperature onsets for thermal runaway in accelerated rate calorimetry testing than cells that have experienced low temperature aging even at relatively mild charging rates. While dendrites and the potential for short circuits are viewed as the typical hazard resulting from lithium plating, the reactivity of lithium metal is also a significant consideration. Reactions between lithium and the electrolyte not only contribute to the growth of the SEI layer but can also be highly exothermic and may play a part in the evolution of thermal runaway. Historically, high temperatures, such as those above 30°C were avoided for battery operation, due to the increased kinetics of SEI formation and other side reactions relative to functional reactions. However, when batteries are subjected to extreme fast charging, higher temperature has a beneficial effect in spite of the increase in kinetic rates of SEI formation, most likely by avoiding operating conditions that would induce lithium plating [23]. Finally, recent work by Yang et al. [23] explored the dependence of the optimal cell temperature on the charging C-rate and cell energy density. The results of their modelling study showed that while both extremely low and extremely high temperatures were generally damaging, fast charging shifted the balance in favour of higher temperatures, particularly for high energy cells.

While the intersection of phenomena, materials chemistry and component design are described in the following sections, anode thickness and its influence on transport provides a useful lens to explore their linkages. While thin electrodes are generally considered to represent ideal transport [26], when electrodes are sufficiently thick, it becomes critical to ensure sufficient Li^+ concentration at the electrode/electrolyte interface throughout the anode to keep the overpotential stable and reduce the chances for lithium plating [28,34]. Strong heterogeneities, whether in electrode microstructures [35] or in lithium concentration gradients observed during the charging process [36], have recently been shown to have significant influence on lithium deposition reactions. Non-uniform SOCs within graphite anodes have also been shown to influence lithium plating [25], with reduced pore tortuosity highlighted as a key lever to avoid electrolyte phase transport limitations and the resulting overpotential increase [17,37]. In relatively thick anodes subjected to fast charging conditions, the lithium salt may become depleted near the current collector, leading to non-uniform electrode utilisation and an increase in the local current densities near the separator [17,29,31]. Local salt depletion at the anode has also been shown to influence the

morphology of lithium deposition, inducing the formation of dendritic structures in place of the more uniform mossy deposits formed when sufficient amounts of lithium are available in the electrolyte [29,38]. To avoid the phenomena that result in plating or dendrite growth, Gallagher et al. recommended operating at current densities below 4 mA cm^{-2} but acknowledged the complex interactions of operating parameters in providing such guidelines [17]. Due to the difference in mass loadings and other characteristics between cells, the general applicability of this recommendation may be questioned.

Alternative anode materials are also the subject of significant research, to assist in addressing the challenges related with lithium plating on graphite anodes during fast charging described above, as well as to increase energy density. Since most studies have been conducted on graphite, much remains to be studied for other systems [39], including the effects of localised current densities on lithium metal anodes [40].

3. Degradation effects

3.1. Thermal effects

In a Li-ion battery, the heat generation occurs as a result of both reversible and irreversible processes [41]. The irreversible heat generation Q_{irr} is given by Ref. [42]:

$$Q_{\mathrm{irr}} = (V_{\mathrm{bat}} - U)I \tag{1}$$

where U is the open circuit potential, V_{bat} is the cell voltage, and I is the current ($I > 0$ during charging). The difference between V_{bat} and U represents the total overpotential of a battery induced by processes such as the charge transfer reactions at the electrode/electrolyte interfaces [43], the diffusion and migration of Li^{+} ions across the electrolyte [44], diffusion and migration of Li^{+} ions in the electrodes [45] and Ohmic losses [46]. A large contribution to the irreversible heat generation is resistive (joule) heating:

$$Q_{\mathrm{joule}} = I^2 R \tag{2}$$

where R is cell resistance. As fast charging requires higher charging currents, more heat is generated due to the quadratic dependency of irreversible heat generation rate Q_{irr} on the current. The heat generated/consumed in the reversible process, also known as entropic heat, originates from the reversible entropy change ΔS during electrochemical reactions [47]. Once the entropy change ΔS is measured [48,49], the reversible heat Q_{rev} can be calculated according to [50]:

$$Q_{\mathrm{rev}} = I\frac{T\Delta S}{nF} \tag{3}$$

where T is the absolute temperature, n is the stoichiometric number of electrons involved in the electrochemical reaction and F is Faraday's constant. To understand heat generation in batteries, Nazari et al. [51] employed a mathematical model to simulate the heat generation in lithium iron phosphate (LFP), lithium manganese oxide (LMO) and lithium cobalt oxide (LCO) batteries with graphite anodes. The results revealed that the total heat generation in all cells investigated is of the same order of magnitude. At low C-rates the reversible heat generation is dominant and at high C-rates the irreversible heat is dominant. Li-ion battery lifetimes vary greatly with cell temperature. To understand this correlation, the US National Renewable Energy Laboratory has developed aging models [52,53] of Li-ion cells that consider the impact of temperature and charge/discharge cycle on battery life. It was found that battery lifetime roughly doubles when the average battery temperature (during storage and cycling) is reduced from 35 °C to 20 °C. The effects of lower temperatures were not explored.

3.1.1. Temperature distribution during cycling

In Li-ion batteries, whether pouch, cylindrical or prismatic, heat can dissipate from some locations more easily than from others: for example, the poor through-plane conductivity of battery materials such as polymer separators causes higher heat accumulation in the core compared to the regions closer to the surface. Furthermore, the current densities and the heat generation rates are not equal at different locations. These inhomogeneities are aggravated for large format cells. For cylindrical cells in particular, the temperature in the battery core is significantly higher than at the surface [54] as shown in Fig. 3. For pouch [55] or prismatic [56] cells, the temperature is higher in the regions close to the tabs [57] as shown in Figs. 4 and 5 due to the higher current densities in those locatons. Furthermore, the temperature near the positive tab is often higher than near the negative tab due to the higher ohmic resistivity of the aluminium current collector on the cathode side compared to copper on the anode side. The heat generation rate among the different regions is not uniform due to the non-uniformly distributed current during cycling. The non-uniformity of current density can be caused by a temperature gradient and the location of tabs [58,59]. High current density near the tabs may lead to local overcharge or overdischarge, potentially resulting in localised failure [60]. The inhomogeneities in the temperature and current distribution can also lead to different local rates of side reactions and therefore different local degradation rates [60]. Zhu et al. [61] recently used micro-Raman spectroscopy as a temperature-sensing platform to investigate the effects of temperature hot spots on lithium dendrite growth in Cu/Li and Cu/LCO optical cells, showing that high local temperature gradients dramatically increased local current densities, leading to dendrite growth and eventual short-circuiting during charging. In Li-ion cells with graphite anodes charged at low temperatures the relationship between hot spots and dendrite growth rates may be more complex due to the interaction between temperature and the local potential of the graphite anode.

Uneven heat generation is not solely a cell-level effect. Design decisions on the pack level, particularly those concerning the pack layout and the thermal management system design, have a strong influence on the temperature variations within a pack. Wu et al. [62] used a coupled electrochemical-thermal model to investigate heat generation in battery packs containing cells connected in parallel. Finite interconnect resistances were shown to result in unequal interconnect overpotentials and, in consequence, lead to load imbalances and heterogeneous heat generation between cells. These effects were aggravated during pulse loading due to the additional heat generation caused by rebalancing between pulses. Over time, different degradation behaviours between individual cells can also be expected to strongly affect the homogeneity of heat generation in an aged pack due to the unequal rise in cell resistances. The resulting temperature gradients may, in turn, further aggravate the differences in the aging behaviours between cells. The design of the thermal management system to minimise temperature inhomogeneity is discussed in Section 6.

3.1.2. Temperature-induced degradation

Many degradation mechanisms that take place in Li-ion batteries show temperature dependence. The temperature effect is correlated with Arrhenius equations [20,63] or modelled with empirical equations fitted to experimental data [64] in the past studies. At high temperatures, the SEI layer on the anode grows faster, becoming more porous and unstable [65]. At the other end of

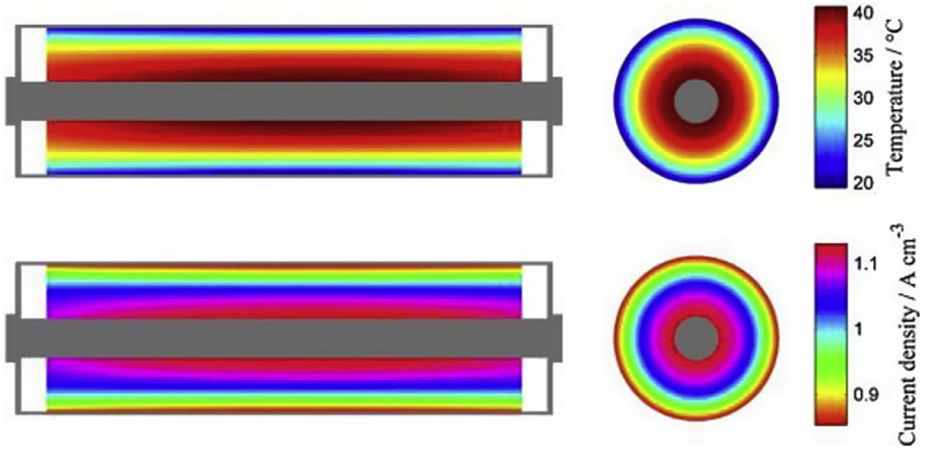

Fig. 3. Simulated temperature and current density distribution in a cylindrical 4.4 Ah cell subjected to SoC-neutral pulse cycling with a pulse amplitude of 70 A [59].

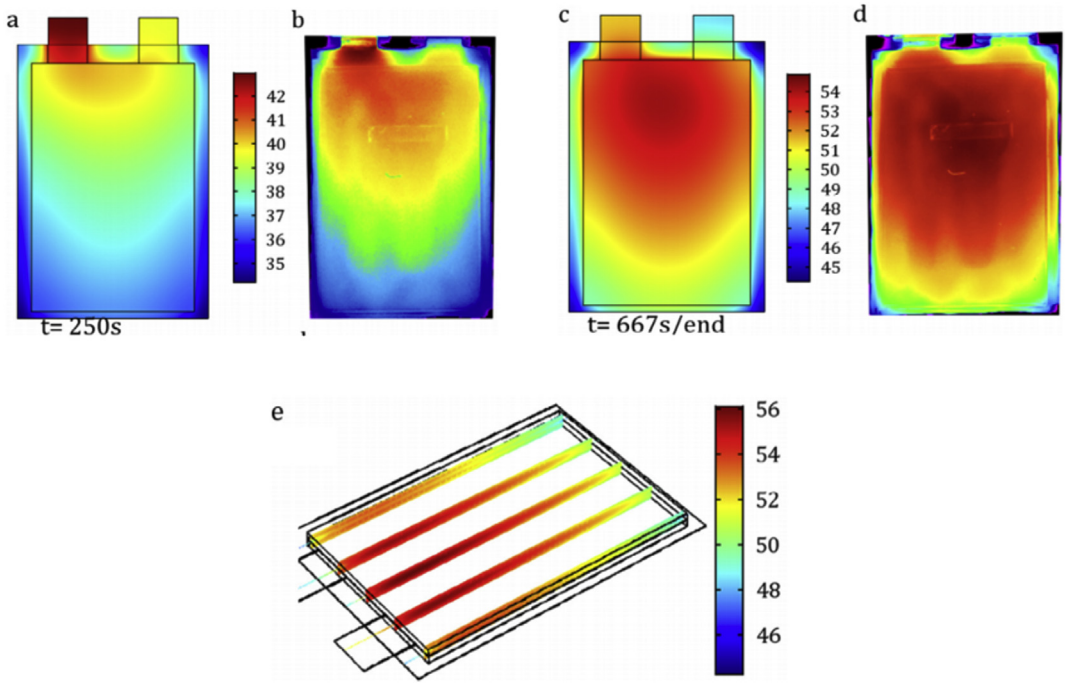

Fig. 4. Surface temperature evolution of a pouch cell during 5C constant current discharge obtained by a) simulation and b) measurement at t = 250 s; c) simulation and d) measurement at the end of discharge/t = 667 s; e) 3D representation of internal temperature distribution [55].

the spectrum, low temperatures lead to slower diffusion and intercalation with the possibility of lithium plating and subsequent lithium dendritic growth [20]. On the cathode, the temperature increases during cycling may lead to binder decomposition [66], phase transitions [67], metal dissolution and CEI growth. The electrolyte, typically ethylene carbonate (EC)/dimethyl carbonate (DMC) (1:1 wt ratio)-$LiPF_6$ (1 M), can decompose to release gaseous species, for example CO_2 [68], when operated at elevated temperatures. In general, most degradation mechanisms are accelerated at high temperatures. Lowering the temperature can suppress the degradation rate but low temperatures also undesirably slow down the diffusion of active species and change the reaction chemistry, leading to accelerated degradation if metallic lithium starts depositing on the anode. Furthermore, operation at low temperatures leads to lower energy efficiency [69] and more heat generation due to the higher overpotential resulting from the increased transport limitations and slower kinetics.

The SEI growth at the anode/electrolyte interface is one of the main degradation mechanisms in Li-ion cells under most cycling conditions. The passive surface layer adds onto the cell impedance and diminishes the power. The lithium consumed by the SEI is not recoverable, resulting in capacity fade. The electrochemical reduction of the electrolyte which generates the complex mixture of SEI with lithium species such as LiF, Li_2CO_3, $(CH_2OCO_2Li)_2$, is highly temperature dependent [70]. The SEI layer formed initially may serve a protective function, but upon further cycling becomes unstable and grows to block pores of the electrode or even penetrate the separator, which causes an impedance rise from the decrease in active surface area and safety issues. At elevated temperatures (60 °C or above), the dissolution and decomposition of SEI species, Li_2CO_3 for example [71], has been found to disrupt the integrity of the protective thin film to form separate islands.

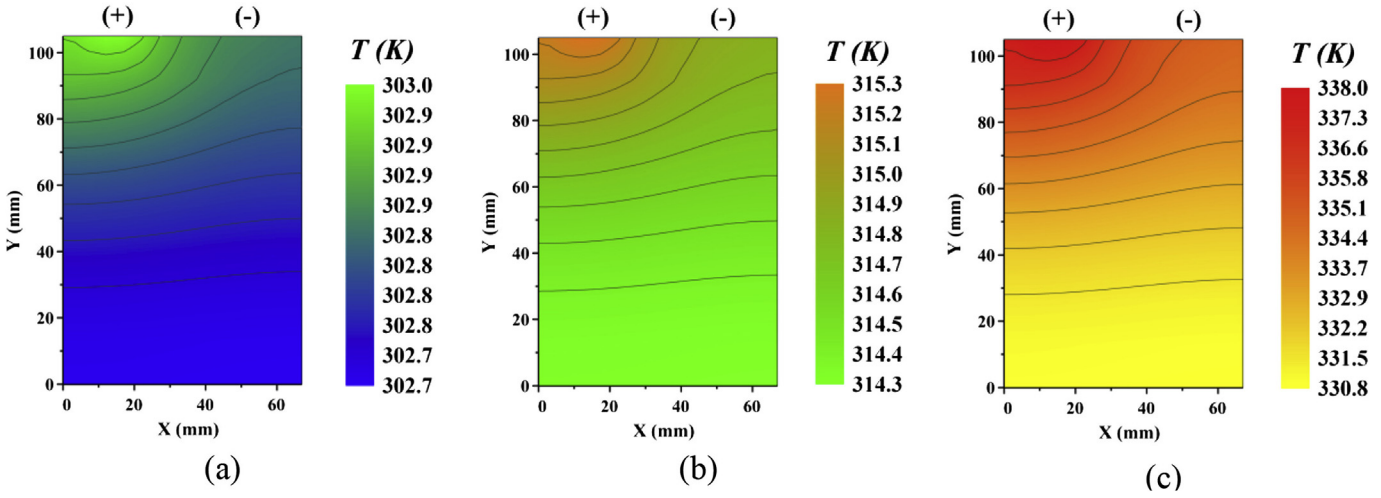

Fig. 5. Temperature distribution of a prismatic LFP cell during a) 1C, b) 2C and c) 5C discharge process. Discharge time is: a) 1020 s, b) 990 s, and c) 360 s [56].

Besides forming the SEI on the graphite anode, thermal decomposition of the carbonate-based electrolyte yields many other possible products, including carbon monoxide, carbon dioxide, hydrogen, ethylene, alkylfluorides, fluorophosporic acids, etc. Gachot et al. [72] recovered lithium methyl carbonate from the separators in Li/chromium-based-oxide (Li/CBO) cells cycled at 55°C. $LiPF_6$ is not stable at 60°C, and its dissociation into PF_5 dissolves the protective SEI and exposes fresh graphite surface [73]. The decomposition reactions are thermally activated and were observed to become significant at 85°C by comparison of nuclear magnetic resonance (NMR) spectra of 1.0 M $LiPF_6$ in EC/DMC/diethyl carbonate (DEC) [74]. The release of gaseous by-product during SEI formation and electrolyte decomposition also compromises the mechanical properties of the anode and the cathode.

As side-products from parasitic reactions accumulate, electrode delamination and particle cracking are also detrimental to a battery after prolonged exposure to elevated temperatures. Delamination was observed by Pieczonka et al. for a polyvinylidene fluoride (PVDF) bound $LiNi_{0.5}Mn_{1.5}O_4$ cathode from the Al current collector after storage in electrolyte at 60°C for three weeks and during cycling [75]. Volume changes in the electrode material, exacerbated by fast charging/discharging and temperature variation, induce stress which generates cracks and eventually delamination when the binders cannot hold the electrode fragments together [76]. The carbon additives in the cathode have been found to be electrochemically active towards PF_6^- intercalation which leads to structural changes in the cathode, with more severe effects observed at 45°C compared to 25°C [77]. Other mechanisms which cause structural instability, for example the interaction of electrolyte oxidation products and corrosion from hydrofluoric acid (HF), are mostly accelerated by higher temperatures.

In the extreme cases when the temperature rises beyond the safety threshold, thermal runaway may occur. Thermal runaway is a process whereby an exothermic reaction rate and the resulting temperature increase run into an uncontrolled positive feedback. The series of reactions during thermal runaway include SEI decomposition, anode/electrolyte and cathode/electrolyte reaction, electrolyte decomposition and reaction with the binder [78]. The breakdown of the SEI layer due to either overheating, overcharging or physical abuse is associated with exothermic decomposition of metastable components such as $(CH_2OCO_2Li)_2$, followed by further exothermic reactions between the anode and the electrolyte [79]. Common polymer separators melt at above 130°C, although some separators are designed to maintain structural integrity and prevent a short circuit. For example, trilayer polypropylene-polyethylene-polypropylene (PP-PE-PP) separators can be engineered to exhibit a shut-down process when temperature rises beyond a threshold. As the PE layer melts down, the separator becomes nonporous and is no longer ionically conductive, stopping the electrochemical function of the cell. At the same time, the PP layers maintain their mechanical properties due to their higher melting point, preventing separator shrinkage and a short circuit [80]. Alternatively, a method of inducing thermal shut-down by introducing an extra material layer between the cathode and the current collector has been proposed by Chen et al. [81] The material consisted of graphene-coated spiky nickel nanoparticles in a polymer matrix and exhibited high electrical conductivity at moderate temperatures. However, at high temperatures (70°C in the study, but tunable depending on the choice of polymer matrix and nickel-to-polymer ratio) its electrical conductivity dropped by seven to eight orders of magnitude within a second, effectively shutting down the cell and preventing thermal runaway. If thermal runaway is not successfully stopped before the separator meltdown occurs, the cell is internally short-circuited, and consequently the cathode breaks down. During thermal runaway, electrolyte decomposition at 250–350°C is severe with rapid release of gaseous species, building up the pressure of the cell and eventually venting flammable vapour into the environment [82].

3.2. Lithium plating

Lithium plating is a Faradaic side reaction in which Li^+ ions in the electrolyte form lithium metal on the surface of the negative electrode instead of intercalating into it [66]. This reaction mainly occurs during fast charging when the electrostatic potential of the negative electrode approaches or falls below that of a Li/Li^+ reference electrode. It is aggravated by factors that slow down the competing intercalation reaction, including low temperatures and insufficient negative electrode material into which to insert lithium.

3.2.1. Structure of lithium deposits

Initially, lithium metal forms in droplets so as to minimise the surface energy [83]. The surface of the droplets quickly reacts with the electrolyte to form SEI. As additional plating occurs on the droplets beneath the SEI, the droplets are subject to increasing

mechanical stress until the SEI is broken and the lithium escapes, in what is variously termed 'mossy' growth, 'root growth' [84] or 'base-controlled growth' [85]. In their X-ray imaging study of lithium deposition in symmetrical lithium metal cells with a 1 M LPF_6 in 1:1 EC/DMC electrolyte, Eastwood et al. [86] showed that the mossy structure may also contain higher atomic number elements in addition to metallic lithium, which were interpreted as lithium salts. New SEI forms on the mossy lithium, preventing the formation of uniform films as observed with less reactive metals such as copper. Continuous mossy growth reduces the electrolyte concentration to values far below equilibrium, decreasing the rate of mossy growth and instead promoting growth perpendicular to the surface, which is referred to as dendritic or 'tip growth' [84]. As the dendrite grows, mechanical stress in the dendrite will act to either break it, or in the worst-case scenario, compress it causing exponential growth. Jana and García [85] use the analogy of squeezing toothpaste out of a tube; in order to do so, there must be sufficient toothpaste in the tube to create the necessary pressure gradients.

3.2.2. Effects on battery performance

Dendritic growth is referred to as a worst-case scenario for good reason; if a dendrite goes all the way through the separator to reach the positive electrode, an internal short-circuit is formed, resulting in rapid heating of the cell [87]. In most cases, the resulting heat generation melts the dendrite immediately and breaks the short [88], but the temperature rise can trigger other degradation mechanisms such as SEI formation, electrolyte drying and dissolution of the positive electrode. While the risk of short-circuit alone is enough to render fast charging at low temperatures unsafe, even mossy growth causes capacity fade through loss of lithium inventory and power fade by reducing the porosity of the negative electrode and/or the amount of electrolyte in the cell. Often plated lithium forms at the electrode-separator interface and thus has the potential to form a blocking layer to the rest of the active material. Metallic lithium is also much more reactive than graphite, promoting further side reactions that result in SEI growth, gas generation and electrolyte decomposition [66].

3.2.3. Model based investigation of lithium plating

The first extension of the standard pseudo-two-dimensional (P2D) model of Fuller, Doyle and Newman [89] to include lithium plating and the inverse process, lithium stripping, was proposed by Arora, Doyle and White [18]. A second Butler-Volmer equation was proposed for the side reaction:

$$j_{n,sr} = \frac{i_{0,sr}}{F}\left[\exp\left(\frac{\alpha_{a,sr}F\eta_{sr}}{RT}\right) - \exp\left(-\frac{\alpha_{c,sr}F\eta_{sr}}{RT}\right)\right], \tag{4}$$

where $j_{n,sr}$ is the side reaction flux (positive for stripping, negative for plating), $i_{0,sr}$ is the side reaction exchange current density, F is Faraday's constant, R is the universal gas constant, T is absolute temperature, the side reaction overpotential η_{sr} is given by

$$\eta_{sr} = \phi_s - \phi_l - U_{sr} - Fj_{n,sr}\frac{\delta_{film}}{\kappa_{film}} \tag{5}$$

and ϕ_s and ϕ_l are the local electrostatic potentials in the solid and electrolyte phases respectively. If the potentials are defined with respect to a Li/Li^+ reference electrode, as in the standard Newman model [89], $U_{sr} = 0$ by definition. Arora, Doyle and White assumed the plating to be partially reversible, choosing values of $\alpha_{a,sr} = 0.3$ and $\alpha_{c,sr} = 0.7$ for the transfer coefficients accordingly. Their model assumed a uniform film, where the film thickness δ_{film} is an additional variable to be solved for:

$$\frac{\partial\delta_{film}}{\partial t} = -j_{n,sr}\frac{M_{film}}{\rho_{film}}. \tag{6}$$

The electrical conductivity κ_{film}, molar mass M_{film} and density ρ_{film} of the film can be either set to those of lithium or modified in order to account for fast side reactions: Arora, Doyle and White consider a film consisting of both lithium metal and lithium carbonate Li_2CO_3. The effect of local electrolyte concentration c on mossy film growth is accounted for by assuming $i_{0,sr}$ to take the form

$$i_{0,sr} = Fk_{sr}c^{\alpha_{c,sr}}, \tag{7}$$

where k_{sr} is a reaction rate constant. Inspection of (4) and (5) shows that plating occurs when the electrostatic potential of the electrolyte exceeds that of the electrode, explaining the potential dependence discussed previously. The above model is hitherto referred to as the Arora model for the sake of brevity.

Perkins et al. devised a control-oriented reduced-order model [90] based on the Arora model. The relative error on $j_{n,sr}$ is less then 10% compared to the full partial differential equation (PDE)-based model for charging rates up to 3C. More important for control purposes is the charge rate required to obtain plating at any given state of charge, for which the relative error is less than 5%. Hein and Latz [91] devised a three-dimensional microstructure-resolved model based on the Arora model. Notably, Hein and Latz also simulated chemical intercalation, a non-Faradaic process where plated lithium intercalates into graphite, assuming a constant flux for said chemical intercalation. Ge et al. [92] used the Arora model to include the effect of low temperatures, by assuming the solid state diffusion coefficients, electrolyte conductivity and reaction rate constants to have Arrhenius temperature dependence. They found that at $-25\,^{\circ}C$, plated lithium accounts for 2% of total charge by the end of a 1.5C charge. The model was also able to reproduce the experimental result that the plated lithium accounted for 1.55% of total charge on reaching 80% SOC, the first direct experimental comparison with a lithium plating model.

Yang et al. [93] added the porosity variation equation of Sikha, Popov and White [94] to the model:

$$\frac{\partial\varepsilon}{\partial t} = -a\frac{\partial\delta_{film}}{\partial t}, \tag{8}$$

where ε is the porosity or electrolyte volume fraction and a is the surface area to volume ratio. Integrating (8) with respect to time and assuming the initial film thickness to be zero yields

$$\varepsilon = \varepsilon_0 - a\delta_{film}, \tag{9}$$

where ε_0 is the initial value of the porosity. Like Arora, Doyle and White, Yang et al. assumed the film to contain SEI as well as lithium metal, but used a separate cathodic Tafel equation for SEI formation. A lumped thermal model was also included. They found that, after around 3000 cycles at room temperature, SEI growth causes enough pore clogging to raise the electrolyte potential above that of the graphite and thus cause plating, at cycling rates as low as C/3. This plating reduces the porosity further, causing positive feedback and nonlinear reduction in useable capacity. However, they did not confirm the presence of plating with a cell teardown.

The same team [95] later devised a modified version of (4) where the stripping rate depends on the concentration c_{Li} of plated lithium:

$$j_{n,sr} = \frac{i_{0,sr}}{F}\left[\frac{c_{Li}}{c^*_{Li}}\exp\left(\frac{\alpha_{a,sr}F\eta_{sr}}{RT}\right) - \frac{c}{c^*}\exp\left(-\frac{\alpha_{c,sr}F\eta_{sr}}{RT}\right)\right], \quad (10)$$

where $i_{0,sr}$ is redefined in terms the reference concentrations c^*_{Li} and c^*:

$$i_{0,sr} = Fk_{sr}\left(c^*_{Li}\right)^{\alpha_{a,sr}}\left(c^*\right)^{\alpha_{c,sr}}. \quad (11)$$

In that paper [95], the film is assumed to consist of only plated lithium with no SEI, resulting in a simple relationship between c_{Li} and δ_{film} in terms of the density ρ_{Li} and molar mass M_{Li} of pure lithium:

$$c_{Li} = a\delta_{film}\frac{\rho_{Li}}{M_{Li}}. \quad (12)$$

In a first attempt to model irreversible capacity loss due to plating, Ren et al. [96] use a modified form of (4) that considers both the reversible lithium, which can be stripped, and irreversible or 'dead' lithium that is electrically isolated and therefore cannot be stripped.

3.2.4. Detection

Non-destructive diagnosis of lithium plating is of great significance for onboard application as well as periodic inspection. Characterisation techniques that can be used to observe the morphology and distribution of lithium plating include optical microscopy [97–100], scanning electron microscopy (SEM) [101–103], transmission electron microscopy (TEM) [104–106], NMR spectroscopy [107–109] and X-ray diffraction (XRD) [20,110]. However, these methods generally require the cell to be disassembled or manufactured with a special structure. The commonly used non-destructive methods to detect lithium plating take advantage of observable external characteristics, including aging rates, voltage plateaus exhibited during lithium stripping, model-based prediction and others.

Lithium deposits gradually accumulate at the microscale during cycling. The side reaction between the plated lithium and the electrolyte forms new SEI, resulting in capacity fade and the rise of the impedance. Trends in these aging behaviours can be used to identify lithium plating. Available methods include the Arrhenius plot [20,111], resistance-capacity plot [111], impedance spectroscopy [112] and coulombic efficiency analysis [113].

The relationship between the aging rate r and the temperature T can be described by the Arrhenius equation, the parameters of which are acquired from cycling tests under different temperatures [20]. An example is shown in Fig. 6a. The aging rates increase at low temperatures (<0°C) due to the increased likelihood of lithium plating, whereas aging due to SEI growth accelerates with increasing temperatures. The resistance-capacity plot [111] reveals that lithium plating primarily influences the rate of capacity fade and has a lesser effect on the rate of impedance rise due to the higher conductivity of lithium metal compared to SEI [111]. Two aging modes can therefore be distinguished: one dominated by lithium plating, with a lower rate of impedance rise but high rate of capacity fade ("Aging mode 2″ in Fig. 6b), and the other dominated by SEI growth, with a higher rate of impedance rise and less prominent capacity fade ("Aging mode 1").

Impedance spectroscopy can also reflect lithium plating. Nonlinear frequency response analysis (NFRA) provides a new potential detection criterion in the form of the correlation between two harmonics as described in Ref. [112]. The authors showed that the analysis of higher harmonic responses by NFRA captured changes in the impedance response with aging that could not be observed by only analysing the first harmonic as measured with electrochemical impedance spectroscopy (EIS). The evolution of the second and third harmonics (Y_2 and Y_3 respectively in Fig. 6c) was observed for cells aged at -10°C and 25°C. The ratio between their values was proposed as an indicator of lithium plating, with the third harmonic increasing significantly more sharply than the second with cycling at -10°C but not at 25°C. This observation was attributed to the high sensitivity of the third harmonic to the increasing charge transfer resistance between the anode and the electrolyte caused by the lithium plated on the surface of the anode.

High precision coulometry can be used to detect lithium plating based on variations in coulombic efficiency. A slight drop of coulombic efficiency as shown in Fig. 6d indicates the consumption of active lithium as a result of the plating reaction. Burns et al. [113] measured the coulombic efficiency with a high precision charger, revealing that lithium deposited slightly at a charging rate of C/2 at 12°C.

Parts of the plated lithium can re-intercalate into the anode or become stripped during a discharge. These processes can give rise to voltage plateaus during the relaxation or discharging periods immediately after charging as shown in Fig. 7. The occurrence of these plateaus can be explained by the changes in total overpotential during the rest or discharge period after charge due to the re-intercalation and stripping of lithium as shown in Fig. 7a. The depressions in the differential voltage and incremental capacity curves in Fig. 7b and c indicate lithium plating had occurred. However, care must be taken to distinguish depressions resulting from lithium stripping from those resulting from phase changes in the electrode materials [114]. Furthermore, Campbell et al. [114] have shown that the absence of a plateau does not prove that lithium plating has not occurred. Self-heating and concentration equilibration phenomena immediately after a fast charge may also influence the shape of the voltage curve [114]. Differential voltage analysis (DVA) [96,114–116] and incremental capacity analysis (ICA) [114,117–119] are useful techniques to identify the occurrence of voltage plateaus. However, these methods require using slow discharge rates to capture the necessary detail; high currents lead to higher overpotentials which become dominant over the features of interest in the voltage curve [114]. Abnormal exothermic peaks may also be observed during the lithium plating and stripping process [110], acting as another indicator of deposition.

Increases in the cell thickness may provide an alternative indicator of lithium plating, but the mechanisms require further study [120,121]. Finally, electrochemical models can be used to predict the occurrence of plating depending on the charging conditions as discussed earlier. However, these complex and computationally intensive models would require simplification to be used for online detection.

Few methods for *in-situ* diagnosis and quantification of lithium plating after abnormal charging have been proposed to date. We believe the detection approaches that rely on the abnormal voltage plateaus are the most promising to be used onboard. However, there is still a significant knowledge and technological gap before these methods can be reliably applied in devices.

3.3. Mechanical effects

Mechanical pulverisation is another important aspect of fast charging induced degradation, and widely observed for various electrode materials including graphite [122–124], lithium nickel manganese cobalt oxide (NMC) [125–127], LCO [128–130], LMO [131], NCA [132], Si [133,134] and others.

Here we summarised mechanical degradation based on scale: cracks within the electrode particles [125–127,129,130,135], isolation of electrode particles, conductive material and binders [136], separation between active material and current collector,

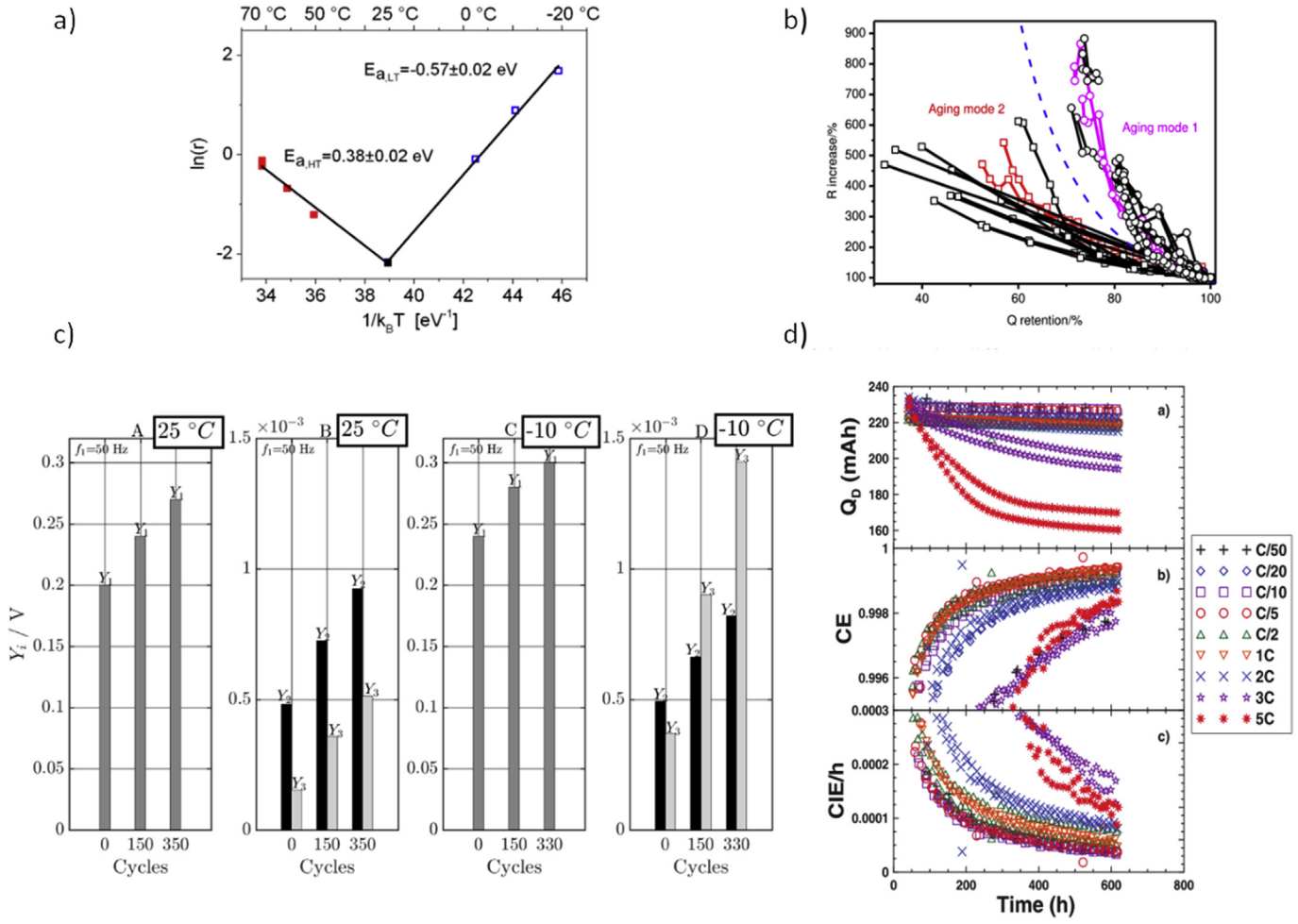

Fig. 6. Lithium plating detection methods based on aging behaviours. a) Arrhenius plot [20], b) Resistance-capacity plot [111], c) Nonlinear frequency response analysis (NFRA) [112], d) Coulombic efficiency [113].

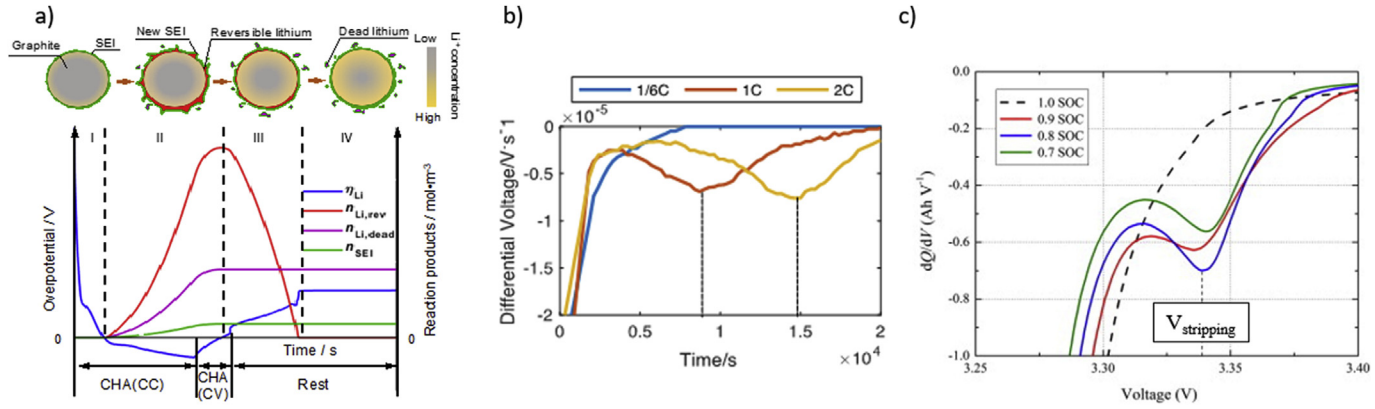

Fig. 7. Detection of lithium plating based on the lithium stripping process. a) Simulated evolution of overpotentials during a CC-CV charge and subsequent rest period, explaining the occurrence of the lithium stripping voltage plateau. In Stage I, no lithium is plated on the particle; during Stage II, lithium plating occurs; during Stage III (the start of the rest period), the reversible part of lithium reintercalates into the anode or is stripped, while the remaining lithium becomes electrically isolated from the anode ('dead lithium'); in Stage IV, steady state is achieved, with the dead lithium no longer being available for cycling [96]. b) Differential Voltage Analysis (DVA). The curves show the differential voltage of Li-ion cells during a rest period after charging at 1/6C, 1C, and 2C at -5°C. The peaks seen in the 1C and 2C curves correspond to voltage plateaus and may indicate lithium stripping [96]. c) Incremental Capacity Analysis (ICA) showing the incremental capacity of cells during a C/20 discharge after being charged at 1C to 0.7, 0.8, 0.9 and 1.0 SOC at -20°C. Again, peaks correspond to voltage plateaus [118].

delamination between electrode sheets. The main reason for these phenomena is the strain mismatch resulted from the lithium concentration gradient [125,128,136], which is aggravated by fast charging. During fast charging, Li^+ ions intercalate into the anode

and deintercalate from the cathode rapidly, leading to a severe lithium concentration gradient, strain mismatch between different parts of the electrode particle and stress development. Cracks propagate in particles when the energy release rate or stress intensity factor exceeds a certain value [128,129]. This is always accompanied by SEI/CEI cracks. Furthermore, the lattice strain along different directions varies for almost all kinds of electrode materials [131]. Primary particles are randomly oriented [125], in direct contact with adjacent primary particles. As a result, fast charging induced strain between nearby primary particles cannot be concordantly accommodated, which may cause isolation between electrode particles or conductive material and binders. The strain mismatch between electrode materials and current collector can also lead to cracks [137] or detachment [138]. Since higher C-rates induce more severe current inhomogeneity across electrode sheets, delamination may occur for cells without tight external constraints [139].

The effects of mechanical disintegration on cell performance can be divided into loss of active material (LAM), loss of lithium inventory (LLI) and impedance growth. Firstly, cracks lead to poor electrical conductivity and even total detachment [125]. Secondly, more fresh surface is uncovered by the cracks and reacts with the electrolyte [126,130,140]. Such side reactions are facilitated by the high temperature induced by fast charging [131]. The process results in further growth of the SEI layer which increases the resistance and causes both LAM and LLI. Finally, consumption of the electrolyte may also reduce the wettability of electrodes and hinder ion transport [126]. The following positive feedback mechanism has been proposed [126]: higher rates result in increased microcrack formation; cracks then aggravate the difference between electron and ion transport as the ions are able to diffuse through the electrolyte infiltrated into the cracks while electrons cannot, leading to severe SOC inhomogeneity and further cracking.

Many studies on the mechanical effects of fast charging have discussed size dependence. Smaller particles are more resilient to cracks because of lower lithium gradients [140] and energy release rates [141]. However, small particles have higher specific surface areas, leading to more SEI and impedance growth. Moreover, small particles result in a lower energy density due to their lower packing density [126,135,140]. Thus, primary particles are sometimes packed into secondary particles. However, the mechanical strength of secondary particles is much lower than the intrinsic material strength of primary particles due to the weak Van der Waals interactions [127]. Another way to increase energy density is to fabricate larger primary particles [135,140]. Researchers have attempted to explore the critical size. Model-based shock maps for LCO [129] and LMO [128,131] have been proposed, showing that for relatively low C-rates and small particle size zones fracture is not expected. Similar results have also been obtained experimentally for Si nano-pillars [142] and Si nano-particles [141]. For a very small diameter of Si nano-pillars [142] (140 nm), cracks are avoided at any C-rate; while for large diameters (290 nm, 360 nm), fracture occurs at most C-rates. Models based on fracture mechanics in terms of stress intensity factor [128] or energy release rate [129] give some guidance for particle design. However, most of such models are not validated and their implementation into real electrodes may be difficult since many parameters, including the fracture strength factor or initial crack length, are difficult to obtain. The real boundary conditions are also more complicated compared to the free-standing conditions in these models.

Whether higher C-rates certainly cause more cracks for secondary particles is still subject to debate. For NMC333 in Ref. [125], operation at 1C did not lead to more cracks than 0.1C. This is consistent with the results for NMC532 under 0.5C and 2C [127]. However, for NMC622 operated at 1–10C cracks increased with C-rates, which is similar for NMC532 in Ref. [135] and NCA in Ref. [143]. This may be due to the so-called skin effect [127]. The hoop stress at first increases with current rate, then drops after a maximum according to simulations. Most Li^+ ions may aggregate at the particle surface while the lithium in other regions remains dispersed even when too high C-rates are applied. Therefore, hoop stress drops quickly within a thin region near the surface, and the stress intensity factor will not be large.

Mechanical constraints can be used to design fast charging protocols [144,145]. Lu et al. designed an exponential charge current protocol using the hoop stress on the particle surface as a constraint [144]. This protocol can theoretically shorten the charge time, with little loss of cycle life. However, no other degradation effects are considered in the model and no experimental validation of capacity retention has been carried out. Spingler et al. proposed a stepwise charging protocol based on constraining the maximum local irreversible swelling of the cell and temperature rise [145]. Experiments proved that the method could shorten charge time and prolong cycle life compared to a 1C constant current - constant voltage (CC-CV) protocol.

Overall, much remains to be studied regarding mechanical degradation in Li-ion batteries under fast charging conditions. Experimental studies on the subject have reached different conclusions, and there is still disagreement regarding important issues such as the dependence of the rate of crack formation on the charging C-rate. Mechanical degradation is often difficult to decouple from other aging mechanisms, although a recent study has proposed a method to identify the effects caused by cracking using ICA, finding it to be the dominant degradation mechanism in single layer NMC532/gaphite cells charged at 9C [146]. Compared to degradation mechanisms such as SEI layer growth or lithium plating, relatively few modelling studies on mechanical effects under high currents have been published, and even fewer have been validated. The difficulty of obtaining the required parameters and formulating realistic boundary conditions remains a major hindrance to developing reliable models.

4. Multi-scale design for fast charging

The extent and mode of fast charging induced degradation can be affected by the battery material components (inherent properties of the electrodes and electrolyte), operational conditions (high rate of charge/discharge, extreme voltages and temperatures), battery manufacturing processes and pack design [147]. Multi-scale design and hybrid approaches present significant opportunities towards developing high performance fast charging batteries.

4.1. Electrode materials

The selection of suitable electrolyte and electrode chemistries with high capacities that can also be operated at a high rate is one of the most challenging issues in cell design. Extensive research has been carried out to develop fast charging anode materials which can prevent the formation of lithium dendrites. Some well-known anode materials, such as the carbon-based alternatives (graphite, carbon nanotubes, graphene or graphene oxides), metal based composites (TiO_2, lithium titanium oxide (LTO), MnO, Co_3O_4, Fe_3O_4, NiO) and alloy composites (such as Si and Sn based compounds), have been investigated with some success.

Conventional graphite anodes are characterised by potentials very close to the potential of Li/Li^+ formation, making them desirable for maximising cell energy density but also particularly susceptible to lithium plating. Modifying anode materials has therefore been one of the most fruitful approaches toward improving the fast charging capability of Li-ion cells. For example,

surface engineered graphite with only 1 wt% Al_2O_3 coating exhibits a reversible capacity of about 337.1 mAh g^{-1} at a high rate of 4000 mA g^{1} [148]. In another instance, LTO materials are desirable for batteries capable of extreme fast charging with long lifetimes due to the fact that they do not exhibit lithium plating or SEI layer formation, but they are seriously limited by their high operating potentials, leading to decreased full cell voltage and limited energy density [149]. The modification of LTO mainly aims to increase its electronic conductivity, lithium-diffusion coefficient or to maximise the active powder content per unit volume by in situ introducing carbon sources [150], carbon coating [151], and metal/nonmetal ion doping [152,153].

Alternatively, some metal oxide and alloy based materials have been proposed for high power Li-ion battery applications. However, these materials are often limited by their fast charge useable capacity and cycling stability because of their severe volume change, pulverisation and agglomeration of primary particles, and their poor electronic conductivities. 2D-structured graphenes have shown great advantages [154] such as a high intrinsic carrier mobility, excellent thermal and electrical conductivity, high theoretical specific surface area, and superior mechanical strength. They can potentially be applied as anode materials by N-doping [155,156] (achieving high reversible capacity of over 1040 mAh g^{1} at 50 mA g^{1}) or integrating with large volume change anode materials such as Si and Sn. For example, Agyeman et al. [157]. reported a carbon coated Si/rGO composite anode with a sandwich structure, which simultaneously achieved a high capacity and a stable cycle life (about 93% capacity retention over 400 cycles).

Other graphene-like 2D materials have been extensively explored as promising anode materials due to their high surface-to-mass ratio and unique physical and chemical properties, leading to shortened Li^{+} diffusion pathways, fast electron transport and increased number of sites for ion storage. Such 2D anode materials mainly include transition metal oxides (TMOs, such as Co_3O_4, NiO, Fe_3O_4, and MnO_2), transition metal dichalcogenides (TMDs, such as MoS_2, WS_2, $MoSe_2$, and WSe_2, FeS, FeS_2, and CoS_2) and the transition metal carbides/nitrides (mainly highly conductive MXenes, such as $Ti_3C_2T_x$, Ti_2CT_x, $Mo_2Ti_2C_2T_x$, $Cr_2TiC_xT_x$, $Nb_4C_3T_x$ and V_2CT_x). Among the TMOs, titanium and niobium based oxides are proposed as promising anode candidates with beneficial redox potentials ranging from 1.0 to 1.6 V, in good match with commercial electrolytes [158–160]. Recently, Goodenough's group proposed the high rate $TiNb_2O_7$ anode with a theoretical capacity comparable to graphite which can achieve rapid Li^{+} intercalation/deintercalation and longer cycle life, demonstrating potential to replace LTO [161].

Electrode structure designs in the nano-scale have also been demonstrated to achieve increased energy and power densities. 2D structures with hollow, core-shell, and yolk-core designs, e.g. 2D holey $ZnMn_2O_4$ nanosheets [162] showed a capacity of 770 mAh g^{-1} at 200 mA g^{-1} and 430 mAh g^{-1} at 1200 mA g^{-1}, while the control spinel $ZnMn_2O_4$ only achieved 32% and 6% of these values respectively. Integration of 2D materials into 3D macroscopic structures, such as porous films, scaffolds, and networks, can enhance both ionic and electronic transport in electrode materials. The 3D hierarchical structures, e.g. MoS_2 with column-like structures [163] have been shown to achieve a high reversible specific capacity of 840 mAh g^{1} at 200 mA g^{1}, cyclic stability up to 500 cycles, and outstanding rate performance. The electrically conductive and electro-active MXenes have been attracting increasing attention since their discovery in 2011 [164]. Strategies were successfully proposed to achieve 3D hierarchical structures, including fabricating 2D MXene flakes into hollow spheres and 3D architectures [165] to prepare free-standing, flexible, and highly conductive 3D macroporous MXene based films and thick vertically aligned MXenes with high rate charging/discharging capabilities [166].

Metallic lithium is one of the most favoured anode material choices for increasing energy density [167] but suffers from low power density due to the low surface area of a pure lithium foil. However, incorporating Li metal into 3D structural matrices can be beneficial to rate capability by enabling faster Li-ion diffusion. For example, a composite material prepared by lithium melt infusion into an electrospun 3D porous carbon matrix showed stable cycling with a small Li plating/stripping overpotential (below 90 mV) [168].

Approaches to enhance the fast charging performance are not limited to anode material selection, modification and nanoscale structure design. Electrolyte and interfaces are also critical elements that affect the performance of anodes [169]. Available approaches towards optimising the anode/electrolyte interface include amorphous carbon coatings for graphite [170,171] that result in more homogeneous SEI layer formation with suppression of unwanted active points on graphite where lithium deposition is more likely [171], metal coating and doping, especially with Cu and Sn on the anode [172], and smart choice of Li salt and co-solvents [38]. Qian et al. [173] reported a high rate and non-dendritic lithium metal anode by using highly concentrated electrolytes. Their Cu/Li cell was cycled at 4 mA cm^{-2} for 41,000 cycles with a high Coulombic efficiency of 98.4% in the 4 M LiFSI-DME electrolyte. Also beyond nano structured materials, Griffith et al. reported $Nb_{16}W_5O_{55}$ and $Nb_{18}W_{16}O_{93}$ anode materials which achieved excellent high-rate performance without nanoscaling [174], delivering a potential low cost way to produce fast charging electrode materials. Research effort has also been dedicated to electrode microstructure optimisation to enable faster diffusion, improving the rate capability. Billaud et al. [175] reported architectured graphite electrodes composed of graphite flakes aligned perpendicularly to the current collector using a low magnetic field that achieved three times higher specific charge compared to similarly loaded conventional graphite anodes when cycled at up to 2C. Low magnetic field was also used by Sander et al. [176] to fabricate LCO electrodes with directional pore arrays that were capable of maintaining significantly higher areal capacities compared to regular LCO electrodes at high C-rates. Also in conventional carbon/graphite anodes, crystal structure has a strong influence on the diffusion of lithium. Fang et al. [177] investigated the electrochemical performance of mesophase soft carbon (MSC), mesophase graphite (SMG) and hard carbon (HC) anodes, finding that MSC exhibited the highest specific capacity at high C-rates, likely due to more extensive interlayer spacing. The more crystalline SMG was characterised by markedly lower capacity than the other two materials at high C-rates, which was contributed to narrower interlayer spacing that obstructed diffusion.

Material selection and modification is undoubtedly a promising direction for future research. Many materials or material architectures have shown improved fast charging characteristics compared to the materials commonly used today. However, it is important to stress that early material development and large scale commercialisation are usually separated by a relatively long period of time. In many cases, new manufacturing techniques and facilities need to be developed to enable the production of a novel material at the required scale. Furthermore, any such material needs to be cost-competitive compared to the ones currently in use, which may be a significant hindrance particularly for alternative anode materials. The performance of many materials or structuring approaches discussed here has only been assessed on a laboratory scale, which may not always translate to similar improvements when integrated into commercial cells and packs. While material science will play an important role in the development of future batteries, other engineering efforts are certainly needed to address the issue of fast charging capability in the near term.

4.2. Cell and pack design

Apart from the choice of materials and their microstructure, the choice of electrode geometrical parameters is also an important design aspect. Increasing the porosity [178] and the width of the anode [179] can help suppress lithium plating but may also cause capacity loss. The negative-to-positive electrode (N/P) capacity ratio can significantly influence lithium deposition [18], with values greater than 1 used in commercial cells for that reason. Additionally, while graphite cracking is not expected during lithiation [26], the higher N/P ratio may also help reduce mechanical stresses on the anode, which would reduce additional SEI formation and associated LLI [180]. The N/P ratio has been shown to decrease in NMC811/graphite cells charged at high C-rates due to the areal capacity of graphite reducing more sharply with the charging rate compared to the areal capacity of the NMC811 electrode [22]. The effect was found to be significant, with the N/P ratio falling from 1.15 at 0.1C to 1.0 at 3C and reaching 0.5 at 4C. Kim et al. [181] investigated 0.85C charging of 1.40 Ah pouch cells with different N/P capacity ratios at 25°C and found that having 20% more capacity in the negative electrode than in the positive electrode was the best compromise between maximising capacity and preventing plating. For faster charging rates and lower temperatures, this may have to be increased. The optimal ratio may also depend on other factors such as the electrode materials or cell form factor. Historically, the anode has often been designed to be slightly larger than the cathode in order to prevent lithium plating [182]. The additional area is known as the anode overhang and was long assumed to be a passive part, essentially not participating in the lithiation or delithiation of the anode [183]. However, the tendency of lithium plating to develop in the anode areas adjacent to the overhang has recently prompted more thorough research into the processes taking place. It was found that during rest times, the lithium from the main anode area tends to diffuse into the overhang due to the concentration gradient [184]. During the following discharge, the edge area of the cathode receives more lithium as an effect. Then, during the subsequent charge, the extra lithium is transferred to the area of the anode directly opposite the cathode edge and adjacent to the overhang. This causes a higher local concentration of lithium with lower local anode potential, increasing the probability of lithium plating [184]. The anode overhang should therefore be minimised in order to avoid deposition.

Cell geometrical design is another factor that can significantly affect the fast charging capability of Li-ion batteries. Cell shape and form factor influence the distribution of temperature and current, with large form factor cells being particularly prone to developing inhomogeneities [185]. Tab position within the cell, tab materials, structures, and welding methods are very important to homogenise the current distribution and limit localised heating and degradation as described in Section 3.1 [185,186]. Erhard et al. [187] simulated and measured current density distributions in large form factor single layer NMC/graphite pouch cells by placing multiple tabs at different locations along the electrodes. Current was always applied to the same pair of reference tabs, located at one side of the cell. Although the temperature differences along the cell length were negligible due to the single layer design, significant differences in local current densities were reported, highlighting the importance of tab placement. Locating the tabs at opposite sides of the cell and increasing the number of tabs [188] can reduce current and temperature gradients.

The links between pack-level performance and cell-level characteristics are still not well understood [34]. While modelling of degradation induced by fast charging at cell level is relatively developed, few studies have so far attempted to extend similar approaches to pack design, largely due to the added complexity and multitude of design and operating parameters that need to be considered. Tanim et al. [34] demonstrated that Nissan LEAF battery packs charged at 2C experienced significantly higher rates of capacity fade compared to individual cells charged at the same C-rate. Liu et al. [189] recently investigated the effects of cell-to-cell variations on pack performance using a thermally coupled single particle (SP) model, showing that significant current imbalances existed between cells. These imbalances had the effect of reducing the overall accessible energy as well as increasing the degradation rate. Interestingly, placing higher resistance cells near the load points reduced the imbalance. Meintz et al. [190] reviewed the implications of fast (over 400 kW) charging on vehicle system design, concluding that there was a number of problems with EV electrical architecture and vehicle components that would need to be addressed before higher charging powers can be safely implemented. Many challenges remain for successful design of fast charging battery packs, including: 1) fast charging packs require high performance cells with low cell-to-cell variability, new materials and advanced manufacturing; 2) more advanced BMSs with additional sensing and control circuits are required for monitoring and balancing purposes; 3) advanced thermal management systems are needed to maintain safe temperatures and reduce thermal gradients within the cells and packs.

5. Fast charging strategies

While many of the material level solutions discussed in Section 4.1 do indeed show promising results, most are not expected to reach the market on a wider scale in the near future. Many researchers have therefore turned towards cell and pack level approaches which can often be implemented in real world systems in a significantly shorter time. Charging strategies, which determine how the current density is varied during the charging process, are an important category of such solutions.

5.1. Types of charging protocols

Standard protocols. Numerous charging protocols have been proposed for Li-ion batteries. CC-CV is by far the most common one. It consists of a constant current charging phase where the battery voltage increases up to a cut-off value (CC phase), followed by a constant voltage hold until the current falls to near-zero (CV phase). The CV phase allows for the concentration gradients within the electrode particles to disperse and is usually necessary to obtain high capacity utilisation without exceeding the maximum voltage. However, since the current gradually decreases during the CV phase, the charging time is significantly increased compared to CC-only charging. The simplicity and ease of implementation of CC-CV has made it the standard charging protocol in most applications. However, many other protocols have been shown to achieve reduced charging times, increased efficiencies and/or improved capacity or power retention. Fig. 8 illustrates some of the alternative protocols proposed for fast charging.

Zhang et al. [192] studied the effects of the CC-CV charging protocol on the reversible capacity and anode potential evolution in experimental LCO/graphite cells with embedded reference electrodes as they were charged at ambient temperatures from -20°C to 10°C with C-rates between 0.16C and 1.2C. The results showed a positive correlation between increasing charging current in the CC phase and increasing time taken by the CV phase to complete. The authors observed that increasing the current beyond a certain value did not bring any further reduction in overall charging time due to this correlation. Both increasing the charging current and decreasing the ambient temperature was shown to result in a reduction in anode potential, with all test schemes causing the

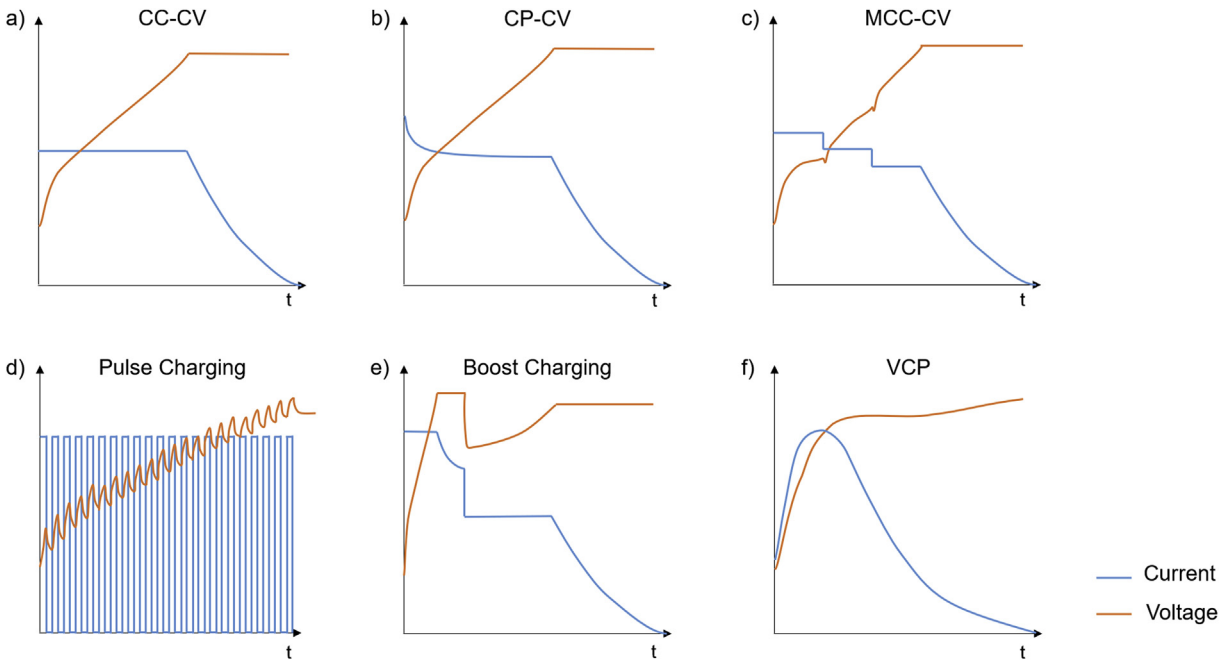

Fig. 8. Schematic representation of common types of charging protocols proposed for fast charging. a) Constant Current - Constant Voltage (CC-CV), b) Constant Power - Constant Voltage (CP-CV), c) Multistage Constant Current - Constant Voltage (MCC-CV), d) Pulse charging, e) Boostcharging with a CC-CV-CC-CV scheme, f) Variable Current Profile (VCP, based on Ref. [191]).

anode potential to become negative versus Li/Li^+ at some point during charging. Negative anode potential was assumed to inevitably cause lithium plating, which was suggested as the main reason for the reduction in charged capacity at high currents and low temperatures. However, the occurrence of plating was not confirmed through other methods. Ouyang et al. [193] demonstrated that the shape of the voltage profile of large format LFP cells changed significantly with the number of cycles at 0.5C CC-CV at -10°C, resulting in an elevated average voltage in the CC stage and longer duration of the CV stage. In comparison, the voltage profile of cells charged at 0.2 and 0.3C at the same temperature retained a similar shape. The increased average voltage as a result of repeated cycling at higher C-rates may contribute to increased degradation rate.

Multistage constant current (MCC) protocols. Many researchers have proposed that adjusting the current levels during the charging process may limit cell degradation while reducing the charging time. Such approaches are often motivated by reducing heat generation, avoiding conditions that enable lithium plating or reducing mechanical stresses when the diffusion of Li^+ ions is constrained. MCC protocols are one of the earliest types designed specifically for fast charging. Such protocols consist of two or more constant current stages, often followed by a CV stage. Higher current levels are usually chosen for the earlier CC stages since the anode potential is less likely to become negative in the beginning of the charging process. Nevertheless, some authors have used the opposite approach with current levels increasing in later CC stages due to the lower cell resistance. Zhang [194] observed faster capacity loss in cells charged with the latter MCC-CV approach compared to CC-CV and constant power - constant voltage CP-CV protocols with the same average C-rate of 1C. The study concluded that CP-CV resulted in best capacity retention when the cell was fast charged (1C), while CC-CV was less damaging for cells charged at 0.5C. Another work [195] reported an 83% capacity retention after 4200 cycles in an LFP cell charged with a 25-min MCC-CV protocol with two CC stages of decreasing current. Waldmann et al. [19] studied the anode potential evolution in reconstructed commercial NCA/graphite cells. Three MCC charging protocols were then tested in fresh cells of the same type. Current level was decreased just before reaching a voltage at which negative anode potential was observed in the reconstructed cells. All three protocols were faster than 0.25C CC-CV protocol and led to a comparable rate of capacity fade. However, this protocol design method is both time consuming and expensive as it requires reconstructing the cell with a reference electrode and measuring the anode potential in the range of temperatures and currents of interest in the practical application. Spingler et al. [145] postulated that lithium deposition leads to local volume changes which can be directly measured in pouch cells *in operando* using laser triangulation, removing the need to measure the anode potential. Based on this assumption, they designed an MCC protocol with multiple stages in which current level was decreased every time the maximum local expansion reached a predetermined value. Cells cycled with this protocol experienced dramatically improved capacity retention compared to a CC-CV protocol with the same average current. However, the method still requires extensive experimentation and is limited in application to pouch cells.

Pulse charging protocols. Pulse charging protocols, where the charging current is periodically interrupted by short rest periods or discharge pulses, are also common in literature. The strategy aims to reduce concentration polarisation, reducing the risk of local anode potential becoming negative or reducing mechanical stresses due to uneven insertion and extraction of lithium in the solid particles. Aryanfar et al. [196] used a Monte Carlo simulation of lithium dendrite growth to show that pulse charging can also potentially inhibit dendrite propagation. One of the early studies [197] reported that a 1C pulse charging protocol could reduce the charging time from 3.5 h for a 1C CC-CV protocol to approximately 1 h due to the absence of the CV stage that accounted for most of the total charging time in CC-CV. Higher discharge capacities were observed for the pulse protocol relative to CC-CV which was attributed to better active material utilisation. However, since the

capacities of the cells were not determined in a standard characterisation test at the beginning of life and the rate of capacity fade did not vary substantially, the discrepancy in capacities could be caused by manufacturing differences. The same study [197] compared SEM images of both electrodes after 300 cycles, finding cracks in the cathode particles of all cells but significantly less SEI formation on the anodes of the pulse charged cells. Abdel-Monem et al. [198] monitored capacity fade and impedance changes in LFP cells cycled with eight different fast charging protocols, all belonging to CC-CV, MCC or pulse charging categories. They observed comparable rates of capacity fade until the 700th cycle, when the capacity of the cell charged by CC-CV started deteriorating considerably faster. The rate of capacity fade between pulse charging and MCC remained similar, however a higher rate of impedance rise was observed for the MCC protocol than for pulse charging. The discrepancy in the rates of capacity fade and impedance rise was interpreted as a manifestation of different aging mechanisms occurring for each protocol. Chen et al. [199] proposed a sinusoidal-ripple-current (SRC) charging strategy using the minimum impedance frequency signal to minimise heat generation. Experiments revealed that the SRC strategy could offer signficant improvements in charging time, efficiency, temperature rise and lifetime compared to 1C CC-CV, and slight improvements compared to a square pulse charge with the same parameters. The method was only validated with one type of cell at a relatively high starting temperature of 28.5°C, and it is unclear if the ambient temperature was controlled in any way during the tests. Amanor-Boadu et al. [200] used the Taguchi orthogonal arrays method to optimise the pulse charging parameters to maximise charging efficiency, again finding the minimum AC impedance frequency to be optimal for charging. Significantly shorter charging times and higher efficiencies were reported for the pulse charging protocol compared to CC-CV with the same average current in the CC phase at 23°C, however the temperature rise was higher and the effects on cycle life were not studied. Yin et al. [201] designed a module charger that performed pulse parameter optimisation on-line to limit battery polarisation. The authors implemented the charger on four cells connected in series, showing that the charge time could be reduced compared to 2C CC-CV, although the resulting temperature rise was slightly higher. No cycle life experiments were performed, while the complexity of implementation was acknowledged by the authors. As mentioned in Section 3.1, pulse loads may lead to increased and uneven heat generation in packs connected in parallel due to the rebalancing events between pulses [62]. The implications of these effects have not been extensively studied in the context of charging protocol optimisation.

Boostcharging. Boostcharging is characterised by high average current in the beginning of charge, followed by a CC-CV part with more moderate currents. The first, boostcharge stage could simply comprise a CC profile (making the protocol identical to MCC-CV), a CV profile where the cell is immediately brought to a set maximum voltage by means of high initial current (CV-CC-CV), or an entire CC-CV profile (CC-CV-CC-CV) [202]. The boostcharge stage should, in any case, allow higher currents or higher maximum voltage compared to the following CC-CV part in order to reduce the overall charging time. Notten et al. [202] tested a few variations of the boostcharge protocol on both cylindrical and prismatic LCO cells with a 5 min boostcharge period. Compared to a 1C CC-CV protocol, the charging time was reduced by about 30–40% with no noticeable acceleration in capacity fade for cylindrical cells. For prismatic cells, a smaller reduction in charging time was reported along with slightly higher rates of capacity fade. Interestingly, some of the boostcharging protocols seemed to achieve marginally better capacity utilisation at the beginning of life compared to the slower 1C CC-CV. It is, however, unclear whether this could be due to manufacturing differences as cell capacities were not measured by a standardised test at the beginning of life. Keil and Jossen [203] arrived at contradicting conclusions after experimentally comparing cycling data from three types of 18650 cells of different chemistries charged by CC-CV, boostcharging and pulse charging protocols. An increased rate of capacity fade was reported for boostcharging compared to CC-CV with a similar charging time, while no significant differences in capacity fade rates were observed for pulse charging. The authors concluded CC-CV was suitable for fast charging high power cells, however mentioning that MCC could be useful in conditions when lithium plating is likely to occur.

Variable current profiles. A number of more complex variable current profiles have also been proposed for fast charging. Sikha et al. [204] investigated a Varying Current Decay VCD) protocol, designed to charge faster than a conventional CC-CV protocol while being less damaging than pure CV charging. The proposed protocol achieved improved capacity utilisation in the early cycles, but still resulted in a significantly higher rate of capacity fade compared to CC-CV with a similar average current. Possible overcharge of the cathode was suggested as the reason for accelerated degradation. Building on a similar idea, the Universal Voltage Protocol (UVP) [191] was designed to reduce both charging time and energy losses due to heating, thus improving charging efficiency. The UVP is derived from a set of CC-CV charging curves using an optimisation algorithm for a specified charging time and target terminal voltage. A variable current profile is then calculated from the UVP and cell resistance. As the cell ages, the current profile needs to be recalculated due to changes in resistance while the voltage profile remains the same as for a fresh cell. Irrespective of the cell age, the current is always very low and rapidly increasing in the beginning of charge due to the cell resistance being highest at 0% SOC and then rapidly dropping. Maximum current is reached at relatively low SOCs, and subsequently it is gradually reduced due to the mass transport of Li becoming more constrained in increasingly lithiated graphite particles. The study demonstrated that a very high charging efficiency could be maintained even for highly aged cells. The capacity of the tested LCO/NMC cell dropped to 80% after 370 cycles with the UVP protocol compared to only 100 cycles achieved by the 2C CC-CV protocol with a similar charging time. While the voltage profile was shown to be universal with respect to cell age, the effects of the charging conditions, most notably temperature, on the cycling performance were not investigated. Ye et al. [205] developed a multistage constant heating rate charging protocol aiming to minimise charging time and temperature rise while maintaining the same charge capacity as in CC-CV. The heating rate was decreased in stages as the battery SOC increased, producing a variable current profile. Reduced charging time and temperature rise compared to CC-CV were reported at ambient temperatures ranging from 10°C to 40°C, although the effects on cycle life were not studied. Another charging strategy concept, Constant Temperature - Constant Voltage (CT-CV) was proposed by Patnaik et al. [206]. The temperature was set to a pre-defined maximum value during the CT stage and then decreased during CV, producing a current profile similar to boostcharging. The method was demonstrated to achieve about 20% shorter charge time compared to CC-CV with the same temperature rise, however the cycling performance was again not investigated. It should be stressed that while temperature plays a key role in determining degradation rates, the assumption that higher temperature rise is always detrimental may not apply in all cases. Temperature gradients within packs and cells are crucial but often not considered in charging protocol studies that use surface temperature as the main indicator of degradation rate.

Schindler et al. [207] took the novel approach of combining

previously published physically-motivated fast charging strategies. Four current-neutral current profiles were superimposed, separately and in combination, on a 1C CC-CV protocol. The profiles are shown in Fig. 9 and included: a) AC pulse, motivated by a decrease in cell resistance due to additional irreversible heating; b) cold derating, a profile in which a very low current is used initially due to high resistance at 0% SOC and the current is brought to a higher constant level as soon as the resistance drops; c) overpotential reserve, a profile in which the overpotential is always maintained below a certain safety limit to prevent negative anode potential, producing a gradually decreasing current profile; and d) pulse charging. Capacity fade was monitored in eighteen cells charged by different protocols, and compared to four cells charged by standard CC-CV. The best performing cell, charged by a combination of all profiles, retained 80% capacity after 800 cycles. In comparison, cells charged by CC-CV alone experienced the same capacity fade after only about 400 cycles, while the worst performing cell, charged by CC-CV combined with cold derating, completed about 330 cycles. In general, protocols that included the overpotential reserve profile resulted in best capacity retention. All tests were conducted at a temperature of 25°C and the results should not be generalised to other conditions.

While many fast charging protocols have been proposed based on an array of physical motivations, most of them have only been validated at standard temperatures and for certain cell chemistries or form factors. Since high currents induce higher mechanical stresses in electrode particles along with more severe current and temperature distributions, care must be taken when generalising the results of experimental studies to different cell types. At the moment, the applicability of many charging protocols to different conditions is difficult to establish without further experiments, which are often time consuming and expensive to conduct. There is a clear need for accurate cell and pack models that would enable the design of charging protocols without the need for extensive and complicated laboratory testing. As the EV industry grows in colder climates, more research on charging protocols suitable for low temperature fast charging will also be necessary. More consideration should also be given to the cell temperature profiles induced by different charging protocols, as it is the cell temperature rather than ambient that determines performance. Finally, studies on the effects of the fast charging protocols discussed in this section at the pack level are still lacking.

5.2. Model-based protocol optimisation

5.2.1. Optimisation based on ECM type models

Some researchers have attempted to design optimal charging protocols by using equivalent circuit model (ECM)-based models, which are reformulated and embedded into single-objective or multi-objective constrained optimisation problems.

In these problems, first-order [191,208–212] or high-order ECMs [213,214] are used to describe cell behaviour, and various cost functions are set to achieve maximum charging efficiency or minimum charging loss while fast charging. The charging loss is determined by the internal resistance, current rate, and charging time.

The thermal effect or battery aging caused by charging can be embedded into the basic ECM with an electro-thermal-aging coupling model to diminish temperature rise or battery degradation during charging. Except for the commonly used lumped thermal model in which the cell is taken as a whole, some enhanced models that can distinguish the core and surface temperature or have improved fidelity at higher rates have been proposed as well [212,213]. The aging effect is modelled in terms of an extended Arrhenius formula, which is related to the current rate, activation energy, total discharged capacity, temperature, etc. [212].

Once the framework of the optimisation problem is established, an appropriate optimisation algorithm should be used according to the cost functions and constraints. The conventional algorithms include: dynamic programming [211], Pontiac minimum principle

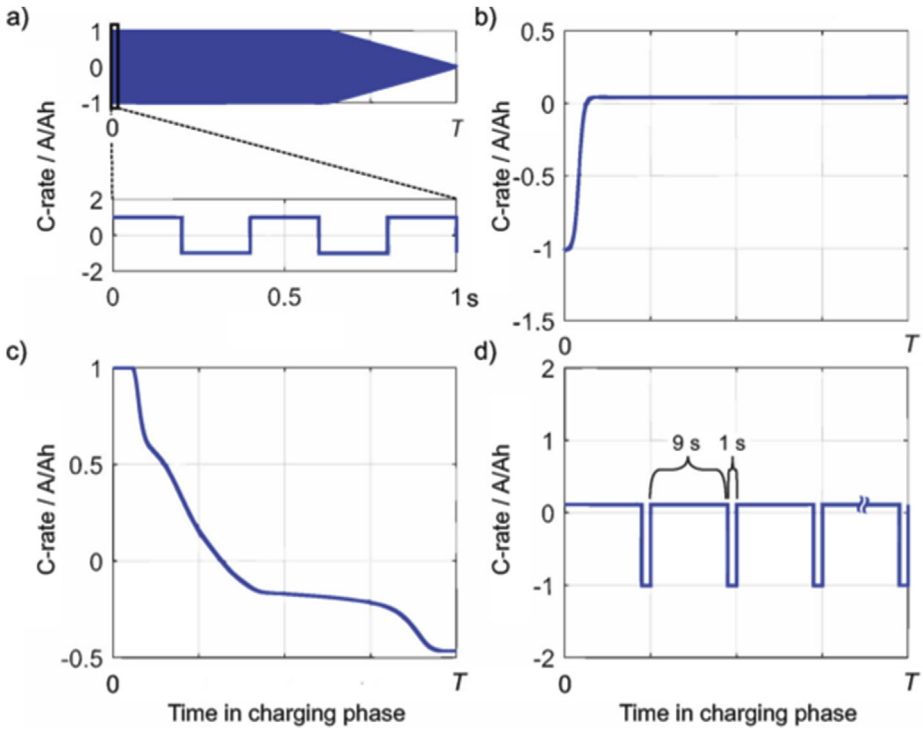

Fig. 9. Current trajectories of superimposed profiles from Ref. [207]. a) AC pulse, b) Cold derating, c) Overpotential reserve, d) Pulse charging.

[210], genetic algorithm [191,213], Legendre-Gauss-Radau (LGR) pseudo-spectral method [212], and minimum-maximum strategy [209].

ECMs can capture the external characteristics of the battery but fail to provide internal state information, especially for side reactions caused by charging such as SEI growth, lithium deposition, etc. Therefore, electrochemical models have drawn increasing attention.

5.2.2. Optimisation based on electrochemical models

The electrochemical-based models can be used to predict side reactions during charging due to their abilities to estimate internal states such as solid and electrolyte potential, ion concentration, and reaction flux. The most commonly used electrochemical model is the P2D model proposed by Doyle, Fuller, and Newman [215], into which key degradation mechanisms such as lithium plating can be incorporated as discussed in Section 3.2.3. However, it is computationally intensive to solve the PDEs in the full order model (FOM). Therefore, efforts were made to reduce the order of the FOM to achieve a faster computational speed with similar fidelity, allowing for realistic application. Purushothaman et al. [216] derived an analytical solution of the solid phase concentration through variable separation method. Fast charge methods of variable current pulse and nonlinear decay current were developed aiming at limiting the solid surface concentration within the boundary. Essentially, the model used in this case was a simplified form of the single particle (SP) model with a number of simplifying assumptions: only diffusion was modelled without considering reaction kinetics, a constant diffusion coefficient was assumed and all lithium-ion reduction was assumed to take place at the anode/separator interface. The model was not validated. The SP model can also predict the temperature, ion concentration distribution or overpotential by extension. The extended models are embedded into optimisation problems to solve for fast charging strategies with temperature or ion concentration restrictions [217,218]. In order to improve the fidelity of the model at various temperatures, the SP-thermal coupling model is established by adding parameter-temperature correlation. By using the coupling model, the performance of fast charging strategies at wider temperature ranges can be enhanced [219,220]. It is important to mention that while some of these models are validated against experimental results [218,219], others are only validated against other models [220] or not validated at all [216,217]. SP models generally lose accuracy at high current densities [221] and thus the results of studies should be interpretted with caution unless parameterised and validated against independent experimental data sets.

Some modelling approaches have been developed that consider side reactions. Rahimian et al. [222] used an SP-based model that included SEI layer growth to optimise the battery cycle life through adjusting the charging C-rate as the cell aged. The simulation results suggested that cycle life could be improved if charging C-rate was increased after a certain number of cycles. The model was not validated. SEI growth models were also used to develop MCC [223] and variable current protocol [224], but neither of these studies included full experimental validation. Lithium deposition prevention has drawn intensive attention in recent years [193,225]. The models that aim to limit lithium plating normally do so by maintaining positive anode potential, which can be estimated by a reduced order model (ROM). Klein et al. built a time-optimal charging problem based on a reduced-order electrochemical-thermal coupling model to predict anode potential and temperature during fast charging [226,227]. The model was validated against the FOM and experimental data for a fresh cell. Han et al. proposed a novel approach to simplify the FOM to form a simplified P2D model (SP2D) while maintaining the FOMs fidelity at high rates [228,229]. Experimental validation was not conducted. The SP2D model was then used to develop a non-destructive fast charging strategy with a variable current profile by maintaining the anode potential above a safety threshold [230]. Two cells were inspected post-mortem after five cycles using the proposed protocol and a CC-CV protocol with a comparable charging time (1.15C), revealing visible lithium deposition on the anode of the cell charged with CC-CV but no visible deposition on the cell charged with the proposed protocol.

Recently, some physics-based ECM models have also been developed that capture key electrochemical processes and internal states of the battery while being easier to parameterise than P2D models [231] or including additional effects such as double layer capacitance [232]. Such hybrid models vary in terms of computational demand and accuracy of prediction. While the more complex physics-informed ECMs could be useful for assessing effects in the frequency domain that standard P2D models do not capture, the simpler ones could have the advantage of being less computationally expensive or easier to parameterise than P2D with an improved fidelity and physical insight compared to standard ECMs. To the best of the authors' knowledge, these models have not yet been applied to charging protocol optimisation.

Overall, model-based charging optimisation studies often use ECM, SP or ROM rather than FOM approaches due to their lower computational demand, which makes them potentially suitable for real-time implementation. However, this advantage often comes at the expense of accuracy, prompting the need for careful validation particularly when abuse conditions such as fast charging are being modelled. While many model-based approaches to fast charging optimisation have been proposed, relatively few of them have been fully validated against experimental results. Furthermore, validation is often conducted only against fresh cell data, which may not be sufficient for modelling studies where the main purpose is to limit long-term degradation.

6. Implications on thermal management

Section 3.1 outlined the effects of fast charging on the temperature uniformity within cells and packs along with potential local degradation effects that may evolve. Fast charging is normally accompanied by high heat generation rates and significant inhomogeneities. At the same time, high charging currents applied at low temperatures may be detrimental to battery lifetime and safety. As such, effective and flexible thermal management strategies are critical to enabling fast charging in all conditions. The requirements on the Battery Thermal Management Systems (BTMSs) can vary greatly depending on temperature. While high thermal conductivity is crucial when cooling a hot battery pack, low temperature operation prompts the desire for good insulation to retain the heat produced by the battery. Passive thermal regulators that adjust their thermal conductance depending on temperature could be one way to address this problem [233].

6.1. Cooling

The cooling media commonly used for EV battery packs can be divided into air, liquid and phase change materials (PCMs). Air cooling systems are low cost and relatively simple, but fail to achieve sufficient cooling rates or good temperature uniformity due to the low heat capacity and thermal conductivity of air [234–236] and are therefore unsuitable for fast charging. Liquid cooling can be 3500 times more efficient than air [235] but its drawbacks include high cost, complexity and potential of leakage. Liquid immersion cooling, whereby batteries are immersed directly in the cooling medium, has been receiving attention from researchers due to its

effectiveness and ability to achieve good temperature homogenization [237]. To prevent short circuits, it is vital that the cooling liquid is dielectric. Examples of such liquids include deionised water and mineral oils. While liquid immersion cooling has not yet been widely adopted in EV battery packs [235], some researchers have shown promising results. For example, the two-phase thermal management liquid Novec7000 (3 M, USA) has been shown to achieve very good surface temperature uniformity in an immersion-cooled cylindrical Li-ion battery, particularly when the battery temperature was high enough to induce boiling [237]. The same liquid has also been reported to effectively maintain the temperature of a battery module around 35˚C even at a 20C discharge rate [238]. In PCM cooling, the latent heat of phase change of the cooling medium is used to absorb heat produced by the battery. However, the method has significant drawbacks: at high ambient temperatures, the PCM could melt completely without any heat being produced by the battery, and the low thermal conductivity of the liquid PCM would then act as a barrier to heat transfer [235]. On the other hand, Hmery et al. [239] coupled PCM with a liquid cooling system to enable solidification of the melted PCM. The coupled system was shown to effectively cool a battery module during a 2C fast charge.

Since fast charging inevitably leads to higher temperature gradients, both within a pack and within a cell, effective and uniform cooling becomes even more critical than under standard charging conditions. Heat generated during charging is more difficult to dissipate from the centre of a cell compared to the regions closer to the outer surfaces due to poor thermal conductivity across the electrodes [235]. At the same time, it is the outer surface of cells that is typically in contact with the cooling medium, further amplifying the temperature gradients. Similar observations apply to battery modules and packs. The dense packing of cells in EV battery packs to minimise the volume aggrevates the issue [240], making the cooling system design critical to pack safety and longevity. Lu et al. modelled the performance of a forced air cooling system with either 15 or 59 air flow channels, showing the latter option to achieve more uniform temperature distribution [240]. The diameters of the channels were adjusted so that both systems required the same volume within the pack and the same heat flux was imposed. Xia et al. [235] reviewed a number of cooling system configurations, concluding that parallel and mixed series-parallel configurations were more effective in minimising temperature gradients between cells compared to parallel configurations in fluid (air or liquid) cooled packs. However, cooling efficiency and uniformity are sometimes in contradiction. Hunt et al. [241] reported substantially lower rates of capacity fade for tab cooled pouch cells compared to surface cooled ones, which was attributed to lower temperature gradients between cell layers. Zhao et al. [242] modelled the effects of surface and tab cooling on the temperature distribution in a prismatic Li-ion cell. The study demonstrated that tab cooling resulted in a substantially more uniform temperature distribution across the cell thickness compared to surface cooling. However, surface cooling was able to reduce the average cell temperature more effectively than tab cooling. The model assumed a set coolant temperature for both methods, which may not be representative of the conditions in operation.

Finally, recent developments in increasing EV charging powers have been accompanied by some interest in external cooling technologies that could be provided by the charging stations. Such an approach, if successful, could help reduce the cost and weight of onboard cooling systems. Ford Global Technologies LLC have applied to patent a charging station that communicates with the connected EV and supplies cooled air to the vehicle radiator during fast charging [243]. Lightning Energy patented a charging station with coolant pipes integrated into the charging connector [244]. The connector locks in place to prevent coolant spillage if removed, and coolant is cycled through by the controller in the charger in response to battery information from the car. Tesla patented a similar idea, with an automated charging connector placed beneath the vehicle and being capable of supplying both cold and hot liquid to optimise the battery temperature during charging [245]. None of these technologies have been commercialised at the time of writing and their ability to provide sufficiently uniform cooling for fast charging applications has not been proven. Leakage of the thermal fluid is a potential issue.

6.2. Preheating in cold conditions

As explained in earlier sections, low temperature fast charging of Li-ion cells proves particularly difficult. While relatively few studies have attempted to address the issue through designing appropriate charging protocols, significant research effort has been dedicated to exploring different preheating strategies. In this section, only the methods that can result in rapid heating of the entire cell are discussed. This is because high speed is an imperative requirement for any preheating strategy that could be integrated with fast charging.

Internal preheating methods are favourable due to higher efficiency (as less heat is lost to the surroundings) and better uniformity [246,247]. Ji and Wang [248] used a coupled electrochemical-thermal model to compare the performance of four heating methods: self-heating by discharging the battery, convective heating using a fan and a resistance heater powered by the battery, mutual pulse heating, and AC heating. Mutual pulse heating is a strategy whereby a battery pack is divided into two groups of equal capacity and charge is exchanged between the two groups in pulses, taking advantage of the resistance to generate heat. Self-heating by discharging was found inefficient, as can be expected considering the cell generates both heat and power during discharge. Convective heating resulted in relatively fast but inefficient and non-uniform heating. The efficiency of the mutual pulse heating strategy was, on the other hand, shown to be much higher and mainly limited by the efficiency of the DC/DC converter used. Only 120 s were needed to raise the temperature of the simulated 2.2 Ah 18650 cell from -20˚C to 20˚C using this method. AC heating could reach even higher heating speeds, achieving the same temperature rise in 80 s with a 10 mV sinusoidal voltage wave at a frequency of 1000 Hz. However, the impacts on degradation and cyclability were not studied.

For AC heating, the time to reach the desired cell temperature can theoretically be minimised by using high current amplitudes, yet exceeding a safe current limit can lead to non-uniformity (as the resistance may vary within the cell), exceeding maximum cell voltage, and to the anode potential becoming negative [246]. Ge et al. [247] used an ECM-type model to estimate the maximum alternating current that could be applied depending on the frequency and temperature while maintaining a positive anode potential and therefore preventing lithium deposition. The study found that the maximum permissible current amplitude increased with increasing temperature and signal frequency. Based on these observations, a method for designing a stepwise AC heating strategy with the current amplitudes increasing with the average cell temperature was proposed. The frequency of the signal was kept constant at 100 Hz as it was demonstrated that gradually increasing the current had a stronger effect on the heating rate than lowering the frequency. The 1 Ah pouch cell used in the study could be heated from -20˚C to 5˚C in 800 s according to both the model and experimental data. However, the effects on the cyclability were not reported. The method for designing the AC profile required placing a reference electrode within the cell in order to obtain EIS spectra of

both electrodes needed to fit the model. The authors argued that preparing and testing one cell per cell type would not be a considerable cost to manufacturers. However, even assuming all cells of a certain type can be reproduced with the same equivalent circuit with the same parameters, it is crucial to note that these parameters would change as the cells age, and may change differently for different cells. Another study [246] proposed a similar AC heating profile with gradually increasing current amplitudes, again confirming that adjusting the amplitude was more beneficial than adjusting the frequency as the cell temperature increased. Based on an electro-thermal coupled model, the optimal frequency resulting in highest heat generation for the study case was calculated at 1377 Hz, slightly lower than the minimum impedance frequency. The frequency optimisation process used a simple model requiring only overall cell data without the need for a reference electrode. However, it was assumed that only cell voltage limits needed to be adhered to; the effect of the AC signal on the anode potential was not considered. The commercial 18650 cell of 2.75 Ah capacity was heated up from -15.4 °C to 5.6 °C in 338 s. No signs of aging were observed in incremental capacity (IC) curves after 300 heating tests. Capacity retention in preheated and subsequently cycled cells was not explored. Zhu et al. [249] experimented with different frequencies and amplitudes for a preheating AC profile on a 30 Ah LFP pouch cell, although the maximum amplitudes were low relative to the cell capacity (60 A, or 2C). With amplitudes limited to this value, a low frequency signal was more successful in heating the cell rapidly compared to higher frequencies. The most effective AC profile tested was able to heat the cell from -25 °C to 5 °C in 1800 s using a frequency of 0.5 Hz and an amplitude of 60 A. SEM images of the anode after 240 heating tests did not feature signs of lithium deposition. While these were compared to images of an anode subjected to 36 DC charge/discharge cycles at 0.5C and -25 °C which showed a clearly altered morphology, no attempt was made to study a cell subjected to the AC preheating procedure with subsequent cycling. A thermocouple inserted in one of the cells enabled the authors to quantify the variation between the internal and surface temperature of the AC heated cell at about 5 °C, providing a useful insight into the homogeneity of the AC heating method.

Designing Li-ion cells specifically to enable rapid preheating is another approach to address low temperature fast charging. Electrically insulated thin nickel foils inserted between two single-sided anode layers of a cell provide a means to raise the temperature when necessary using standard direct current [16,250,251]. Current through the foils can be controlled using an activation switch. Turning the switch on directs the current to the nickel foils, causing rapid heat generation. When the switch is in the 'off' position, the current flows through the electrodes only, and the nickel foils are electrically isolated. Yang et al. [251] modelled this cell design, using 10 Ah and 40 Ah prismatic cells as examples. The study demonstrated that heating uniformity and speed improved substantially with the number of nickel foils inserted, even when the total thickness of the foils was unchanged. The total thickness of nickel foils was 200 μm which reduced the volumetric energy density by only about 0.58%. The same group [16] followed up with an experimental study on a 9.5 Ah NMC622 pouch cell with two nickel foils. The results showed that the cell could be preheated and charged to 80% SOC in 15 min even from -50 °C. Cycling tests at 0 °C ambient revealed a cycle life of 4500 cycles before reaching 20% capacity fade for a cell preheated and subsequently fast charged at 3.5C, compared to only 50 cycles for a cell that was not preheated.

Although it is generally accepted that internal heating methods offer both better efficiency and more homogeneous temperature distribution, still little research has been done to evaluate the effects of internal preheating in conjunction with fast charging on cycle life. Since current flows preferentially through paths of lower resistance and therefore higher temperature, it is possible that even small temperature gradients produced by internal preheating methods would be exacerbated if immediately followed by a fast charge. Since internal temperature is difficult to measure experimentally, cycle life testing or reliable models will be needed to fully assess the performance of AC preheating. Nickel foil preheating, while potentially promising, would require a non-standard cell design with additional weight, instrumentation, and possible reliability issues. As the technology was proposed only recently, more research on its performance and cost will be needed before potential commercialisation.

7. Safety

7.1. Effects of fast charging on thermal runaway characteristics

Lithium plating [30,96,252] and the temperature rise due to the heat accumulated in the cells or bus-bars at the end of fast charging [253,254] pose potential safety risks in addition to causing accelerated degradation.

Research has shown that the thermal runaway behaviour of batteries changes after experiencing fast charging [255]. By conducting ARC tests on a fast-charged high energy pouch battery, it was found that the self-heating temperature and the thermal runaway triggering temperature drastically reduced for cells subjected to fast charging compared to fresh cells. These effects do, however, seem to be reversible if sufficient rest time is allowed. Waldmann et al. [256,257] conducted ARC tests on batteries rested for different periods of time after fast charging. While a significant change in thermal runaway characteristics was observed for cells after only a short rest time, the thermal runaway behaviour of cells subjected to long rest times was similar to that of a fresh cell. This phenomenon can be explained by the re-intercalation of lithium into the anode during the rest time, as well the reaction of the plated lithium with electrolyte to form new SEI [96,115]. With the rest time extending, the active plated-lithium content participating in the thermal runaway process is reduced, and the thermal runaway characteristics of the battery recover to their normal state.

Thermal runaway is known as being composed of a series of chain reactions [258]. In a fresh battery it is generally triggered by an internal short circuit, and the maximum temperature is quickly reached with the participation of the electrolyte [259–266]. To clearly describe the chain reactions of fast-charged batteries, the evolution process of thermal runaway can be divided into three stages, as shown in Fig. 10. For the fast charged battery which exhibits abnormal thermal runaway behaviour, the reaction between lithium and electrolyte is dominant in the thermal runaway process, as opposed to that of fresh batteries. In the first stage ($60\,^{\circ}C < T < 110\,^{\circ}C$), the plated lithium reacts with the electrolyte and heats the battery. The SEI film on the plated lithium surface is continuously decomposed and regenerated, while the temperature rise rate remains relatively low. In the second stage (thermal runaway triggering process), the plated lithium is consumed in a large amount in the violent reaction with the electrolyte, causing a sharp increase in temperature. The separator collapses, and the cathode and anode connect with each other. In the third stage (thermal runaway developing to the highest temperature), other reactions are involved. The reaction of the anode and electrolyte, the reaction of the anode and the cathode, and the reaction of the cathode and electrolyte are triggered due to the sudden rise of temperature. As a result, the battery reaches the maximum

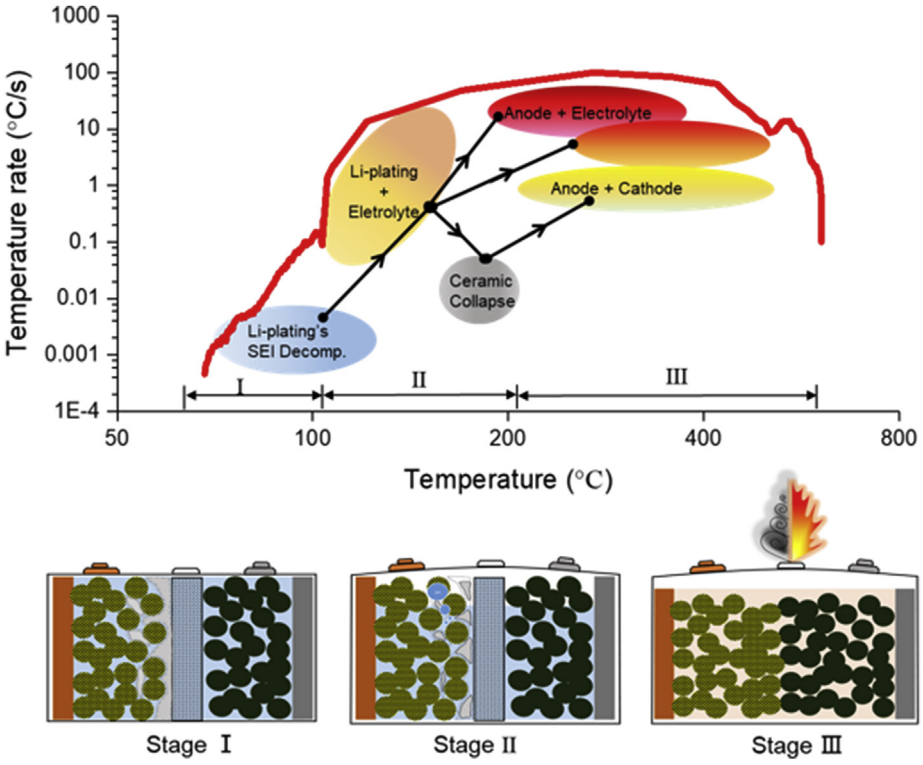

Fig. 10. Chain reactions of the thermal runaway process in fast charged batteries [255].

temperature of thermal runaway.

7.2. Overcharge-induced thermal runaway

Some cells in a fast-charged battery pack may become overcharged due to the inconsistency among the cells [34,267,268], potentially leading to thermal runaway [269,270]. This process consists of four stages [259].

Stage 1 (100% < SOC < 120%): The battery voltage exceeds the cut-off voltage and increases slowly. The excess anode material, normally incorporated in Li-ion cells for safety, can still withstand excessive embedded lithium in the beginning of overcharging [271–273]. Some side reactions of the battery material may be triggered and the temperature and internal resistance of the battery slightly increase.

Stage 2 (120% < SOC < 140%): A dissolution reaction of transition metal ions such as Mn^{2+} may be triggered in positive electrodes of certain chemistries, due to the excessive deintercalation of lithium [274,275]. At the same time, electrolyte oxidation may also begin since the battery potential exceeds the stable operating window. The negative electrode of the battery gradually becomes unable to withstand further transfer of lithium atoms, leading to significant amounts of Li depositing on its surface [275,276]. The deposited lithium reacts with the electrolyte to form new SEI film, increasing the internal resistance of the cell [276,277]. The joule heating effect of the overcharge current causes a significant increase in the battery temperature.

Stage 3 (140% < SOC < 160%): The heat produced by the exothermic reactions of the battery material begins to be comparable to and subsequently dominant over the joule heat due to the further removal of lithium from the positive electrode, the large deposition of lithium in the negative electrode, and the increase of the electrode potential. Oxidative decomposition of the electrolyte produces a greater amount of heat [278,279], accompanied by the generation of gas, causing the battery to expand. The lithium-electrolyte reaction also becomes more pronounced as the amount of lithium deposition increases. When the SOC is close to 160%, a large amount of Mn^{2+} is dissolved if present in the cathode material; the SEI film gradually collapses [280,281]; the structure of the cathode material changes, causing the battery voltage to reach a maximum value and then begin to decrease [282–284].

Stage 4 (140% < SOC < 160%): The oxidative decomposition of the electrolyte generates a large amount of gas, resulting in the battery rupture instantaneously. The battery separator is displaced by the shock, and a large internal short circuit occurs in the battery. The contact between the positive and negative electrodes of the battery produces a severe redox reaction [260]. Thermal runaway occurs eventually.

High-precision thermo-electrochemical coupling models have been created to investigate overcharged batteries, based on the amount of internal materials and reaction kinetic parameters of the battery, and proposed two design methods to help protect the battery from overcharging [259]:

1) Raising the electrolyte oxidation reaction potential from 4.4 V to 4.7 V. This results in a more stable electrolyte and the SOC of thermal runaway increased to 183%. It can be achieved by adding functional additives or redox shuttle additives [285,286], i.e. chemical species that can be reversibly reduced and oxidised at potentials slightly higher than the maximum safe cathode potential, thus preventing it from increasing further [287]. Due to the range of requirements for such compounds, including stable electrochemistry over many cycles, appropriate redox potential and non-reactivity in both oxidised and reduced forms with any of the components of a Li-ion cell, still more research is needed to find suitable redox shuttle species [287].

2) Increasing the temperature at which the battery thermal runaway occurs to 300°C can delay the occurrence of large-scale internal short circuit inside the battery, and increase the SOC of

thermal runaway to 180%. This measure could potentially be realised by optimising the battery pressure relief design or using a diaphragm with a higher heat exchange stability [80,260] to postpone the rupture of the battery [259].

8. Conclusion

Electrification of transport is undisputably one of the key strategies to address climate change. The need to reduce range anxiety and meet customer expectations has driven many manufacturers to target fast charging capability as a critical design feature for EV battery packs. While significant research efforts have been dedicated to various aspects of fast charging in the recent years, many knowledge gaps still exist.

- To date, no reliable onboard methods exist to detect the occurrence of crucial degradation phenomena such as lithium plating or mechanical cracking. Techniques for detecting lithium plating based on the characteristic voltage platueaus are promising for online application, but fully reliable methods to distinguish lithium stripping from other plateau-inducing phenomena, or to detect plating where no plateau is observed, have not yet been reported.
- Many alternative electrode materials have been proposed that could potentially improve fast charging capabilities of Li-ion cells, however much remains to be studied regarding their stability, possible degradation mechanisms, ease of manufacture, and cost. Despite the fact that graphite anodes are particularly susceptible to lithium plating, they will likely continue to dominate the Li-ion battery market in the foreseeable future due to their low cost, wide availability, and technology maturity.
- Existing modelling approaches have significant limitations: ECM-based models, with the exclusion of some physics-informed ones, do not capture information about the internal states of the battery and are only reliable in a limited range of conditions which cannot normally be extended to abuse conditions. On the other hand, the high fidelity of full order electrochemical models renders them inappropriate for real-time implementation. There is therefore a clear need for accurate reduced order models capable of reproducing key internal states that could be implemented in future fast charging enabled BMSs. Physics-based ECMs could also offer advantages in terms of computational demand or ability to capture phenomena not reflected by standard P2D models.
- Many studies on fast charging protocols have been of empirical or experimental nature, and therefore their performance has only been assessed for a limited range of cell chemistries, form factors, and operating conditions. Such results cannot be easily extended to other cell types or ambient temperatures, as supported by the often conflicting findings reported by different authors. On the other hand, many of the model-based charging optimisation studies are based on SP or ECM type models that may not be accurate at high currents, while their results are often validated only against other models or not at all. Accurate and validated cell and pack models and improved understanding of limiting phenomena are needed to enable the design of charging protocols without the need for extensive laboratory testing.
- Few charging optimisation studies to date have addressed the special case of low temperature fast charging, which will be increasingly important as deployment of EVs accelerates in colder climates.
- To further optimise the charging process for individual cells in a pack and avoid local degradation or overcharge, advanced BMSs with cell balancing capabilities will be required.
- While much attention has been afforded to the design of thermal management systems already, further research is still needed to assess the efficiency and homogeneity achieved by various preheating and cooling technologies. For instance, few studies have attempted to assess the implications of AC preheating with subsequent fast charging on cell lifetime, or to quantify the temperature gradients induced by this method. Optimisation of tab design and placement and of the geometrical design of cooling systems may be another significant route to improving temperature and current homogeneity. External cooling technologies integrated with EV chargers could be helpful in reducing the weight and cost of on-board cooling systems, but whether such solutions could achieve the required cooling rates or temperature uniformity remains to be studied.
- Finally, the links between cell level and pack level degradation rates are still not well understood. Multiple charging and preheating strategies have been demonstrated for single cells, but the effects, feasibility, and cost of their implementation in battery packs have not been studied. It is conceivable that some charging protocols that result in improved performance for single cells may lead to current or temperature heterogeneities when performed on a pack. Research on this topic will be required before any non-conventional protocols are applied in real-world systems. Furthermore, few modelling works have addressed the impacts of cell-to-cell variation on pack level performance. Since fast charging can be expected to amplify heterogeneities, such multiscale studies are urgently needed. Advancements in multiscale modelling will be critical to integrating cell and pack level design and control, playing an important role in linking research on different scales to improvements in the performance of commercial systems.

Acknowledgements

The authors gratefully acknowledge the helpful discussions held with the Advanced Energy Storage team at Shell. This work was kindly supported by: Shell, the EPSRC Faraday Institution Multi-Scale Modelling Project (EP/S003053/1, grant number FIRG003), energy storage for low carbon grids project (EP/K002252/1), the EPSRC Joint UK-India Clean Energy centre (JUICE) (EP/P003605/1), Integrated Development of Low-Carbon Energy Systems (IDLES) (EP/R045518/1), the Innovate UK Advanced Battery Lifetime Extension (ABLE), the Innovate UK Battery Advanced for Future Transport Applications (BAFTA) project and the National Natural Science Foundation of China (grant number U1564205, 51706117).

References

[1] Howell D, Duong T, Faguy P, Cunningham B. DOE vehicle battery R&D: progress update 2011. Tech. rep. 2011. https://www.hydrogen.energy.gov/pdfs/htac{_}nov2011{_}howell.pdf.
[2] Lane B. Porsche installs first 350 kW ultra-rapids in Berlin - zap-Map. 2017. https://www.zap-map.com/porsche-installs-first-350-kw-ultra-rapids-in-berlin/.
[3] Szymkowski S. Porsche installs first 350-kW electric car charging station in Berlin. 2017. https://www.motorauthority.com/news/1111847{_}mercedes-outlines-3-pronged-approach-to-self-driving-cars.
[4] Porsche taycan price and specifications - EV database. 2018. https://ev-database.uk/car/1116/Porsche-Taycan.
[5] Audi e-tron GT price and specifications - EV Database. 2018. https://ev-database.uk/car/1153/Audi-e-tron-GT.
[6] Research project FastCharge: ultra-fast charging technology. https://www.siemens.com/press/en/feature/2018/energymanagement/2018-12-fastcharge.php; 2018.
[7] Tech. rep. 2014 LEAF owner's manual. 2014. https://owners.nissanusa.com/nowners/.
[8] Berman B. Quick charging of electric cars | PluginCars.com. 2014. https://plugincars.com/electric-car-quick-charging-guide.html.
[9] Mussa AS, Klett M, Behm M, Lindbergh G, Lindström RW. Fast-charging to a partial state of charge in lithium-ion batteries: a comparative ageing study.

Journal of Energy Storage 2017;13:325–33. https://doi.org/10.1016/J.EST.2017.07.004. https://www.sciencedirect.com/science/article/pii/S2352152X17301913?via{%}3Dihub{#}bib0070.
[10] BMW i3. Charging guide | pod point (2018), https://pod-point.com/guides/vehicles/bmw/2018/i3; 2018.
[11] Zhu G, Zhao C, Huang J, He C, Zhang J, Chen S, Xu L, Yuan H, Zhang Q. Fast charging lithium batteries: recent progress and future prospects. Small 2019;15(15):1805389. https://doi.org/10.1002/smll.201805389. https://onlinelibrary.wiley.com/doi/abs/10.1002/smll.201805389.
[12] Liu Y, Zhu Y, Cui Y. Challenges and opportunities towards fast-charging battery materials. Nature Energy 2019;4(7):540–50. https://doi.org/10.1038/s41560-019-0405-3. http://www.nature.com/articles/s41560-019-0405-3.
[13] Shen Weixiang, Vo Thanh Tu, Kapoor A. Charging algorithms of lithium-ion batteries: an overview. In: 2012 7th IEEE conference on industrial electronics and applications (ICIEA). IEEE; 2012. p. 1567–72. https://doi.org/10.1109/ICIEA.2012.6360973. http://ieeexplore.ieee.org/document/6360973/.
[14] Gao Y, Zhang X, Cheng Q, Guo B, Yang J. Classification and review of the charging strategies for commercial lithium-ion batteries. IEEE Access 2019;7:43511–24. https://doi.org/10.1109/ACCESS.2019.2906117. https://ieeexplore.ieee.org/document/8669683/.
[15] Chen C, Shang F, Salameh M, Krishnamurthy M. Challenges and advancements in fast charging solutions for EVs: a technological review. In: 2018 IEEE transportation electrification conference and expo (ITEC). IEEE; 2018. p. 695–701. https://doi.org/10.1109/ITEC.2018.8450139. https://ieeexplore.ieee.org/document/8450139/.
[16] Yang X-G, Zhang G, Ge S, Wang C-Y. Fast charging of lithium-ion batteries at all temperatures. Proc. Natl. Acad. Sci. U.S.A 2018;115(28):7266–71. https://doi.org/10.1073/pnas.1807115115. www.pnas.org/cgi/doi/10.1073/pnas.1807115115.
[17] Gallagher KG, Trask SE, Bauer C, Woehrle T, Lux SF, Tschech M, Lamp P, Polzin BJ, Ha S, Long B, Wu Q, Lu W, Dees DW, Jansen AN. Optimizing areal capacities through understanding the limitations of lithium-ion electrodes. J Electrochem Soc 2016;163(2):138–49. https://doi.org/10.1149/2.0321602jes. http://jes.ecsdl.org/content/163/2/A138.full.pdf.
[18] Arora P, Doyle M, White RE. Mathematical modeling of the lithium deposition overcharge reaction in lithium-ion batteries using carbon-based negative electrodes. J Electrochem Soc 1999;146(10):3543. https://doi.org/10.1149/1.1392512. http://jes.ecsdl.org/cgi/doi/10.1149/1.1392512.
[19] Waldmann T, Kasper M, Wohlfahrt-Mehrens M. Optimization of charging strategy by prevention of lithium deposition on anodes in high-energy lithium-ion batteries electrochemical experiments. Electrochim Acta 2015;178:525–32. https://doi.org/10.1016/J.ELECTACTA.2015.08.056. https://www.sciencedirect.com/science/article/pii/S0013468615303066.
[20] Waldmann T, Wilka M, Kasper M, Fleischhammer M, Wohlfahrt-mehrens M. Temperature dependent ageing mechanisms in Lithium-ion batteries: a Post-Mortem study. J Power Sources 2014;262:129–35. https://doi.org/10.1016/j.jpowsour.2014.03.112. https://doi.org/10.1016/j.jpowsour.2014.03.112.
[21] Bach TC, Schuster SF, Fleder E, Müller J, Brand MJ, Lorrmann H, Jossen A, Sextl G. Nonlinear aging of cylindrical lithium-ion cells linked to heterogeneous compression. Journal of Energy Storage 2016;5:212–23. https://doi.org/10.1016/J.EST.2016.01.003. https://www.sciencedirect.com/science/article/pii/S2352152X16300032?via{%}3Dihub.
[22] Mao C, Ruther RE, Li J, Du Z, Belharouak I. Identifying the limiting electrode in lithium ion batteries for extreme fast charging. Electrochem Commun 2018;97:37–41. https://doi.org/10.1016/J.ELECOM.2018.10.007. https://www.sciencedirect.com/science/article/pii/S1388248118302601.
[23] Yang X-G, Wang C-Y. Understanding the trilemma of fast charging, energy density and cycle life of lithium-ion batteries. J Power Sources 2018;402:489–98. https://doi.org/10.1016/J.JPOWSOUR.2018.09.069. https://www.sciencedirect.com/science/article/pii/S0378775318310462?via{%}3Dihub.
[24] Trentadue G, Lucas A, Otura M, Pliakostathis K, Zanni M, Scholz H. Evaluation of fast charging efficiency under extreme temperatures. Energies 2018;11(8):1937. https://doi.org/10.3390/en11081937. http://www.mdpi.com/1996-1073/11/8/1937.
[25] Jow TR, Delp SA, Allen JL, Jones J-P, Smart MC. Factors limiting Li + charge transfer kinetics in Li-ion batteries. J Electrochem Soc 2018;165(2):361–7. https://doi.org/10.1149/2.1221802jes. http://jes.ecsdl.org/content/165/2/A361.full.pdf.
[26] Takahashi K, Srinivasan V. Examination of graphite particle cracking as a failure mode in lithium-ion batteries: a model-experimental study. J Electrochem Soc 2015;162(4):A635–45. https://doi.org/10.1149/2.0281504jes. http://jes.ecsdl.org/lookup/doi/10.1149/2.0281504jes.
[27] Persson K, Sethuraman VA, Hardwick LJ, Hinuma Y, Meng YS, van der Ven A, Srinivasan V, Kostecki R, Ceder G. Lithium diffusion in graphitic carbon. J Phys Chem Lett 2010;1(8):1176–80. https://doi.org/10.1021/jz100188d. https://pubs.acs.org/doi/10.1021/jz100188d.
[28] Hall DS, Eldesoky A, Logan ER, Tonita EM, Ma X, Dahn JR. Exploring classes of Co-solvents for fast-charging lithium-ion cells. J Electrochem Soc 2018;165(10):A2365–73. https://doi.org/10.1149/2.1351810jes. http://jes.ecsdl.org/lookup/doi/10.1149/2.1351810jes.
[29] Chang HJ, Ilott AJ, Trease NM, Mohammadi M, Jerschow A, Grey CP. Correlating microstructural lithium metal growth with electrolyte salt depletion in lithium batteries using 7Li MRI. J Am Chem Soc 2015;137(48):15209–16. https://doi.org/10.1021/jacs.5b09385. http://pubs.acs.org/doi/10.1021/jacs.5b09385.
[30] Waldmann T, Hogg B-I, Wohlfahrt-Mehrens M. Li plating as unwanted side reaction in commercial Li-ion cells A review. J Power Sources 2018;384(February):107–24. https://doi.org/10.1016/j.jpowsour.2018.02.063.
[31] Du Z, Wood DL, Daniel C, Kalnaus S, Li J. Understanding limiting factors in thick electrode performance as applied to high energy density Li-ion batteries. J Appl Electrochem 2017;47(3):405–15. https://doi.org/10.1007/s10800-017-1047-4. http://link.springer.com/10.1007/s10800-017-1047-4.
[32] Liu QQ, Petibon R, Du CY, Dahn JR. Effects of electrolyte additives and solvents on unwanted lithium plating in lithium-ion cells. J Electrochem Soc 2017;164(6):1173–83. https://doi.org/10.1149/2.1081706jes. http://jes.ecsdl.org/content/164/6/A1173.full.pdf.
[33] Waldmann T, Quinn JB, Richter K, Kasper M, Tost A, Klein A, Wohlfahrt-Mehrens M. Electrochemical, post-mortem, and ARC analysis of Li-ion cell safety in second-life applications. J Electrochem Soc 2017;164(13):A3154–62. https://doi.org/10.1149/2.0961713jes. http://jes.ecsdl.org/lookup/doi/10.1149/2.0961713jes.
[34] Tanim TR, Shirk MG, Bewley RL, Dufek EJ, Liaw BY. Fast charge implications: pack and cell analysis and comparison. J Power Sources 2018;381(February):56–65. https://doi.org/10.1016/j.jpowsour.2018.01.091.
[35] Müller S, Eller J, Ebner M, Burns C, Dahn J, Wood V. Quantifying inhomogeneity of lithium ion battery electrodes and its influence on electrochemical performance. J Electrochem Soc 2018;165(2):A339–44. https://doi.org/10.1149/2.0311802jes. http://jes.ecsdl.org/lookup/doi/10.1149/2.0311802jes.
[36] Yao KPC, Okasinski JS, Kalaga K, Shkrob IA, Abraham DP. Quantifying lithium concentration gradients in the graphite electrode of Li-ion cells using operando energy dispersive X-ray diffraction. Energy Environ Sci 2019;12(2):656–65. https://doi.org/10.1039/C8EE02373E. http://xlink.rsc.org/?DOI=C8EE02373E.
[37] Malifarge S, Delobel B, Delacourt C. Experimental and modeling analysis of graphite electrodes with various thicknesses and porosities for high-energy-density Li-ion batteries. J Electrochem Soc 2018;165(7):A1275–87. https://doi.org/10.1149/2.0301807jes. http://jes.ecsdl.org/lookup/doi/10.1149/2.0301807jes.
[38] Liu Q, Du C, Shen B, Zuo P, Cheng X, Ma Y, Yin G, Gao Y. Understanding undesirable anode lithium plating issues in lithium-ion batteries. RSC Adv 2016;6(91):88683–700. https://doi.org/10.1039/c6ra19482f.
[39] Ahmed S, Bloom I, Jansen AN, Tanim T, Dufek EJ, Pesaran A, Burnham A, Carlson RB, Dias F, Hardy K, Keyser M, Kreuzer C, Markel A, Meintz A, Michelbacher C, Mohanpurkar M, Nelson PA, Robertson DC, Scoffield D, Shirk M, Stephens T, Vijayagopal R, Zhang J. Enabling fast charging A battery technology gap assessment. J Power Sources 2017;367:250–62. https://doi.org/10.1016/J.JPOWSOUR.2017.06.055. https://www.sciencedirect.com/science/article/pii/S0378775317308388.
[40] Abboud AW, Dufek EJ, Liaw B. CommunicationImplications of local current density variations on lithium plating affected by cathode particle size. J Electrochem Soc 2019;166(4):A667–9. https://doi.org/10.1149/2.0711904jes. http://jes.ecsdl.org/lookup/doi/10.1149/2.0711904jes.
[41] Raijmakers L, Danilov D, Eichel R-A, Notten P. A review on various temperature-indication methods for Li-ion batteries. Appl Energy 2019;240:918–45. https://doi.org/10.1016/J.APENERGY.2019.02.078. https://www.sciencedirect.com/science/article/pii/S0306261919303757?via{%}3Dihub.
[42] Schuster E, Ziebert C, Melcher A, Rohde M, Seifert HJ. Thermal behavior and electrochemical heat generation in a commercial 40 Ah lithium ion pouch cell. J Power Sources 2015;286:580–9. https://doi.org/10.1016/J.JPOWSOUR.2015.03.170. https://www.sciencedirect.com/science/article/pii/S0378775315006047?via{%}3Dihub.
[43] Heubner C, Schneider M, Lämmel C, Michaelis A. Local heat generation in a single stack lithium ion battery cell. Electrochim Acta 2015;186:404–12. https://doi.org/10.1016/J.ELECTACTA.2015.10.182. https://www.sciencedirect.com/science/article/pii/S0013468615307581?via{%}3Dihub.
[44] Danilov D, Notten P. Mathematical modelling of ionic transport in the electrolyte of Li-ion batteries. Electrochim Acta 2008;53(17):5569–78. https://doi.org/10.1016/J.ELECTACTA.2008.02.086. https://www.sciencedirect.com/science/article/pii/S0013468608003046?via{%}3Dihub.
[45] Grazioli D, Magri M, Salvadori A. Computational modeling of Li-ion batteries. Comput Mech 2016;58(6):889–909. https://doi.org/10.1007/s00466-016-1325-8. http://link.springer.com/10.1007/s00466-016-1325-8.
[46] Andre D, Meiler M, Steiner K, Wimmer C, Soczka-Guth T, Sauer D. Characterization of high-power lithium-ion batteries by electrochemical impedance spectroscopy. I. Experimental investigation. J Power Sources 2011;196(12):5334–41. https://doi.org/10.1016/J.JPOWSOUR.2010.12.102. https://www.sciencedirect.com/science/article/pii/S0378775311000681?via{%}3Dihub.
[47] Jalkanen K, Aho T, Vuorilehto K. Entropy change effects on the thermal behavior of a LiFePO4/graphite lithium-ion cell at different states of charge. J Power Sources 2013;243:354–60. https://doi.org/10.1016/J.JPOWSOUR.2013.05.199. https://www.sciencedirect.com/science/article/pii/S0378775313010203?via{%}3Dihub.
[48] Schmidt JP, Weber A, Ivers-Tiffée E. A novel and precise measuring method for the entropy of lithium-ion cells: ΔS via electrothermal impedance spectroscopy. Electrochim Acta 2014;137:311–9. https://doi.org/10.1016/J.ELECTACTA.2014.05.153. https://www.sciencedirect.com/science/article/

pii/S0013468614011682?via{%}3Dihub.
[49] Osswald PJ, del Rosario M, Garche J, Jossen A, Hoster HE. Fast and accurate measurement of entropy profiles of commercial lithium-ion cells. Electrochim Acta 2015;177:270–6. https://doi.org/10.1016/J.ELECTACTA.2015.01.191. https://www.sciencedirect.com/science/article/pii/S0013468615002376?via{%}3Dihub.
[50] Murashko K, Mityakov A, Mityakov V, Sapozhnikov S, Jokiniemi J, Pyrhönen J. Determination of the entropy change profile of a cylindrical lithium-ion battery by heat flux measurements. J Power Sources 2016;330:61–9. https://doi.org/10.1016/J.JPOWSOUR.2016.08.130. https://www.sciencedirect.com/science/article/pii/S0378775316311508?via{%}3Dihub.
[51] Nazari A, Farhad S. Heat generation in lithium-ion batteries with different nominal capacities and chemistries. Appl Therm Eng 2017;125:1501–17. https://doi.org/10.1016/J.APPLTHERMALENG.2017.07.126. https://www.sciencedirect.com/science/article/pii/S1359431117304441?via{%}3Dihub.
[52] Keyser M, Pesaran A, Li Q, Santhanagopalan S, Smith K, Wood E, Ahmed S, Bloom I, Dufek E, Shirk M, Meintz A, Kreuzer C, Michelbacher C, Burnham A, Stephens T, Francfort J, Carlson B, Zhang J, Vijayagopal R, Hardy K, Dias F, Mohanpurkar M, Scoffield D, Jansen AN, Tanim T, Markel A. Enabling fast charging Battery thermal considerations. J Power Sources 2017;367:228–36. https://doi.org/10.1016/J.JPOWSOUR.2017.07.009. https://www.sciencedirect.com/science/article/pii/S0378775317308819?via{%}3Dihub.
[53] Smith K, Shi Y, Wood E, Pesaran A. Optimizing battery usage and management for long life (presentation). Tech. rep. NREL (National Renewable Energy Laboratory); 2016. https://www.nrel.gov/docs/fy16osti/66708.pdf.
[54] Veneri O, editor. Technologies and applications for smart charging of electric and plug-in hybrid vehicles. Cham: Springer International Publishing; 2017. https://doi.org/10.1007/978-3-319-43651-7. http://link.springer.com/10.1007/978-3-319-43651-7.
[55] Goutam S, Nikolian A, Jaguemont J, Smekens J, Omar N, Van Dan Bossche P, Van Mierlo J. Three-dimensional electro-thermal model of li-ion pouch cell: analysis and comparison of cell design factors and model assumptions. Appl Therm Eng 2017;126:796–808. https://doi.org/10.1016/J.APPLTHERMALENG.2017.07.206. https://www.sciencedirect.com/science/article/pii/S1359431117325565?via{%}3Dihub.
[56] Xu M, Zhang Z, Wang X, Jia L, Yang L. A pseudo three-dimensional electrochemicalthermal model of a prismatic LiFePO4 battery during discharge process. Energy 2015;80:303–17. https://doi.org/10.1016/J.ENERGY.2014.11.073. https://www.sciencedirect.com/science/article/pii/S0360544214013437?via{%}3Dihub.
[57] Liu J, Kunz M, Chen K, Tamura N, Richardson TJ. Visualization of charge distribution in a lithium battery electrode. J Phys Chem Lett 2010;1(14):2120–3. https://doi.org/10.1021/jz100634n. https://pubs.acs.org/doi/10.1021/jz100634n.
[58] Zhang G, Shaffer CE, Wang C-Y, Rahn CD. In-situ measurement of current distribution in a Li-ion cell. J Electrochem Soc 2013;160(4):A610–5. https://doi.org/10.1149/2.046304jes. http://jes.ecsdl.org/lookup/doi/10.1149/2.046304jes.
[59] Fleckenstein M, Bohlen O, Roscher MA, Bäker B. Current density and state of charge inhomogeneities in Li-ion battery cells with LiFePO4 as cathode material due to temperature gradients. J Power Sources 2011;196(10):4769–78. https://doi.org/10.1016/J.JPOWSOUR.2011.01.043. https://www.sciencedirect.com/science/article/pii/S0378775311001558.
[60] Song W, Chen M, Bai F, Lin S, Chen Y, Feng Z. Non-uniform effect on the thermal/aging performance of Lithium-ion pouch battery. Appl Therm Eng 2018;128:1165–74. https://doi.org/10.1016/J.APPLTHERMALENG.2017.09.090. https://www.sciencedirect.com/science/article/pii/S1359431117350986?via{%}3Dihub.
[61] Zhu Y, Xie J, Pei A, Liu B, Wu Y, Lin D, Li J, Wang H, Chen H, Xu J, Yang A, Wu C-L, Wang H, Chen W, Cui Y. Fast lithium growth and short circuit induced by localized-temperature hotspots in lithium batteries. Nat Commun 2019;10(1):2067. https://doi.org/10.1038/s41467-019-09924-1. http://www.nature.com/articles/s41467-019-09924-1.
[62] Wu B, Yufit V, Marinescu M, Offer GJ, Martinez-Botas RF, Brandon NP. Coupled thermalelectrochemical modelling of uneven heat generation in lithium-ion battery packs. J Power Sources 2013;243:544–54. https://doi.org/10.1016/J.JPOWSOUR.2013.05.164. https://www.sciencedirect.com/science/article/pii/S0378775313009622.
[63] Barré A, Deguilhem B, Grolleau S, Gérard M, Suard F, Riu D. A review on lithium-ion battery ageing mechanisms and estimations for automotive applications. J Power Sources 2013;241:680–9. https://doi.org/10.1016/J.JPOWSOUR.2013.05.040. https://www.sciencedirect.com/science/article/pii/S0378775313008185{#}fd1.
[64] Erdinc O, Vural B, Uzunoglu M. A dynamic lithium-ion battery model considering the effects of temperature and capacity fading. In: 2009 international conference on clean electrical power. IEEE; 2009. p. 383–6. https://doi.org/10.1109/ICCEP.2009.5212025. http://ieeexplore.ieee.org/document/5212025/.
[65] Zhang S, Xu K, Jow T. Optimization of the forming conditions of the solid-state interface in the Li-ion batteries. J Power Sources 2004;130(1–2):281–5. https://doi.org/10.1016/J.JPOWSOUR.2003.12.012. https://www.sciencedirect.com/science/article/pii/S0378775303012114.
[66] Vetter J, Novák P, Wagner M, Veit C, Möller K-C, Besenhard J, Winter M, Wohlfahrt-Mehrens M, Vogler C, Hammouche A. Ageing mechanisms in lithium-ion batteries. J Power Sources 2005;147(1–2):269–81. https://doi.org/10.1016/J.JPOWSOUR.2005.01.006. https://www.sciencedirect.com/science/article/pii/S0378775305000832.
[67] Wohlfahrt-Mehrens M, Vogler C, Garche J. Aging mechanisms of lithium cathode materials. J Power Sources 2004;127(1–2):58–64. https://doi.org/10.1016/J.JPOWSOUR.2003.09.034. https://www.sciencedirect.com/science/article/pii/S0378775303009376.
[68] Imhof R, Novák P. Oxidative electrolyte solvent degradation in lithium-ion batteries an in situ differential electrochemical mass spectrometry investigation. Tech. Rep. 1999;5. http://jes.ecsdl.org/content/146/5/1702.full.pdf.
[69] Ji Y, Zhang Y, Wang C-Y. Li-ion cell operation at low temperatures. J Electrochem Soc 2013;160(4):A636–49. https://doi.org/10.1149/2.047304jes. http://jes.ecsdl.org/lookup/doi/10.1149/2.047304jes.
[70] Smith AJ, Burns JC, Zhao X, Xiong D, Dahn JR. A high precision coulometry study of the SEI growth in Li/graphite cells. J Electrochem Soc 2011;158(5):447–52. https://doi.org/10.1149/1.3557892. http://jes.ecsdl.org/content/158/5/A447.full.pdf.
[71] Andersson AM, Edström K. Chemical composition and morphology of the elevated temperature SEI on graphite. J Electrochem Soc 2001;148:1100–9. https://doi.org/10.1149/1.1397771. http://jes.ecsdl.org/content/148/10/A1100.full.pdf.
[72] Gachot G, Grugeon S, Armand M, Pilard S, Guenot P, Tarascon J-M, Laruelle S. Deciphering the multi-step degradation mechanisms of carbonate-based electrolyte in Li batteries. J Power Sources 2008;178(1):409–21. https://doi.org/10.1016/J.JPOWSOUR.2007.11.110. https://www.sciencedirect.com/science/article/abs/pii/S0378775307026377{#}fig1.
[73] Lee HH, Wan CC, Wang YY. Thermal stability of the solid electrolyte interface on carbon electrodes of lithium batteries. J Electrochem Soc 2004;151:542–7. https://doi.org/10.1149/1.1647568. http://jes.ecsdl.org/content/151/4/A542.full.pdf.
[74] Ravdel B, Abraham K, Gitzendanner R, DiCarlo J, Lucht B, Campion C. Thermal stability of lithium-ion battery electrolytes. J Power Sources 2003;119–121:805–10. https://doi.org/10.1016/S0378-7753(03)00257-X. https://www.sciencedirect.com/science/article/pii/S037877530300257X.
[75] Pieczonka NPW, Borgel V, Ziv B, Leifer N, Dargel V, Aurbach D, Kim J-H, Liu Z, Huang X, Krachkovskiy SA, Goward GR, Halalay I, Powell BR, Manthiram A. Lithium polyacrylate (LiPAA) as an advanced binder and a passivating agent for high-voltage Li-ion batteries. Adv. Energy Mater.. 2015;5(23):1501008. https://doi.org/10.1002/aenm.201501008. https://doi.org/10.1002/aenm.201501008.
[76] Yuca N, Zhao H, Song X, Ferhat Dogdu M, Yuan W, Fu Y, Battaglia VS, Xiao X, Liu G. A systematic investigation of polymer binder flexibility on the electrode performance of lithium-ion batteries. www.acsami.org.
[77] Syzdek J, Marcinek M, Kostecki R. Electrochemical activity of carbon blacks in LiPF6-based organic electrolytes. J Power Sources 2014;245:739–44. https://doi.org/10.1016/J.JPOWSOUR.2013.07.033. https://www.sciencedirect.com/science/article/pii/S0378775313012147?via{%}3Dihub{#}fig3.
[78] Wang Q, Ping P, Zhao X, Chu G, Sun J, Chen C. Thermal runaway caused fire and explosion of lithium ion battery. J Power Sources 2012;208:210–24. https://doi.org/10.1016/J.JPOWSOUR.2012.02.038. https://www.sciencedirect.com/science/article/pii/S0378775312003989{#}sec0020.
[79] Wang Q, Sun J, Yao X, Chen C. Thermal behavior of lithiated graphite with electrolyte in lithium-ion batteries. J Electrochem Soc 2006;153:329–33. https://doi.org/10.1149/1.2139955. http://jes.ecsdl.org/content/153/2/A329.full.pdf.
[80] Arora P, Zhang Z. Battery separators. Chem Rev 2004;104(10):4419–62. https://doi.org/10.1021/cr020738u.
[81] Chen Z, Hsu P-C, Lopez J, Li Y, To JWF, Liu N, Wang C, Andrews SC, Liu J, Cui Y, Bao Z. Fast and reversible thermoresponsive polymer switching materials for safer batteries. Nature Energy 2016;1(1):15009. https://doi.org/10.1038/nenergy.2015.9. http://www.nature.com/articles/nenergy20159.
[82] Roth EP, Orendorff CJ. How electrolytes influence battery safety. Interface magazine 2012;21(2):45–9. https://doi.org/10.1149/2.F04122if. http://interface.ecsdl.org/cgi/doi/10.1149/2.F04122if.
[83] Pei A, Zheng G, Shi F, Li Y, Cui Y. Nanoscale nucleation and growth of electrodeposited lithium metal. Nano Lett 2017;17(2):1132–9. https://doi.org/10.1021/acs.nanolett.6b04755. http://pubs.acs.org/doi/10.1021/acs.nanolett.6b04755.
[84] P. Bai, J. Li, F. R. Brushett, M. Z. Bazant, Transition of lithium growth mechanisms in liquid electrolytes, Energy Environ Sci doi:10.1039/c6ee01674j.
[85] Jana A, García RE. Lithium dendrite growth mechanisms in liquid electrolytes. Nano Energy 2017;41:552–65. https://doi.org/10.1016/J.NANOEN.2017.08.056. https://www.sciencedirect.com/science/article/pii/S2211285517305244.
[86] Eastwood DS, Bayley PM, Chang HJ, Taiwo OO, Vila-Comamala J, Brett DJL, Rau C, Withers PJ, Shearing PR, Grey CP, Lee PD. Three-dimensional characterization of electrodeposited lithium microstructures using synchrotron X-ray phase contrast imaging. Chem Commun 2015;51(2):266–8. https://doi.org/10.1039/C4CC03187C. http://xlink.rsc.org/?DOI=C4CC03187C.
[87] Birkl CR, Roberts MR, McTurk E, Bruce PG, Howey DA. Degradation diagnostics for lithium ion cells. J Power Sources 2017;341:373–86. https://doi.org/10.1016/J.JPOWSOUR.2016.12.011. https://www.sciencedirect.com/science/article/pii/S0378775316316998.
[88] Santhanagopalan S, Ramadass P, Zhang JZ. Analysis of internal short-circuit in a lithium ion cell. J Power Sources 2009;194(1):550–7. https://doi.org/10.1016/J.JPOWSOUR.2009.05.002. https://www.sciencedirect.com/science/

article/pii/S037877530900843X.
[89] Fuller TF, Doyle M, Newman J. Simulation and optimization of the dual lithium ion insertion cell. J Electrochem Soc 1994;141(1):1. https://doi.org/10.1149/1.2054684. http://jes.ecsdl.org/cgi/doi/10.1149/1.2054684.
[90] Perkins RD, Randall AV, Zhang X, Plett GL. Controls oriented reduced order modeling of lithium deposition on overcharge. J Power Sources 2012;209:318–25. https://doi.org/10.1016/J.JPOWSOUR.2012.03.003. https://www.sciencedirect.com/science/article/pii/S0378775312005423.
[91] Hein S, Latz A. Influence of local lithium metal deposition in 3D microstructures on local and global behavior of Lithium-ion batteries. Electrochim Acta 2016;201:354–65. https://doi.org/10.1016/J.ELECTACTA.2016.01.220. https://www.sciencedirect.com/science/article/pii/S0013468616302456.
[92] Ge H, Aoki T, Ikeda N, Suga S, Isobe T, Li Z, Tabuchi Y, Zhang J. Investigating lithium plating in lithium-ion batteries at low temperatures using electrochemical model with NMR assisted parameterization. J Electrochem Soc 2017;164(6):A1050–60. https://doi.org/10.1149/2.0461706jes. http://jes.ecsdl.org/lookup/doi/10.1149/2.0461706jes.
[93] X. G. Yang, Y. Leng, G. Zhang, S. Ge, C. Y. Wang, Modeling of lithium plating induced aging of lithium-ion batteries: transition from linear to nonlinear aging, J Power Sourcesdoi:10.1016/j.jpowsour.2017.05.110.
[94] Sikha G, Popov BN, White RE. Effect of porosity on the capacity fade of a lithium-ion battery. J Electrochem Soc 2004;151(7):A1104. https://doi.org/10.1149/1.1759972. http://jes.ecsdl.org/cgi/doi/10.1149/1.1759972.
[95] Yang X-G, Ge S, Liu T, Leng Y, Wang C-Y. A look into the voltage plateau signal for detection and quantification of lithium plating in lithium-ion cells. J Power Sources 2018;395:251–61. https://doi.org/10.1016/J.JPOWSOUR.2018.05.073. https://www.sciencedirect.com/science/article/pii/S0378775318305573.
[96] Ren D, Han X, Feng X, Smith K, Lu L, Ouyang M, Guo D, Li J. Investigation of lithium plating-stripping process in Li-ion batteries at low temperature using an electrochemical model. J Electrochem Soc 2018;165(10):A2167–78. https://doi.org/10.1149/2.0661810jes.
[97] Osaka T, Homma T, Momma T, Hideki Y. In situ observation of Li deposition processes in solid polymer and gel electrolytes. J Electroanal Chem 1997;421:153.
[98] Crowther O, West AC. Effect of electrolyte composition on lithium dendrite growth. J Electrochem Soc 2008;155(11):A806——811. https://doi.org/10.1149/1.2969424.
[99] Aryanfar A, Brooks DJ, Colussi AJ, Hoffmann MR. Quantifying the dependence of dead lithium losses on the cycling period in lithium metal batteries. Phys Chem Chem Phys 2014;16(45):24965–70. https://doi.org/10.1039/c4cp03590a.
[100] Guo Z, Zhu J, Feng J, Du S. Direct in situ observation and explanation of lithium dendrite of commercial graphite electrodes. RSC Adv 2015;5(85):69514–21. https://doi.org/10.1039/C5RA13289D.
[101] Shao M. In situ microscopic studies on the structural and chemical behaviors of lithium-ion battery materials. J Power Sources 2014;270:475–86. https://doi.org/10.1016/j.jpowsour.2014.07.123.
[102] Steiger J, Richter G, Wenk M, Kramer D, Mönig R. Comparison of the growth of lithium fi laments and dendrites under different conditions. Electrochem Commun 2015;50:11–4. https://doi.org/10.1016/j.elecom.2014.11.002. https://doi.org/10.1016/j.elecom.2014.11.002.
[103] Bieker G, Winter M, Bieker P. Electrochemical in situ investigations of SEI and dendrite formation on the lithium metal anode. Phys Chem Chem Phys 2015;17(14):8670–9. https://doi.org/10.1039/c4cp05865h.
[104] Liu XH, Zhong L, Zhang LQ, Kushima A, Mao SX, Li J, Ye ZZ, Sullivan JP, Huang JY. Lithium fiber growth on the anode in a nanowire lithium ion battery during charging. Appl Phys Lett 2011;98(18):183107. https://doi.org/10.1063/1.3585655.
[105] Ghassemi H, Au M, Chen N, Heiden PA, Yassar RS. Real-time observation of lithium fibers growth inside a nanoscale lithium-ion battery. Appl Phys Lett 2011;99(12):123113. https://doi.org/10.1063/1.3643035.
[106] Sacci RL, Dudney NJ, Unocic RR, Parent LR, Nigel D. Direct visualization of initial SEI morphology and growth kinetics during lithium deposition with in situ electrochemical transmission electron microscopy. Chem Commun 2014;50(17):2104–7.
[107] Bhattacharyya R, Key B, Chen H, Best AS, Hollenkamp AF, Grey CP. In situ NMR observation of the formation of metallic lithium microstructures in lithium batteries. Nat Mater 2010;9(6):504–10. https://doi.org/10.1038/nmat2764. NIHMS150003. https://doi.org/10.1038/nmat2764.
[108] Arai J, Okada Y, Sugiyama T, Izuka M, Gotoh K, Takeda K. In situ solid state Li-7 NMR observations of lithium metal deposition during overcharge in lithium ion batteries. J Electrochem Soc 2015;162(6):A952–8. https://doi.org/10.1149/2.0411506jes.
[109] Letellier M, Chevallier F, Morcrette M. In situ Li-7 nuclear magnetic resonance observation of the electrochemical intercalation of lithium in graphite; 1st cycle. Carbon 2007;45(5):1025–34. https://doi.org/10.1016/j.carbon.2006.12.018.
[110] Downie LE, Krause LJ, Burns JC, Jensen LD, Chevrier VL, Dahn JR. In situ detection of lithium plating on graphite electrodes by electrochemical calorimetry. J Electrochem Soc 2013;160(4):A588–94. https://doi.org/10.1149/2.049304jes. http://jes.ecsdl.org/cgi/doi/10.1149/2.049304jes.
[111] Zhang Y, Li X, Li Z, Zhang J, Su L, Liaw BY. Lithium plating detection and quantification in Li-ion cells from degradation behaviors. ECS Transactions 2017;75(23):37–50. https://doi.org/10.1149/07523.0037ecst.
[112] Harting N, Wolff N, Krewer U. Identification of lithium plating in lithium-ion batteries using nonlinear frequency response analysis (NFRA). Electrochim Acta 2018;281:378–85. https://doi.org/10.1016/j.electacta.2018.05.139. https://doi.org/10.1016/j.electacta.2018.05.139.
[113] Burns JC, Stevens DA, Dahn JR. In-situ detection of lithium plating using high precision coulometry. J Electrochem Soc 2015;162(6):A959–64. https://doi.org/10.1149/2.0621506jes.
[114] Campbell ID, Marzook M, Marinescu M, Offer GJ. How observable is lithium plating? Differential voltage analysis to identify and quantify lithium plating following fast charging of cold lithium-ion batteries. J Electrochem Soc 2019;166(4):A725–39. https://doi.org/10.1149/2.0821904jes. http://jes.ecsdl.org/lookup/doi/10.1149/2.0821904jes.
[115] Lüders CV, Zinth V, Erhard SV, Osswald PJ, Hofmann M, Gilles R, Jossen A. Lithium plating in lithium-ion batteries investigated by voltage relaxation and in situ neutron diffraction. J Power Sources 2017;342:17–23. https://doi.org/10.1016/j.jpowsour.2016.12.032. https://doi.org/10.1016/j.jpowsour.2016.12.032.
[116] Uhlmann C, Illig J, Ender M, Schuster R, Ivers-Tiffée E. In situ detection of lithium metal plating on graphite in experimental cells. J Power Sources 2015;279:428–38. https://doi.org/10.1016/j.jpowsour.2015.01.046.
[117] Schindler S, Bauer M, Petzl M, Danzer MA. Voltage relaxation and impedance spectroscopy as in-operando methods for the detection of lithium plating on graphitic anodes in commercial lithium-ion cells. J Power Sources 2016;304:170–80. https://doi.org/10.1016/j.jpowsour.2015.11.044. https://doi.org/10.1016/j.jpowsour.2015.11.044.
[118] Petzl M, Danzer MA. Nondestructive detection, characterization, and quantification of lithium plating in commercial lithium-ion batteries. J Power Sources 2014;254:80–7. https://doi.org/10.1016/j.jpowsour.2013.12.060. https://doi.org/10.1016/j.jpowsour.2013.12.060.
[119] Anseán D, Dubarry M, Devie A, Liaw BY, García VM, Viera JC, González M. Operando lithium plating quantification and early detection of a commercial LiFePO4cell cycled under dynamic driving schedule. J Power Sources 2017;356:36–46. https://doi.org/10.1016/j.jpowsour.2017.04.072.
[120] Bitzer B, Gruhle A. A new method for detecting lithium plating by measuring the cell thickness. J Power Sources 2014;262:297–302. https://doi.org/10.1016/j.jpowsour.2014.03.142.
[121] Rieger B, Schuster SF, Erhard SV, Osswald PJ, Rheinfeld A, Willmann C, Jossen A. Multi-directional laser scanning as innovative method to detect local cell damage during fast charging of lithium-ion cells. Journal of Energy Storage 2016;8:1–5. https://doi.org/10.1016/j.est.2016.09.002.
[122] Lin C, Tang A, Wu N, Xing J. Electrochemical and mechanical failure of graphite-based anode materials in Li-ion batteries for electric vehicles. J Chem 2016;2016:1–7. https://doi.org/10.1155/2016/2940437. https://www.hindawi.com/journals/jchem/2016/2940437/.
[123] Purewal J, Wang J, Graetz J, Soukiazian S, Tataria H, Verbrugge MW. Degradation of lithium ion batteries employing graphite negatives and nickelcobaltmanganese oxide + spinel manganese oxide positives: Part 2, chemicalmechanical degradation model. J Power Sources 2014;272:1154–61. https://doi.org/10.1016/J.JPOWSOUR.2014.07.028. https://www.sciencedirect.com/science/article/pii/S0378775314010726.
[124] Iqbal N, Lee S. Mechanical failure analysis of graphite anode particles with PVDF binders in Li-ion batteries. J Electrochem Soc 2018;165(9):A1961–70. https://doi.org/10.1149/2.0111810jes. http://jes.ecsdl.org/lookup/doi/10.1149/2.0111810jes.
[125] Yan P, Zheng J, Gu M, Xiao J, Zhang JG, Wang CM. Intragranular cracking as a critical barrier for high-voltage usage of layer-structured cathode for lithium-ion batteries. Nat Commun 2017;8:1–9. https://doi.org/10.1038/ncomms14101.
[126] Xia S, Mu L, Xu Z, Wang J, Wei C, Liu L, Pianetta P, Zhao K, Yu X, Lin F, Liu Y. Chemomechanical interplay of layered cathode materials undergoing fast charging in lithium batteries. Nano Energy 2018;53:753–62. https://doi.org/10.1016/J.NANOEN.2018.09.051. https://www.sciencedirect.com/science/article/pii/S2211285518306955?via{%}3Dihub.
[127] Shi J, Li J, de Vasconcelos LS, Xu R, Zhao K. Disintegration of meatball electrodes for LiNi x Mn y Co z O2 cathode materials. Exp Mech 2017;58(4):549–59. https://doi.org/10.1007/s11340-017-0292-0.
[128] Woodford WH, Chiang Y-M, Carter WC. Electrochemical shock of intercalation electrodes: a fracture mechanics analysis. J Electrochem Soc 2010;157(10):A1052. https://doi.org/10.1149/1.3464773.
[129] Zhao K, Pharr M, Vlassak JJ, Suo Z. Fracture of electrodes in lithium-ion batteries caused by fast charging. J Appl Phys 2010;108(7):1–7. https://doi.org/10.1063/1.3492617. https://doi.org/10.1063/1.3492617.
[130] Ning G, Haran B, Popov BN. Capacity fade study of lithium-ion batteries cycled at high discharge rates. J Power Sources 2003;117(1–2):160–9. https://doi.org/10.1016/S0378-7753(03)00029-6.
[131] Woodford WH, Carter WC, Chiang YM. Design criteria for electrochemical shock resistant battery electrodes. Energy Environ Sci 2012;5(7):8014–24. https://doi.org/10.1039/c2ee21874g.
[132] Morigaki K, Hosokawa T, Nakura K, Watanabe S, Kinoshita M. Capacity fade of LiAlyNi1xyCoxO2 cathode for lithium-ion batteries during accelerated calendar and cycle life tests (surface analysis of LiAlyNi1xyCoxO2 cathode after cycle tests in restricted depth of discharge ranges). J Power Sources 2014;258:210–7. https://doi.org/10.1016/j.jpowsour.2014.02.018. https://doi.org/10.1016/j.jpowsour.2014.02.018.
[133] Zhang S, Zhao K, Zhu T, Li J. Electrochemomechanical degradation of high-

capacity battery electrode materials. Prog Mater Sci 2017;89:479–521. https://doi.org/10.1016/j.pmatsci.2017.04.014.
[134] Wei C, Zhang Y, Lee SJ, Mu L, Liu J, Wang C, Yang Y, Doeff M, Pianetta P, Nordlund D, Du XW, Tian Y, Zhao K, Lee JS, Lin F, Liu Y. Thermally driven mesoscale chemomechanical interplay in Li0.5Ni0.6Mn0.2Co0.2O2 cathode materials. J Mater Chem 2018;6(45):23055–61. https://doi.org/10.1039/c8ta08973f.
[135] Z. Zhang, C. Yang, Z. Zuo, Z. Huang, G. Li, H. Zhou, Understanding the accumulated cycle capacity fade caused by the secondary particle fracture of LiNi1-x-yCoxMnyO2 cathode for lithium ion batteries, J Solid State Electrochem doi:10.1007/s10008-016-3399-9
[136] Mukhopadhyay A, Sheldon BW. Deformation and stress in electrode materials for Li-ion batteries. Prog Mater Sci 2014;63:58–116. https://doi.org/10.1016/j.pmatsci.2014.02.001. https://doi.org/10.1016/j.pmatsci.2014.02.001.
[137] Eberman KW, Turner RL, Beaulieu LY, Dahn JR, Krause LJ. Colossal reversible volume changes in lithium alloys. Electrochem Solid State Lett 2002;4(9). https://doi.org/10.1149/1.1388178. A137.
[138] Evans AG, Hepp AF, Maranchi JP, Kumta PN, Nuhfer NT. Interfacial properties of the a-SiCu:ActiveInactive thin-film anode system for lithium-ion batteries. J Electrochem Soc 2007;153(6):A1246. https://doi.org/10.1149/1.2184753.
[139] Zhao Y, Patel Y, Hunt IA, Kareh KM, Holland AA, Korte C, Dear JP, Yue Y, Offer GJ. Preventing lithium ion battery failure during high temperatures by externally applied compression. Journal of Energy Storage 2017;13:296–303. https://doi.org/10.1016/j.est.2017.08.001. https://doi.org/10.1016/j.est.2017.08.001.
[140] Xu Z, Rahman MM, Mu L, Liu Y, Lin F. Chemomechanical behaviors of layered cathode materials in alkali metal ion batteries. J Mater Chem 2018;6(44):21859–84. https://doi.org/10.1039/c8ta06875e. https://doi.org/10.1039/C8TA06875E.
[141] Liu XH, Zhong L, Huang S, Mao SX, Zhu T, Huang JY. Size-dependent fracture of silicon during lithiation. ACS Nano 2012;6(2):1522–31.
[142] Berla LA, McDowell MT, Cui Y, Nix WD, Lee SW. Fracture of crystalline silicon nanopillars during electrochemical lithium insertion. Proc Natl Acad Sci 2012;109(11):4080–5. https://doi.org/10.1073/pnas.1201088109.
[143] Watanabe S, Kinoshita M, Hosokawa T, Morigaki K, Nakura K. Capacity fading of LiAlyNi1-x-yCoxO 2 cathode for lithium-ion batteries during accelerated calendar and cycle life tests (effect of depth of discharge in charge-discharge cycling on the suppression of the micro-crack generation of LiAlyNi 1-x-yCoxO2 parti. J Power Sources 2014;260:50–6. https://doi.org/10.1016/j.jpowsour.2014.02.103.
[144] Lu B, Zhao Y, Song Y, Zhang J. Stress-limited fast charging methods with time-varying current in lithium-ion batteries. Electrochim Acta 2018;288:144–52. https://doi.org/10.1016/J.ELECTACTA.2018.09.009. https://www.sciencedirect.com/science/article/pii/S0013468618319704.
[145] Spingler FB, Wittmann W, Sturm J, Rieger B, Jossen A. Optimum fast charging of lithium-ion pouch cells based on local volume expansion criteria. J Power Sources 2018;393:152–60. https://doi.org/10.1016/J.JPOWSOUR.2018.04.095. https://www.sciencedirect.com/science/article/pii/S0378775318304440.
[146] Tanim TR, Dufek EJ, Evans M, Dickerson C, Jansen AN, Polzin BJ, Dunlop AR, Trask SE, Jackman R, Bloom I, Yang Z, Lee E. Extreme fast charge challenges for lithium-ion battery: variability and positive electrode issues. J Electrochem Soc 2019;166(10):1926–38. https://doi.org/10.1149/2.0731910jes. http://jes.ecsdl.org/content/166/10/A1926.full.pdf.
[147] Palacín MR. Understanding ageing in Li-ion batteries: a chemical issue. Chem Soc Rev 2018;47(13):4924–33. https://doi.org/10.1039/c7cs00889a.
[148] Kim DS, Kim YE, Kim H. Improved fast charging capability of graphite anodes via amorphous Al 2 O 3 coating for high power lithium ion batteries. J Power Sources 2019;422(December 2018):18–24. https://doi.org/10.1016/j.jpowsour.2019.03.027.
[149] Vasileiadis A, de Klerk NJ, Smith RB, Ganapathy S, Harks PPR, Bazant MZ, Wagemaker M. Toward optimal performance and in-depth understanding of spinel Li 4 Ti 5 O 12 electrodes through phase field modeling. Adv Funct Mater 2018;28(16):1–18. https://doi.org/10.1002/adfm.201705992.
[150] Zheng XD, Dong CC, Huang B, Lu M. High-rate Li4Ti5O12/C composites as anode for lithium-ion batteries. Ionics 2013;19(3):385–9. https://doi.org/10.1007/s11581-012-0767-z.
[151] Yuan T, Yu X, Cai R, Zhou Y, Shao Z. Synthesis of pristine and carbon-coated Li4Ti5O12 and their low-temperature electrochemical performance. J Power Sources 2010;195(15):4997–5004. https://doi.org/10.1016/j.jpowsour.2010.02.020.
[152] Yang A-R, Na B-K. Manufacturing and electrochemical characteristics of SnO 2/Li 4 Ti 5 O 12 for lithium ion battery. Cleanroom Technol 2016;21(4):265–70. https://doi.org/10.7464/ksct.2015.21.4.265.
[153] Tian B, Xiang H, Zhang L, Li Z, Wang H. Niobium doped lithium titanate as a high rate anode material for Li-ion batteries. Electrochim Acta 2010;55(19):5453–8. https://doi.org/10.1016/j.electacta.2010.04.068.
[154] Xu C, Xu B, Gu Y, Xiong Z, Sun J, Zhao XS. Graphene-based electrodes for electrochemical energy storage. Energy Environ Sci 2013;6(6):1388–414. https://doi.org/10.1039/c3ee23870a.
[155] Wu ZS, Ren W, Xu L, Li F, Cheng HM. Doped graphene sheets as anode materials with superhigh rate and large capacity for lithium ion batteries. ACS Nano 2011;5(7):5463–71. https://doi.org/10.1021/nn2006249.
[156] Reddy ALM, Srivastava A, Gowda SR, Gullapalli H, Dubey M, Ajayan PM. Synthesis of nitrogen-doped graphene films for lithium battery application. ACS Nano 2010;4(11):6337–42. https://doi.org/10.1021/nn101926g. http://pubs.acs.org/doi/10.1021/nn101926g.
[157] Agyeman DA, Song K, Lee GH, Park M, Kang YM. Carbon-coated Si nanoparticles anchored between reduced graphene oxides as an extremely reversible anode material for high energy-density Li-ion battery. Adv. Energy Mater. 2016;6(20):1–10. https://doi.org/10.1002/aenm.201600904.
[158] Kang SH, Abraham DP, Yoon WS, Nam KW, Yang XQ. First-cycle irreversibility of layered Li-Ni-Co-Mn oxide cathode in Li-ion batteries. Electrochim Acta 2008;54(2):684–9. https://doi.org/10.1016/j.electacta.2008.07.007.
[159] Han J-T, Liu D-Q, Song S-H, Kim Y, Goodenough JB. Lithium ion intercalation performance of niobium oxides: KNb_5O_{13} and $K_6Nb_{10.8}O_{30}$. Chem Mater 2009;21(20):4753–5. https://doi.org/10.1021/cm9024149.
[160] Reddy MA, Varadaraju UV. ChemInform abstract: facile insertion of lithium into nanocrystalline AlNbO 4 at room temperature. ChemInform 2008;39(43):4557–9. https://doi.org/10.1002/chin.200843014.
[161] Han J-T, Goodenough JB. 3-V full cell performance of anode framework TiNb 2 O 7/spinel LiNi 0.5 Mn 1.5 O 4. Chem Mater 2011;23(15):3404–7. https://doi.org/10.1021/cm201515g.
[162] L. Peng, P. Xiong, L. Ma, Y. Yuan, Y. Zhu, D. Chen, X. Luo, J. Lu, K. Amine, G. Yu, Holey two-dimensional transition metal oxide nanosheets for efficient energy storage, Nat Commun 8. doi:10.1038/ncomms15139
[163] Ding J, Zhou Y, Li Y, Guo S, Huang X. MoS2 nanosheet assembling superstructure with a three-dimensional ion accessible site: a new class of bifunctional materials for batteries and electrocatalysis. Chem Mater 2016;28(7):2074–80. https://doi.org/10.1021/acs.chemmater.5b04815.
[164] Naguib M, Kurtoglu M, Presser V, Lu J, Niu J, Heon M, Hultman L, Gogotsi Y, Barsoum MW. Two-dimensional nanocrystals produced by exfoliation of Ti 3AlC 2. Adv Mater 2011;23(37):4248–53. https://doi.org/10.1002/adma.201102306.
[165] Zhao MQ, Xie X, Ren CE, Makaryan T, Anasori B, Wang G, Gogotsi Y. Hollow MXene spheres and 3D macroporous MXene frameworks for Na-ion storage. Adv Mater 2017;29(37):1–7. https://doi.org/10.1002/adma.201702410.
[166] Xia Y, Mathis TS, Zhao MQ, Anasori B, Dang A, Zhou Z, Cho H, Gogotsi Y, Yang S. Thickness-independent capacitance of vertically aligned liquid-crystalline MXenes. Nature 2018;557(7705):409–12. https://doi.org/10.1038/s41586-018-0109-z.
[167] Lin D, Liu Y, Cui Y. Reviving the lithium metal anode for high-energy batteries. Nat Nanotechnol 2017;12(3):194–206. https://doi.org/10.1038/nnano.2017.16.
[168] Liang Z, Lin D, Zhao J, Lu Z, Liu Y, Liu C, Lu Y, Wang H, Yan K, Tao X, Cui Y. Composite lithium metal anode by melt infusion of lithium into a 3D conducting scaffold with lithiophilic coating. Proc Natl Acad Sci 2016;113(11):2862–7. https://doi.org/10.1073/pnas.1518188113.
[169] Zhao Q, Tu Z, Wei S, Zhang K, Choudhury S, Liu X, Archer LA. Building organic/inorganic hybrid interphases for fast interfacial transport in rechargeable metal batteries. Angew Chem Int Ed 2018;57(4):992–6. https://doi.org/10.1002/anie.201711598.
[170] Nagaoka K, Hoshi K, Bitoh S, Inagaki M, Ohta N. Carbon-coated graphite for anode of lithium ion rechargeable batteries: graphite substrates for carbon coating. J Power Sources 2009;194(2):985–90. https://doi.org/10.1016/j.jpowsour.2009.06.013.
[171] Dimov N, Gunawardhana N, Park G-J, Nakamura H, Sasidharan M, Yoshio M. Suppression of lithium deposition at sub-zero temperatures on graphite by surface modification. Electrochem Commun 2011;13(10):1116–8. https://doi.org/10.1016/j.elecom.2011.07.014. https://doi.org/10.1016/j.elecom.2011.07.014.
[172] Nobili F, Mancini M, Dsoke S, Tossici R, Marassi R. Low-temperature behavior of graphite-tin composite anodes for Li-ion batteries. J Power Sources 2010;195(20):7090–7. https://doi.org/10.1016/j.jpowsour.2010.05.001. https://doi.org/10.1016/j.jpowsour.2010.05.001.
[173] J. Qian, W. A. Henderson, W. Xu, P. Bhattacharya, M. Engelhard, O. Borodin, J. G. Zhang, High rate and stable cycling of lithium metal anode, Nat Commun 6. doi:10.1038/ncomms7362
[174] Griffith KJ, Wiaderek KM, Cibin G, Marbella LE, Grey CP. Niobium tungsten oxides for high-rate lithium-ion energy storage. Nature 2018;559(7715):556–63. https://doi.org/10.1038/s41586-018-0347-0.
[175] Billaud J, Bouville F, Magrini T, Villevieille C, Studart AR. Magnetically aligned graphite electrodes for high-rate performance Li-ion batteries. Nature Energy 2016;1(8):16097. https://doi.org/10.1038/nenergy.2016.97. http://www.nature.com/articles/nenergy201697.
[176] Sander JS, Erb RM, Li L, Gurijala A, Chiang YM. High-performance battery electrodes via magnetic templating. Nature Energy 2016;1(8):1–7. https://doi.org/10.1038/nenergy.2016.99.
[177] Fang M-D, Ho T-H, Yen J-P, Lin Y-R, Hong J-L, Wu S-H, Jow J-J. Preparation of advanced carbon anode materials from mesocarbon microbeads for use in high C-rate lithium ion batteries. Materials 2015;8(6):3550–61. https://doi.org/10.3390/ma8063550. http://www.mdpi.com/1996-1944/8/6/3550.
[178] Hasan MF, Chen C-F, Shaffer CE, Mukherjee PP. Analysis of the implications of rapid charging on lithium-ion battery performance. J Electrochem Soc 2015;162(7):A1382–95. https://doi.org/10.1149/2.0871507jes.
[179] Verbrugge MW, Koch BJ. The effect of large negative potentials and overcharge on the electrochemical performance of lithiated carbon. J Electroanal Chem 1997;436(1–2):1–7. https://doi.org/10.1016/S0022-0728(97)00031-4.

[180] Xu J, Deshpande RD, Pan J, Cheng Y-T, Battaglia VS. Electrode side reactions, capacity loss and mechanical degradation in lithium-ion batteries. J Electrochem Soc 2015;162(10):A2026–35. https://doi.org/10.1149/2.0291510jes. http://jes.ecsdl.org/lookup/doi/10.1149/2.0291510jes.

[181] Kim C-S, Jeong KM, Kim K, Yi C-W. Effects of capacity ratios between anode and cathode on electrochemical properties for lithium polymer batteries. Electrochim Acta 2015;155:431–6. https://doi.org/10.1016/J.ELECTACTA.2014.12.005. https://www.sciencedirect.com/science/article/pii/S0013468614024402?via{%}3Dihub.

[182] Tang M, Albertus P, Newman J, Energy E, Division T, Berkeley L. Two-dimensional modeling of lithium deposition during cell charging. J Electrochem Soc 2009;156(5):390–9. https://doi.org/10.1149/1.3095513.

[183] Hüfner T, Oldenburger M, Bedürftig B, Gruhle A. Lithium flow between active area and overhang of graphite anodes as a function of temperature and overhang geometry. Journal of Energy Storage 2019;24:100790. https://doi.org/10.1016/J.EST.2019.100790. https://www.sciencedirect.com/science/article/pii/S2352152X19301768{#}bib0010.

[184] Grimsmann F, Gerbert T, Brauchle F, Gruhle A, Parisi J, Knipper M. Hysteresis and current dependence of the graphite anode color in a lithium-ion cell and analysis of lithium plating at the cell edge. Journal of Energy Storage 2018;15:17–22. https://doi.org/10.1016/J.EST.2017.10.015. https://www.sciencedirect.com/science/article/pii/S2352152X17302268.

[185] Zhang G, Shaffer CE, Wang C-Y, Rahn CD. Effects of non-uniform current distribution on energy density of Li-ion cells. J Electrochem Soc 2013;160(11):A2299–305. https://doi.org/10.1149/2.061311jes.

[186] Yao XY, Pecht MG. Tab design and failures in cylindrical li-ion batteries. IEEE Access 2019;7:24082–95. https://doi.org/10.1109/ACCESS.2019.2899793.

[187] Erhard SV, Osswald PJ, Keil P, Höffer E, Haug M, Noel A, Wilhelm J, Rieger B, Schmidt K, Kosch S, Kindermann FM, Spingler F, Kloust H, Thoennessen T, Rheinfeld A, Jossen A. Simulation and measurement of the current density distribution in lithium-ion batteries by a multi-tab cell approach. J Electrochem Soc 2017;164(1):A6324–33. https://doi.org/10.1149/2.0551701jes. http://jes.ecsdl.org/lookup/doi/10.1149/2.0551701jes.

[188] Zhao W, Luo G, Wang CY. Effect of tab design on large-format Li-ion cell performance. J Power Sources 2014;257:70–9. https://doi.org/10.1016/j.jpowsour.2013.12.146. https://doi.org/10.1016/j.jpowsour.2013.12.146.

[189] Liu X, Ai W, Naylor Marlow M, Patel Y, Wu B. The effect of cell-to-cell variations and thermal gradients on the performance and degradation of lithium-ion battery packs. Appl Energy 2019;248:489–99. https://doi.org/10.1016/J.APENERGY.2019.04.108. https://www.sciencedirect.com/science/article/pii/S0306261919307810?dgcid=author{#}b0070.

[190] Meintz A, Zhang J, Vijayagopal R, Kreutzer C, Ahmed S, Bloom I, Burnham A, Carlson RB, Dias F, Dufek EJ, Francfort J, Hardy K, Jansen AN, Keyser M, Markel A, Michelbacher C, Mohanpurkar M, Pesaran A, Scoffield D, Shirk M, Stephens T, Tanim T. Enabling fast charging Vehicle considerations. J Power Sources 2017;367:216–27. https://doi.org/10.1016/j.jpowsour.2017.07.093.

[191] Guo Z, Liaw BY, Qiu X, Gao L, Zhang C. Optimal charging method for lithium ion batteries using a universal voltage protocol accommodating aging. J Power Sources 2015;274:957–64. https://doi.org/10.1016/J.JPOWSOUR.2014.10.185. https://www.sciencedirect.com/science/article/pii/S0378775314018047.

[192] Zhang S, Xu K, Jow T. Study of the charging process of a LiCoO2-based Li-ion battery. J Power Sources 2006;160(2):1349–54. https://doi.org/10.1016/J.JPOWSOUR.2006.02.087. https://www.sciencedirect.com/science/article/pii/S0378775306004162.

[193] Ouyang M, Chu Z, Lu L, Li J, Han X, Feng X, Liu G. Low temperature aging mechanism identification and lithium deposition in a large format lithium iron phosphate battery for different charge profiles. J Power Sources 2015;286:309–20. https://doi.org/10.1016/J.JPOWSOUR.2015.03.178. https://www.sciencedirect.com/science/article/pii/S0378775315006126.

[194] Zhang SS. The effect of the charging protocol on the cycle life of a Li-ion battery. J Power Sources 2006;161(2):1385–91. https://doi.org/10.1016/J.JPOWSOUR.2006.06.040. https://www.sciencedirect.com/science/article/pii/S0378775306011839?via{%}3Dihub.

[195] Anseán D, González M, Viera J, García V, Blanco C, Valledor M. Fast charging technique for high power lithium iron phosphate batteries: a cycle life analysis. J Power Sources 2013;239:9–15. https://doi.org/10.1016/J.JPOWSOUR.2013.03.044. https://www.sciencedirect.com/science/article/pii/S0378775313004357.

[196] Aryanfar A, Brooks D, Merinov BV, Goddard WA, Colussi AJ, Hoffmann MR. Dynamics of lithium dendrite growth and inhibition: pulse charging experiments and Monte Carlo calculations. J Phys Chem Lett 2014;5(10):1721–6. https://doi.org/10.1021/jz500207a.

[197] Li J, Murphy E, Winnick J, Kohl PA. The effects of pulse charging on cycling characteristics of commercial lithium-ion batteries. J Power Sources 2001;102(1–2):302–9. https://doi.org/10.1016/S0378-7753(01)00820-5. https://www.sciencedirect.com/science/article/pii/S0378775301008205.

[198] Abdel-Monem M, Trad K, Omar N, Hegazy O, Van den Bossche P, Van Mierlo J. Influence analysis of static and dynamic fast-charging current profiles on ageing performance of commercial lithium-ion batteries. Energy 2017;120:179–91. https://doi.org/10.1016/J.ENERGY.2016.12.110. https://www.sciencedirect.com/science/article/pii/S0360544216319156.

[199] Chen L-R, Wu S-L, Shieh D-T, Chen T-R. Sinusoidal-ripple-current charging strategy and optimal charging frequency study for Li-ion batteries. IEEE Trans Ind Electron 2013;60(1):88–97. https://doi.org/10.1109/TIE.2012.2186106. http://ieeexplore.ieee.org/document/6140959/.

[200] Amanor-Boadu JM, Guiseppi-Elie A, Sanchez-Sinencio E. Search for optimal pulse charging parameters for Li-ion polymer batteries using Taguchi orthogonal arrays. IEEE Trans Ind Electron 2018;65(11):8982–92. https://doi.org/10.1109/TIE.2018.2807419. https://ieeexplore.ieee.org/document/8294255/.

[201] Yin M, Cho J, Park D, Yin MD, Cho J, Park D. Pulse-based fast battery IoT charger using dynamic frequency and duty control techniques based on multi-sensing of polarization curve. Energies 2016;9(3):209. https://doi.org/10.3390/en9030209. http://www.mdpi.com/1996-1073/9/3/209.

[202] Notten P, het Veld JO, van Beek J. Boostcharging Li-ion batteries: a challenging new charging concept. J Power Sources 2005;145(1):89–94. https://doi.org/10.1016/J.JPOWSOUR.2004.12.038. https://www.sciencedirect.com/science/article/pii/S0378775305000728.

[203] Keil P, Jossen A. Charging protocols for lithium-ion batteries and their impact on cycle lifeAn experimental study with different 18650 high-power cells. Journal of Energy Storage 2016;6:125–41. https://doi.org/10.1016/J.EST.2016.02.005. https://www.sciencedirect.com/science/article/pii/S2352152X16300147.

[204] Sikha G, Ramadass P, Haran BS, White RE, Popov BN. Comparison of the capacity fade of Sony US 18650 cells charged with different protocols. J Power Sources 2003;122(1):67–76.

[205] Ye M, Gong H, Xiong R, Mu H. Research on the battery charging strategy with charging and temperature rising control awareness. IEEE Access 2018;6:64193–201. https://doi.org/10.1109/ACCESS.2018.2876359. https://ieeexplore.ieee.org/document/8493503/.

[206] Patnaik L, Praneeth AVJS, Williamson SS. A closed-loop constant-temperature constant-voltage charging technique to reduce charge time of lithium-ion batteries. IEEE Trans Ind Electron 2019;66(2):1059–67. https://doi.org/10.1109/TIE.2018.2833038. https://ieeexplore.ieee.org/document/8353785/.

[207] Schindler S, Bauer M, Cheetamun H, Danzer MA. Fast charging of lithium-ion cells: identification of aging-minimal current profiles using a design of experiment approach and a mechanistic degradation analysis. Journal of Energy Storage 2018;19:364–78. https://doi.org/10.1016/J.EST.2018.08.002. https://www.sciencedirect.com/science/article/pii/S2352152X18301464.

[208] Wang J. Charging strategy studies for phev batteries based on power loss model. In: SAE 2010 world congress and exhibition. SAE International; 2010. https://doi.org/10.4271/2010-01-1238. https://doi.org/10.4271/2010-01-1238.

[209] Khamar M, Askari J. A charging method for Lithium-ion battery using Min-max optimal control. In: 2014 22nd Iranian conference on electrical engineering (ICEE). IEEE; 2014. p. 1239–43. https://doi.org/10.1109/IranianCEE.2014.6999724. http://ieeexplore.ieee.org/document/6999724/.

[210] Parvini Y, Vahidi A. Maximizing charging efficiency of lithium-ion and lead-acid batteries using optimal control theory. In: 2015 American control conference (ACC). IEEE; 2015. p. 317–22. https://doi.org/10.1109/ACC.2015.7170755. http://ieeexplore.ieee.org/document/7170755/.

[211] Chen Z, Xia B, Mi CC, Xiong R. Loss-minimization-based charging strategy for lithium-ion battery. IEEE Trans Ind Appl 2015;51(5):4121–9. http://ieeexplore.ieee.org/lpdocs/epic03/wrapper.htm?arnumber=7072523http://xplorestaging.ieee.org/ielx7/28/4957013/07072523.pdf?arnumber=7072523.

[212] Hu X, Perez HE, Moura SJ. Battery charge control with an electro-thermal-aging coupling. In: ASME 2015 dynamic systems and control conference. American Society of Mechanical Engineers; 2015. V001T13A002–V001T13A002.

[213] Zhang C, Jiang J, Gao Y, Zhang W, Liu Q, Hu X. Charging optimization in lithium-ion batteries based on temperature rise and charge time. Appl Energy 2017;194:569–77. https://doi.org/10.1016/j.apenergy.2016.10.059. http://www.sciencedirect.com/science/article/pii/S0306261916315033https://ac.els-cdn.com/S0306261916315033/1-s2.0-S0306261916315033-main.pdf?{_}tid=a751af18-175f-448f-8705-77d38159ca17{&}acdnat=1545648344{_}1e1b09f56d7fdd637465abf5e84ea7cd.

[214] Jiuchun J, Qiujiang L, Caiping Z, Weige Z. Evaluation of acceptable charging current of power Li-ion batteries based on polarization characteristics. IEEE Trans Ind Electron 2014;61(12):6844–51. URL inspec:14581758.

[215] Doyle M, Fuller TF, Newman J. Modeling of galvanostatic charge and discharge of the lithium/polymer/insertion cell. J Electrochem Soc 1993;140(6):1526–33.

[216] Purushothaman BK, Landau U. Rapid charging of lithium-ion batteries using pulsed currents a theoretical analysis. J Electrochem Soc 2006;153(3):A533—–542. https://doi.org/10.1149/1.2161580. http://jes.ecsdl.org/content/153/3/A533.

[217] Tsai Y, Gopaluni RB. An algorithm for optimal charging of Li ion batteries using a single particle model. In: 5th international symposium on advanced control of industrial processes (ADCONIP); 2014. https://pdfs.semanticscholar.org/72fe/9f860e3d99ad820529dbd49f37bcb2ae49e9.pdf.

[218] Perez HE, Hu X, Moura SJ. Optimal charging of batteries via a single particle model with electrolyte and thermal dynamics. In: American control conference (ACC), 2016. IEEE; 2016. p. 4000–5.

[219] Choe S-Y, Li X, Xiao M. Fast charging method based on estimation of ion concentrations using a reduced order of Electrochemical Thermal Model for lithium ion polymer battery. In: The international electric vehicle

symposium and exhibition (EVS); 2013. https://doi.org/10.1109/evs.2013.6914966.
[220] Pramanik S, Anwar S. Electrochemical model based charge optimization for lithium-ion batteries. J Power Sources 2016;313:164–77. https://doi.org/10.1016/j.jpowsour.2016.01.096. www.sciencedirect.com/science/article/pii/S0378775316300969. http://ac.els-cdn.com/S0378775316300969/1-s2.0-S0378775316300969-main.pdf?{_}tid=6b15a794-eba6-11e6-bb27-00000aab0f6b{&}acdnat=1486301247{_}83841c2ed1836d99058dc7d923d68d5d.
[221] Li J, Lotfi N, Landers RG, Park J. A single particle model for lithium-ion batteries with electrolyte and stress-enhanced diffusion physics. J Electrochem Soc 2017;164(4):874–83. https://doi.org/10.1149/2.1541704jes. http://jes.ecsdl.org/content/164/4/A874.full.pdf.
[222] Rahimian SK, Rayman SC, White RE. Maximizing the life of a lithium-ion cell by optimization of charging rates. J Electrochem Soc 2010;157(12):A1302–8. http://jes.ecsdl.org/content/157/12/A1302.full.pdf.
[223] Zou Changfu, Manzie C, Nesic D. PDE battery model simplification for charging strategy evaluation. In: 2015 10th asian control conference (ASCC). IEEE; 2015. p. 1–6. https://doi.org/10.1109/ASCC.2015.7244553. http://ieeexplore.ieee.org/document/7244553/.
[224] Yuan S, Wu H, Ma X, Yin C. Optimal charging strategy development based on solid electrolyte interface (sei) film growth model and dynamic programming. In: The international electric vehicle symposium and exhibition (EVS); 2015. http://www.evs28.org/event_file/event_file/1/pfile/EVS28_0452_Full%20paper.pdf.
[225] Campbell ID, Gopalakrishnan K, Marinescu M, Torchio M, Offer GJ, Raimondo D. Optimising lithium-ion cell design for plug-in hybrid and battery electric vehicles. Journal of Energy Storage 2019;22:228–38. https://doi.org/10.1016/J.EST.2019.01.006. https://www.sciencedirect.com/science/article/pii/S2352152X18300094.
[226] Klein R, Chaturvedi NA, Christensen J, Ahmed J, Findeisen R, Kojic A. Optimal charging strategies in lithium-ion battery. In: Proceedings of the 2011 American control conference; 2011. p. 382–7. https://doi.org/10.1109/ACC.2011.5991497. https://ieeexplore.ieee.org/ielx5/5975310/5989965/05991497.pdf?tp={&}arnumber=5991497{&}isnumber=5989965.
[227] Klein R, Chaturvedi Na, Christensen J, Ahmed J, Findeisen R, Kojic A. Electrochemical model based observer design for a lithium-ion battery. IEEE Trans Control Syst Technol 2013;21(2):289–301. https://doi.org/10.1109/TCST.2011.2178604.
[228] Han X, Ouyang M, Lu L, Li J. Simplification of physics-based electrochemical model for lithium ion battery on electric vehicle. Part I: diffusion simplification and single particle model. J Power Sources 2015;278:802–13.
[229] Han X, Ouyang M, Lu L, Li J. Simplification of physics-based electrochemical model for lithium ion battery on electric vehicle. Part II: pseudo-two-dimensional model simplification and state of charge estimation. J Power Sources 2015;278:814–25.
[230] Chu Z, Feng X, Lu L, Li J, Han X, Ouyang M. Non-destructive fast charging algorithm of lithium-ion batteries based on the control-oriented electrochemical model. Appl Energy 2017;204:1240–50. https://doi.org/10.1016/j.apenergy.2017.03.111. https://doi.org/10.1016/j.apenergy.2017.03.111.
[231] Merla Y, Wu B, Yufit V, Martinez-Botas RF, Offer GJ. An easy-to-parameterise physics-informed battery model and its application towards lithium-ion battery cell design, diagnosis, and degradation. J Power Sources 2018;384:66–79. https://doi.org/10.1016/J.JPOWSOUR.2018.02.065. https://www.sciencedirect.com/science/article/pii/S0378775318301861.
[232] von Srbik M-T, Marinescu M, Martinez-Botas RF, Offer GJ. A physically meaningful equivalent circuit network model of a lithium-ion battery accounting for local electrochemical and thermal behaviour, variable double layer capacitance and degradation. J Power Sources 2016;325:171–84. https://doi.org/10.1016/J.JPOWSOUR.2016.05.051. https://www.sciencedirect.com/science/article/pii/S0378775316305973.
[233] Hao M, Li J, Park S, Moura S, Dames C. Efficient thermal management of Li-ion batteries with a passive interfacial thermal regulator based on a shape memory alloy. Nature Energy 2018;3(10):899–906. https://doi.org/10.1038/s41560-018-0243-8. http://www.nature.com/articles/s41560-018-0243-8.
[234] Bandhauer TM, Garimella S, Fuller TF. A critical review of thermal issues in lithium-ion batteries. http://jes.ecsdl.org/content/158/3/R1.full.pdf.
[235] Xia G, Cao L, Bi G. A review on battery thermal management in electric vehicle application. J Power Sources 2017;367:90–105. https://doi.org/10.1016/J.JPOWSOUR.2017.09.046. https://www.sciencedirect.com/science/article/pii/S0378775317312557{#}bib151.
[236] Zolot M, Pesaran AA, Mihalic M. Thermal evaluation of toyota prius battery pack. In: Future car congr.; 2002. https://doi.org/10.4271/2002-01-1962. http://papers.sae.org/2002-01-1962/.
[237] van Gils R, Danilov D, Notten P, Speetjens M, Nijmeijer H. Battery thermal management by boiling heat-transfer. Energy Convers Manag 2014;79:9–17. https://doi.org/10.1016/J.ENCONMAN.2013.12.006. https://www.sciencedirect.com/science/article/pii/S0196890413007826.
[238] Hirano H, Tajima T, Hasegawa T, Sekiguchi T, Uchino M. Boiling liquid battery cooling for electric vehicle. In: 2014 IEEE conference and expo transportation electrification asia-pacific (ITEC asia-pacific). IEEE; 2014. p. 1–4. https://doi.org/10.1109/ITEC-AP.2014.6940931. http://ieeexplore.ieee.org/lpdocs/epic03/wrapper.htm?arnumber=6940931.
[239] Hémery C-V, Pra F, Robin J-F, Marty P. Experimental performances of a battery thermal management system using a phase change material. J Power Sources 2014;270:349–58. https://doi.org/10.1016/J.JPOWSOUR.2014.07.147. https://www.sciencedirect.com/science/article/pii/S0378775314012014.
[240] Lu Z, Meng X, Wei L, Hu W, Zhang L, Jin L. Thermal management of densely-packed EV battery with forced air cooling strategies. Energy Procedia 2016;88:682–8. https://doi.org/10.1016/J.EGYPRO.2016.06.098. https://www.sciencedirect.com/science/article/pii/S187661021630162X.
[241] Hunt IA, Zhao Y, Patel Y, Offer J. Surface cooling causes accelerated degradation compared to tab cooling for lithium-ion pouch cells. J Electrochem Soc 2016;163(9):A1846–52. https://doi.org/10.1149/2.0361609jes. http://jes.ecsdl.org/lookup/doi/10.1149/2.0361609jes.
[242] Zhao Y, Patel Y, Zhang T, Offer GJ. Modeling the effects of thermal gradients induced by tab and surface cooling on lithium ion cell performance. J Electrochem Soc 2018;165(13):3169–78. https://doi.org/10.1149/2.0901813jes. http://jes.ecsdl.org/content/165/13/A3169.full.pdf.
[243] Christen EJ, Fleming M, Siciak RC. Charging station for electrified vehicles, United States Patent US20170088005A1. https://patents.google.com/patent/US20170088005A1/en.
[244] Dyer CK, Epstein ML, Culver D. Station for rapidly charging an electric vehicle battery, United States Patent US8350526B2. https://patents.google.com/patent/US8350526.
[245] Mardall J, Van Dyke CH. Charging station providing thermal conditioning of electric vehicle during charging session, United States Patent US20170096073A1. https://patents.google.com/patent/US20170096073A1/en.
[246] Ruan H, Jiang J, Sun B, Zhang W, Gao W, Wang LY, Ma Z. A rapid low-temperature internal heating strategy with optimal frequency based on constant polarization voltage for lithium-ion batteries. Appl Energy 2016;177:771–82. https://doi.org/10.1016/J.APENERGY.2016.05.151. https://www.sciencedirect.com/science/article/pii/S0306261916307644.
[247] Ge H, Huang J, Zhang J, Li Z. Temperature-adaptive alternating current preheating of lithium-ion batteries with lithium deposition prevention. J Electrochem Soc 2016;163(2):290–9. https://doi.org/10.1149/2.0961602jes. http://jes.ecsdl.org/content/163/2/A290.full.pdf.
[248] Ji Y, Wang CY. Heating strategies for Li-ion batteries operated from subzero temperatures. Electrochim Acta 2013;107:664–74. https://doi.org/10.1016/J.ELECTACTA.2013.03.147. https://www.sciencedirect.com/science/article/pii/S0013468613005707.
[249] Zhu J, Sun Z, Wei X, Dai H, Gu W. Experimental investigations of an AC pulse heating method for vehicular high power lithium-ion batteries at subzero temperatures. J Power Sources 2017;367:145–57. https://doi.org/10.1016/J.JPOWSOUR.2017.09.063. https://www.sciencedirect.com/science/article/pii/S037877531731282X.
[250] Wang C-Y, Zhang G, Ge S, Xu T, Ji Y, Yang X-G, Leng Y. Lithium-ion battery structure that self-heats at low temperatures. Nature 2016;529(7587):515–8. https://doi.org/10.1038/nature16502. http://www.nature.com/articles/nature16502.
[251] Yang X-G, Liu T, Wang C-Y. Innovative heating of large-size automotive Li-ion cells. J Power Sources 2017;342:598–604. https://doi.org/10.1016/J.JPOWSOUR.2016.12.102. https://www.sciencedirect.com/science/article/pii/S0378775316318055.
[252] Li Z, Huang J, Yann Liaw B, Metzler V, Zhang J. A review of lithium deposition in lithium-ion and lithium metal secondary batteries. J Power Sources 2014;254:168–82. https://doi.org/10.1016/j.jpowsour.2013.12.099.
[253] Grandjean T, Barai A, Hosseinzadeh E, Guo Y, McGordon A, Marco J. Large format lithium ion pouch cell full thermal characterisation for improved electric vehicle thermal management. J Power Sources 2017;359:215–25. https://doi.org/10.1016/j.jpowsour.2017.05.016.
[254] Kim US, Yi J, Shin CB, Han T, Park S. Modeling the thermal behaviors of a lithium-ion battery during constant-power discharge and charge operations. J Electrochem Soc 2013;160(6):A990–5. https://doi.org/10.1149/2.146306jes.
[255] Li Y, Feng X, Ren D, Ouyang M, Lu L. Varying thermal runaway mechanism caused by fast charging for high energy pouch batteries. ECS Meeting Abstracts MA2019-01 2019;6:585.
[256] Klein A, Quinn JB, Kasper M, Wohlfahrt-Mehrens M, Richter K, Waldmann T, Tost A. Electrochemical, post-mortem, and ARC analysis of Li-ion cell safety in second-life applications. J Electrochem Soc 2017;164(13):A3154–62. https://doi.org/10.1149/2.0961713jes.
[257] Fleischhammer M, Waldmann T, Bisle G, Hogg BI, Wohlfahrt-Mehrens M. Interaction of cyclic ageing at high-rate and low temperatures and safety in lithium-ion batteries. J Power Sources 2015;274:432–9. https://doi.org/10.1016/j.jpowsour.2014.08.135.
[258] Feng X, Ouyang M, Liu X, Lu L, Xia Y, He X. Thermal runaway mechanism of lithium ion battery for electric vehicles: a review. Energy Storage Materials 2018;10(May 2017):246–67. https://doi.org/10.1016/j.ensm.2017.05.013.
[259] Ren D, Feng X, Lu L, Ouyang M, Zheng S, Li J, He X. An electrochemical-thermal coupled overcharge-to-thermal-runaway model for lithium ion battery. J Power Sources 2017;364:328–40. https://doi.org/10.1016/j.jpowsour.2017.08.035.
[260] Zheng S, Wang L, Feng X, He X. Probing the heat sources during thermal runaway process by thermal analysis of different battery chemistries. J Power Sources 2018;378(July 2017):527–36. https://doi.org/10.1016/j.jpowsour.2017.12.050.
[261] Liu X, Ren D, Hsu H, Feng X, Xu GL, Zhuang M, Gao H, Lu L, Han X, Chu Z, Li J,

He X, Amine K, Ouyang M. Thermal runaway of lithium-ion batteries without internal short circuit. Joule 2018;2(10):2047–64. https://doi.org/10.1016/j.joule.2018.06.015.
[262] Ouyang M, Ren D, Lu L, Li J, Feng X, Han X, Liu G. Overcharge-induced capacity fading analysis for large format lithium-ion batteries with LiyNi1/3Co1/3 Mn1/3 O2 + LiyMn2O4 composite cathode. 2015. https://doi.org/10.1016/j.jpowsour.2015.01.051.
[263] Feng X, He X, Ouyang M, Wang L, Lu L, Ren D, Santhanagopalan S. A coupled electrochemical-thermal failure model for predicting the thermal runaway behavior of lithium-ion batteries. J Electrochem Soc 2018;165(16):A3748–65. https://doi.org/10.1149/2.0311816jes.
[264] Feng X, Ren D, Zhang S, He X, Wang L, Ouyang M. Influence of aging paths on the thermal runaway features of lithium-ion batteries in accelerating rate calorimetry tests. International Journal of Electrochemical Science 2019;14(1):44–58. https://doi.org/10.20964/2019.01.14.
[265] Ren D, Liu X, Feng X, Lu L, Ouyang M, Li J, He X. Model-based thermal runaway prediction of lithium-ion batteries from kinetics analysis of cell components. Appl Energy 2018;228(January):633–44. https://doi.org/10.1016/j.apenergy.2018.06.126.
[266] Feng X, Zheng S, He X, Wang L, Wang Y, Ren D, Ouyang M. Time sequence map for interpreting the thermal runaway mechanism of lithium-ion batteries with LiNixCoyMnzO2 cathode. Frontiers in Energy Research 2018;6(November):1–16. https://doi.org/10.3389/fenrg.2018.00126.
[267] Zhang C, Jiang Y, Jiang J, Cheng G, Diao W, Zhang W. Study on battery pack consistency evolutions and equilibrium diagnosis for serial- connected lithium-ion batteries. Appl Energy 2017;207:510–9. https://doi.org/10.1016/j.apenergy.2017.05.176.
[268] Li Z, Lu L, Ouyang M, Xiao Y. Modeling the capacity degradation of LiFePO4/graphite batteries based on stress coupling analysis. J Power Sources 2011;196(22):9757–66. https://doi.org/10.1016/j.jpowsour.2011.07.080.
[269] Hofmann A, Uhlmann N, Ziebert C, Wiegand O, Schmidt A, Hanemann T. Preventing Li-ion cell explosion during thermal runaway with reduced pressure. Appl Therm Eng 2017;124:539–44. https://doi.org/10.1016/j.applthermaleng.2017.06.056.
[270] Zhu X, Wang Z, Wang Y, Wang H, Wang C, Tong L, Yi M. Overcharge investigation of large format lithium-ion pouch cells with Li(Ni 0.6 Co 0.2 Mn 0.2)O 2 cathode for electric vehicles: thermal runaway features and safety management method. Energy 2019;169:868–80. https://doi.org/10.1016/j.energy.2018.12.041.
[271] Li X, Liang J, Hou Z, Zhang W, Wang Y, Zhu Y, Qian Y. The design of a high-energy Li-ion battery using germanium-based anode and LiCoO 2 cathode. J Power Sources 2015;293:868–75. https://doi.org/10.1016/j.jpowsour.2015.06.031.
[272] Ferg E. Spinel anodes for lithium-ion batteries. J Electrochem Soc 2006;141(11):L147. https://doi.org/10.1149/1.2059324.
[273] Krueger S, Kloepsch R, Li J, Nowak S, Passerini S, Winter M. How do reactions at the anode/electrolyte interface determine the cathode performance in lithium-ion batteries? J Electrochem Soc 2013;160(4):A542–8. https://doi.org/10.1149/2.022304jes.
[274] Zheng H, Sun Q, Liu G, Song X, Battaglia VS. Correlation between dissolution behavior and electrochemical cycling performance for LiNi 1/3Co 1/3Mn 1/3O 2-based cells. J Power Sources 2012;207:134–40. https://doi.org/10.1016/j.jpowsour.2012.01.122.
[275] Arora P. Capacity fade mechanisms and side reactions in lithium-ion batteries. J Electrochem Soc 1998;145(10):3647. https://doi.org/10.1149/1.1838857.
[276] Sharma N, Peterson VK. Overcharging a lithium-ion battery: effect on the LixC 6 negative electrode determined by in situ neutron diffraction. J Power Sources 2013;244:695–701. https://doi.org/10.1016/j.jpowsour.2012.12.019.
[277] P. Arora, Mathematical modeling of the lithium deposition overcharge reaction in lithium-ion batteries using carbon-based negative electrodes, J Electrochem Socdoi:10.1149/1.1392512
[278] Kumai K, Miyashiro H, Kobayashi Y, Takei K, Ishikawa R. Gas generation mechanism due to electrolyte decomposition in commercial lithium-ion cell. J Power Sources 1999;81–82:715–9. https://doi.org/10.1016/S0378-7753(98)00234-1.
[279] Ohsaki T, Kishi T, Kuboki T, Takami N, Shimura N, Sato Y, Sekino M, Satoh A. Overcharge reaction of lithium-ion batteries. J Power Sources 2005;146(1–2):97–100. https://doi.org/10.1016/j.jpowsour.2005.03.105.
[280] Feng X, Fang M, He X, Ouyang M, Lu L, Wang H, Zhang M. Thermal runaway features of large format prismatic lithium ion battery using extended volume accelerating rate calorimetry. J Power Sources 2014;255:294–301. https://doi.org/10.1016/j.jpowsour.2014.01.005.
[281] Roth EP, Doughty DH. Thermal abuse performance of high-power 18650 Li-ion cells. J Power Sources 2004;128(2):308–18. https://doi.org/10.1016/j.jpowsour.2003.09.068.
[282] Wu L, Nam KW, Wang X, Zhou Y, Zheng JC, Yang XQ, Zhu Y. Structural origin of overcharge-induced thermal instability of Ni-containing layered-cathodes for high-energy-density lithium batteries. Chem Mater 2011;23(17):3953–60. https://doi.org/10.1021/cm201452q.
[283] Lin CK, Ren Y, Amine K, Qin Y, Chen Z. In situ high-energy X-ray diffraction to study overcharge abuse of 18650-size lithium-ion battery. J Power Sources 2013;230:32–7. https://doi.org/10.1016/j.jpowsour.2012.12.032.
[284] He YB, Ning F, Yang QH, Song QS, Li B, Su F, Du H, Tang ZY, Kang F. Structural and thermal stabilities of layered Li(Ni1/3Co 1/3Mn1/3)O2 materials in 18650 high power batteries. J Power Sources 2011;196(23):10322–7. https://doi.org/10.1016/j.jpowsour.2011.08.042.
[285] Odom SA, Ergun S, Poudel PP, Parkin SR. A fast, inexpensive method for predicting overcharge performance in lithium-ion batteries. Energy Environ Sci 2014;7(2):760–7. https://doi.org/10.1039/c3ee42305k.
[286] Wen J, Yu Y, Chen C. A review on lithium-ion batteries safety issues: existing problems and possible solutions. Materials Express 2012;2(3):197–212. https://doi.org/10.1166/mex.2012.1075.
[287] Patterson ML. Chemical shuttle additives in lithium ion batteries. Tech. rep. EnerDel, Inc. for U.S. Department of Energy National Energy Technology Laboratory; 2014. https://www.osti.gov/servlets/purl/1163216.